Open access • Report • DOI:10.2172/270727

TOUGH2 simulations of the TEVES Project including the behavior of a single-component NAPL — Source link

S.W. Webb

Published on: 01 May 1996

Topics: Borehole and Soil vapor extraction

SANDIA REPORT

SAND94–1639 • UC–2010
Unlimited Release
Printed May 1996

TOUGH2 Simulations of the TEVES Project Including the Behavior of a Single-Component NAPL

Stephen W. Webb

Prepared by
Sandia National Laboratories
Albuquerque, New Mexico 87185 and Livermore, California 94550
for the United States Department of Energy
under Contract DE-AC04-94AL85000

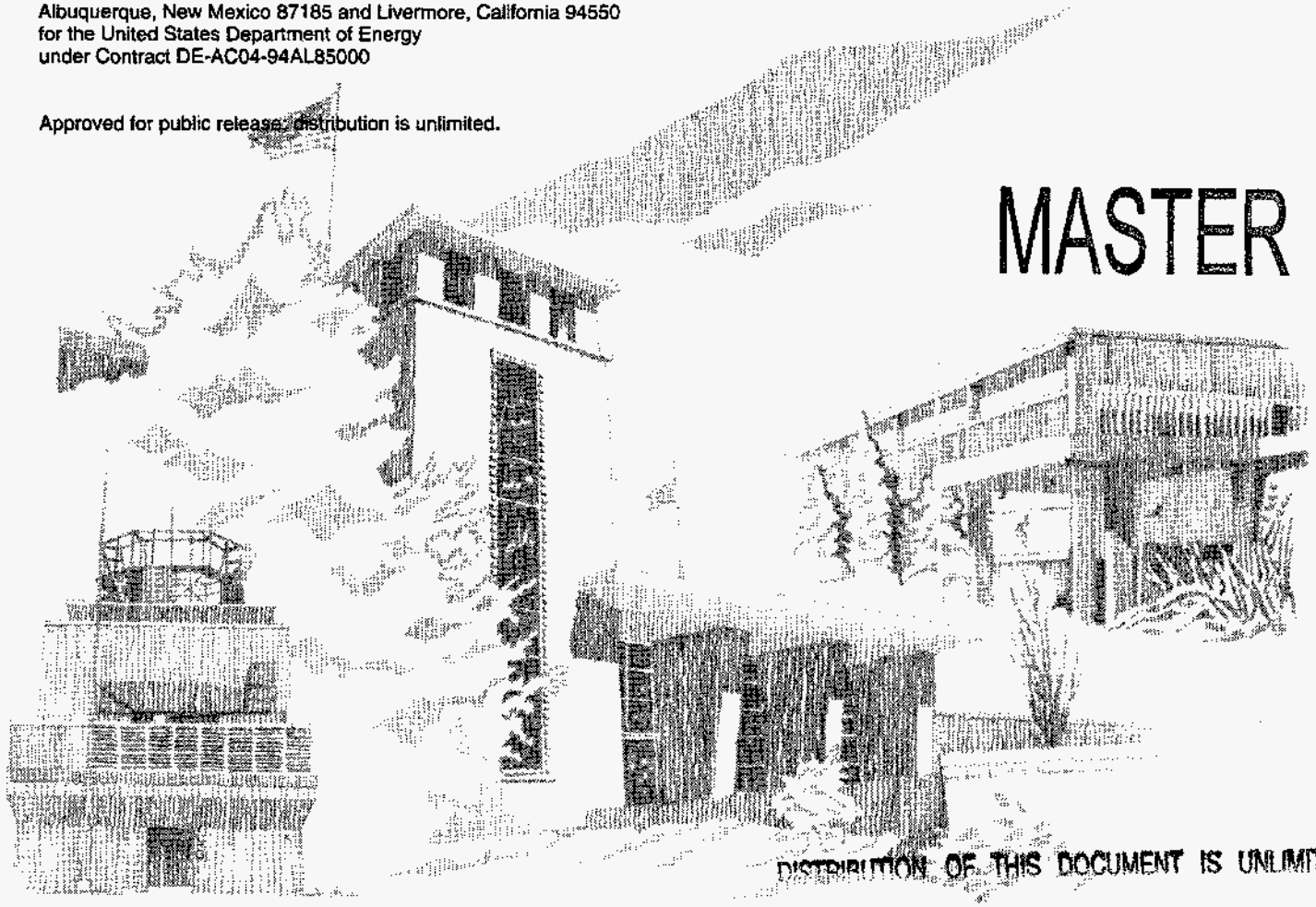

Issued by Sandia National Laboratories, operated for the United States Department of Energy by Sandia Corporation.

Available to DOE and DOE contractors from
Office of Scientific and Technical Information
PO Box 62
Oak Ridge, TN 37831

Prices available from (615) 576-8401, FTS 626-8401

Available to the public from
National Technical Information Service
US Department of Commerce
5285 Port Royal Rd
Springfield, VA 22161

NTIS price codes
Printed copy: A07
Microfiche copy: A01

SAND94-1639
Unlimited Release
Printed May 1996

Distribution
Category UC-2010

TOUGH2 Simulations of the TEVES Project Including the Behavior of a Single-Component NAPL

Stephen W. Webb
Geohydrology Department
Sandia National Laboratories
Albuquerque, NM 87185

ABSTRACT

The TEVES (Thermal Enhanced Vapor Extraction System) Project is a demonstration of a process designed to extract solvents and chemicals contained in the Chemical Waste Landfill at Sandia National Laboratories. In this process, the ground is electrically heated, and borehole(s) within the heated zone are maintained at a vacuum to draw air and evaporated contaminants into the borehole and a subsequent treatment facility. TOUGH2 simulations have been performed to evaluate the fluid flow and heat transfer behavior of the system. The TOUGH2 version used in this study includes air, water, and a single-component non-aqueous phase liquid (NAPL). In the present simulations, an initial o-xylene inventory is assumed in the heated zone for illustration purposes. Variation in borehole (vapor extraction) vacuum, borehole location, and soil permeability were investigated.

Simulations indicate that the temperatures in the soil are relatively insensitive to the magnitude of the borehole vacuum or the borehole locations. In contrast, however, the NAPL and liquid water saturation distributions are sensitive to these borehole parameters. As the borehole vacuum and air flow rate through the soil decrease, the possibility of contaminant (NAPL) migration from the heated zone into the surrounding unheated soil increases. The borehole location can also affect the likelihood of contaminant movement into the unheated soil.

Intentionally Left Blank

Contents

1.0 Introduction 1

2.0 Model Development 3

2.1 TEVES Parameters 3
2.2 TOUGH2 Model 6
2.3 TOUGH2 Simulations 10

3.0 Simulation Results - Inside Extraction 11

3.1 2.5 kPa Borehole Vacuum 11
3.2 1.0 kPa Borehole Vacuum 31
3.3 0.5 kPa Borehole Vacuum 41

4.0 Simulation Results - Outside Extraction 59

4.1 2.5 kPa Borehole Vacuum 59
4.2 1.0 kPa Borehole Vacuum 77

5.0 Simulation Results - Soil Permeability Variation 95

6.0 Discussion 111

6.1 Inside Extraction 111
6.2 Outside Extraction 111
6.3 Soil Permeability Variation 112

7.0 Summary and Conclusions 113

8.0 References 115

Appendix A: Early Simulation Results A-1

Figures

2-1. General TEVES configuration 4
3-1. Inside extraction schematic 12
3-2. Inside extraction nodalization 14

Figures (Continued)

3-3. Heated and unheated zone temperatures, inside extraction; 100 kW - 2.5 kPa (10" water) borehole (BH) vacuum 16
3-4. Temperature contours, top view, inside extraction, 2.5 kPA vacuum 18
3-5. Temperature contours, long-side view, inside extraction, 2.5 kPA vacuum 19
3-6. Temperature contours, short-side view, inside extraction, 2.5 kPA BH vacuum 20
3-7. Heated zone fluid and water mass - inside extraction; 100 kW 2.5 kPa (10" water) BH vacuum 21
3-8. Early-time water and NAPL saturation contours, 2.5 kPA vacuum, top view, inside extraction 22
3-9. Early-time water and NAPL saturation contours, 2.5 kPA vacuum, long-side view, inside extraction 23
3-10. Early-time water and NAPL saturation contours, 2.5 kPA vacuum, short-side view, inside extraction 24
3-11. Late-time water saturation contours, 2.5 kPA vacuum, inside extraction, top view 26
3-12. Late-time water saturation contours, 2.5 kPA vacuum, inside extraction, long-side view 27
3-13. Late-time water saturation contours, 2.5 kPA vacuum, inside extraction, short-side view 28
3-14. Mass rates, inside extraction, 100 kW - 2.5 kPA (10" water) BH vacuum 29
3-15. Gas velocity vectors at 60 days, 2.5 kPa vacuum, inside extraction 30
3-16. Heated and unheated zone temperatures, inside extraction; 100 kW - 1.0 kPA (4" water) BH vacuum 32
3-17. Temperature contours at 60 days, inside extraction, 1.0 kPa BH vacuum 33
3-18. Heated zone fluid masses, inside extraction, 100 kW - 1.0 kPa (4" water) BH vacuum, 0-60 days 34
3-19. Early-time water and NAPL saturation contours, 1.0 kPa vacuum, top view, inside extraction 35
3-20. Early-time water and NAPL saturation contours, long-side view, 1.0 kPa vacuum, inside extraction 36
3-21. Early-time water and NAPL saturation contours, short-side view, 1.0 kPa vacuum, inside extraction 37
3-22. Late-time water saturation contours at 60 days 1.0 kPa vacuum, inside extraction 38
3-23. Mass rates, inside extraction, 100 kW - 1.0 kPa (4" water) BH vacuum 39
3-24. Gas velocity vectors at 60 days - 1.0 kPa vacuum, inside extraction 40
3-25. Heated and unheated zone temperatures, inside extraction; 100 kW - 0.5 kPa (2" water) BH vacuum 42
3-26. Temperature contours at 60 days, inside extraction, 0.5 kPa vacuum 43
3-27. Heated zone fluid masses and O-xylene mass variation, inside extraction, 100 kW, 0.5 kPa (2" water) BH vacuum 44

Figures (Continued)

3-28. Early-time water and NAPL saturation contours, 0.5 kPa vacuum, top view, inside extraction 45
3-29. Early-time water and NAPL saturation contours, 0.5 kPa vacuum, long-side view, inside extraction 47
3-30. Early-time water and NAPL saturation contours, 0.5 kPa vacuum, short-side view, inside extraction 49
3-31. Late-time water saturation contours, 0.5 kPa vacuum, inside extraction, top view . . . 51
3-32. Late-time water saturation contours, 0.5 kPa vacuum, inside extraction, long-side view 52
3-33. Late-time water saturation contours, 0.5 kPa vacuum, inside extraction, short-side view 53
3-34. Mass rates, inside extraction, 100 kW - 0.5 kPa (2" water) BH vacuum 55
3-35. Gas velocity vectors at 60 days, 0.5 kPa vacuum, inside extraction 56
3-36. Details of NAPL migration into unheated zone at 15 days, 0.5 kPa vacuum, inside extraction 57
4-1. Outside extraction schematic 60
4-2. Outside extraction nodalization 62
4-3. Heated and unheated zone temperatures, outside extraction; 100 kW - 2.5 kPa (10" water) BH vacuum 64
4-4. Temperature contours, top view, outside extraction 2.5 kPa vacuum 65
4-5. Temperature contours, long-side view, outside extraction 2.5 kPa vacuum 66
4-6. Temperature contours, short-side view, outside extraction 2.5 kPa vacuum 67
4-7. Heated zone fluid and water masses, outside extraction, 100 kW, 2.5 kPa (10" water) BH vacuum 69
4-8. Early-time water and NAPL saturation contours, 2.5 kPa vacuum, top view, outside extraction 70
4-9. Early-time water and NAPL saturation contours, 2.5 kPa vacuum, long-side view, outside extraction 71
4-10. Early-time water and NAPL saturation contours, 2.5 kPa vacuum, short-side view, outside extraction 72
4-11. Late-time water saturation contours, 2.5 kPa vacuum, outside extraction, top view . . 73
4-12. Late-time water saturation contours, 2.5 kPa vacuum, outside extraction, long-side view 74
4-13. Late-time water saturation contours, 2.5 kPa vacuum, outside extraction, short-side view 75
4-14. Mass ratese, outside extraction, 100 kW, 2.5 kPa (10" water) BH vacuum 76
4-15. Gas velocity vectors at 60 days, 2.5 kPa vacuum, outside extraction 78
4-16. Heated and unheated zone temperatures, outside extraction; 100 kW - 1.0 kPa (4" water) BH vacuum 79
4-17. Temperature contours, at 60 days, outside extraction 1.0 kPa vacuum 80

Figures (Continued)

4-18. Heated zone fluid masses and O-xylene mass variation, outside extraction, 100 kW, 1.0 kPa (4" water) BH vacuum 81
4-19. Early-time water and NAPL saturation contours, 1.0 kPa vacuum, top view, outside extraction 82
4-20. Early-time water and NAPL saturation contours, long-side view, 1.0 kPa vacuum, outside extraction 84
4-21. Early-time water and NAPL saturation contours, short-side view, 1.0 kPa vacuum, outside extraction 86
4-22. Late-time water saturation contours, 1.0 kPa vacuum, outside extraction, top view 88
4-23. Late-time water saturation contours, 1.0 kPa vacuum, outside extraction, long-side view 89
4-24. Late-time water saturation contours, 1.0 kPa vacuum, outside extraction, short-side view 90
4-25. Mass rates, outside extraction, 100 kW - 1.0 kPa (4" water) BH vacuum 92
4-26. Gas velocity vectors at 60 days, 1.0 kPa vacuum, outside extraction 93
4-27. Details of NAPL migration into 94
5-1. Heated and unheated zone temperatures, inside extraction; 100 kW - 2.5 kPa BH vacuum - 10 darcies 96
5-2. Temperature contours at 60 days, inside extraction, 10 darcies 97
5-3. Heated zone fluid masses and O-xylene mass variation, inside extraction, 100 kW, 2.5 kPa BH vacuum, 10 darcies 98
5-4. Early-time water and NAPL saturation contours, 10 darcies, top view, inside extraction 99
5-5. Early-time water and NAPL saturation contours, 10 darcies, long-side view, inside extraction 101
5-6. Early-time water and NAPL saturation contours, 10 darcies, short-side view, inside extraction 103
5-7. Late-time water saturation contours, 10 darcies, inside extraction, top view . . . 105
5-8. Late-time water saturation contours, 10 darcies, inside extraction, long-side view 106
5-9. Late-time water saturation contours, 10 darcies, inside extraction, short-side view 107
5-10. Mass rates, inside extraction, 100 kW, 2.5 kPa BH vacuum, 10 darcies 108
5-11. Gas velocity vectors at 60 days, 10 darcies, inside extraction 109
A-1. Heated and unheated zone temperatures, inside extraction, 100 kW, 0.5 kPa (2" water) BH vacuum A-2
A-2. Temperature contours at 60 days, inside extraction, 0.5 kPa vacuum A-3
A-3. Heated zone fluid masses and O-xylene mass variation, inside extraction, 100 kW, 0.5 kPa (2" water) BH vacuum A-4
A-4. NAPL saturation contours at 8 days, 0.5 kPa vacuum A-5
A-5. Mass rates, inside extraction, 100 kW, 0.5 kPa (2" water) BH vacuum A-6

Tables

2-1 Summary of Model Parameters 5
2-2 Element Dimensions (m) 8

Intentionally Left Blank

TOUGH2 Simulations of the TEVES Project Including the Behavior of a Single-Component NAPL

1.0 Introduction

Contaminant behavior and removal rates from subsurface soils are important in the design of cleanup processes of waste landfills. The TEVES (Thermal Enhanced Vapor Extraction System) Project is a demonstration of a process designed to extract volatile organic chemicals contained in the Chemical Waste Landfill at Sandia National Laboratories. In this process, the ground is electrically heated and borehole(s) within the heated zone are maintained at a vacuum to draw air and contaminants from the ground and into a subsequent treatment facility.

The behavior of the contaminants will be influenced by a number of factors including the soil heating rate and local temperature gradients, the evaporation rate of the liquid water and contaminants, the air flow rate, and the borehole, or vapor extraction, location(s). If the air flow rate is too small, the heating and evaporation processes may drive the contaminant vapors out of the heated zone and into the cooler unheated soil where they may condense, and contaminant migration into previously uncontaminated areas would occur.

In order to address contaminant behavior issues, detailed two-phase calculations have been performed using a single-component non-aqueous phase liquid (NAPL) version of the TOUGH2 computer program (Pruess, 1991). Variations in the borehole vacuum, vapor extraction locations, and soil permeability have been studied to evaluate the effect on system performance. A summary of some of the early simulation results has been given by Phelan and Webb (1994). Differences between the results presented by Phelan and Webb (1994) and those contained herein are discussed in Appendix A of this report.

Intentionally Left Blank

2.0 Model Development

2.1 TEVES Parameters

Figure 2-1 shows the general TEVES process setup. In this process, the ground is electrically heated, and borehole(s) within the heated zone are maintained at a vacuum to draw air and evaporated contaminants into the borehole and a subsequent treatment facility. The ground above the heated zone and beyond is insulated to minimize heat loss to the atmosphere. A vapor barrier is used over an even larger area to provide for a more complete air sweep of the contaminated soil. Details of the heating process, the insulation, and the vapor barrier are discussed by Snow and Bajzek (1993).

The simulated dimensions of the heated zone for the present study are 6.1 m x 15.2 m x 5.6 m deep (20 ft x 50 ft x 18.5 ft deep). Insulation covers the entire top of the heated zone and extends 1.8 m (6 ft) beyond the heated zone in all directions. A vapor barrier extends an additional 0.9 m (3 ft) beyond the insulation. Two different vapor extraction schemes were investigated which are referred to as inside extraction and outside extraction. Vapor extraction can either occur through two vapor extraction wells located near the center of the heated zone (inside extraction), or through four guard electrodes located on the edge of the heated zone (outside extraction). The vapor extraction wells are 10 cm (4 in) in diameter and are assumed to be active only for the heated depth of 5.6 m (18.5 ft). The guard electrodes are 5 cm (2 in) in diameter with an active depth of 8.5 m (28 ft), much deeper than the heated zone.

The nominal borehole vacuum used in the present analysis is 2.5 kPa (10 inches of water). The borehole vacuum is an important parameter, because if the air sweep into the borehole is not sufficient, water vapor and volatile organic compunds (VOCs) generated by the heating process could migrate from the heated zone into the unheated soil resulting in a loss of containment and a larger zone of contamination. As is discussed later, for the assumed soil properties and configurations, this nominal borehole vacuum was sufficient to contain the simulated NAPL within the heated zone in both the inside and outside vapor extraction schemes. Lower borehole vacuums were analyzed for the two vapor extraction schemes to determine the onset of migration of the simulated NAPL into the unheated soil.

Heat is assumed to be uniformly added to the heated zone at the rate of 100 kW for a volumetric heating rate of approximately 190 W/m^3. The insulation is assumed to be 7.6 cm (3 in) thick with a thermal conductivity of 0.0865 W/m-°C (0.05 BTU/hr-ft-°F). The vapor barrier is assumed to be impermeable to flow. For simplicity, the soil properties are assumed to be uniform with a permeability of 50 darcies (Phelan, 1993), a porosity of 0.333 and an initial liquid water saturation of 0.20, which is less than the liquid residual saturation. An initial o-xylene saturation of 0.05 in the heated zone is assumed to simulate an initial NAPL inventory. These and other parameters including some o-xylene properties are summarized in Table 2-1. NAPL is assumed to not be initially present in the unheated zone.

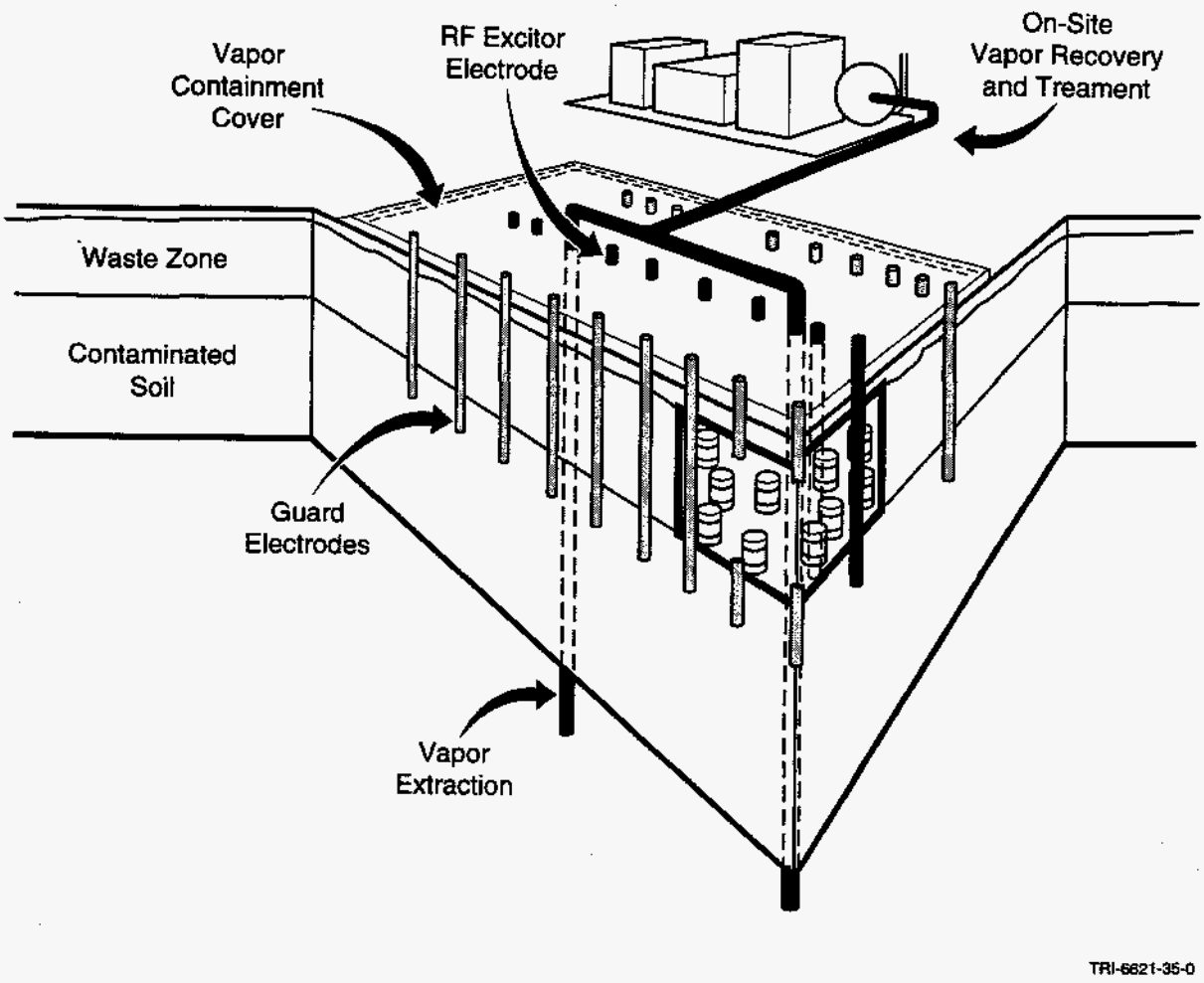

Figure 2-1. General TEVES configuration

Table 2-1
Summary of Model Parameters

Soil Properties	
Grain Density	2650 kg/m^3
Porosity	0.333
Soil Density	1768 kg/m^3
Permeability	50 darcies
Thermal Conductivity	1.5 W/m-°C
Heat Capacity	920. J/kg-°C
Initial Liquid Saturation - water	0.20
Initial Liquid Saturation - NAPL (o-xylene)	0.05
Initial Gas Pressure	83.5 kPa
Initial Temperature	20°C
van Genuchten - Parker two-phase characteristic curves (D.B. Stephens, 1989)	
α	0.00968 cm^{-1}
n	2.0353
$S_{l,r}$ ($S_{l,r}$ for water + 0.05)	0.2845
$S_{l,s}$	1.00
Insulation Properties	
Thickness	7.6 cm (3 inches)
Density	52 kg/m^3
Permeability	0 darcies
Thermal Conductivity	0.0865 W/m-°C
Heat Capacity	700. J/kg-°C
Vapor Barrier Properties (assumed)	
Effective Thickness	0.002 m
Density	1000 kg/m^3
Permeability	0 darcies
Thermal Conductivity	0.1 W/m-°C
Heat Capacity	1000. J/kg-°C
Ambient Conditions	
Pressure	83.5 kPa
Temperature	20°C
Humidity	100%
Heat Transfer Coefficient	20. W/m^2-°C

Table 2-1 (cont)
Summary of Model Parameters

Borehole Conditions		
Pressure (nominal)		81 kPa (2.5 kPa vacuum)
Temperature		20°C
Humidity		100%
o-xylene - Selected Properties (Falta, et al., 1992b)		
Normal Boiling Point		417.6 °K (144.5 °C)
Critical Temperature		630.2 °K
Critical Pressure		37.3 bars
Vapor Pressure Constants*		
a		-7.53357
b		1.40968
c		-3.10985
d		-2.85992
Vapor Pressure	20°C	658 Pa (water = 2337 Pa)
	100°C	26.5 kPa (water = 101.3 kPa)
Liquid Density at 293 °K		880 kg/m^3

* - based on Wagner Equation

$$P_{sat} = P_{crit} \exp\left(\frac{ax + bx^{1.5} + cx^3 + dx^6}{1 - x}\right)$$

where

$$x = 1 - \frac{T}{T_{crit}}$$

2.2 TOUGH2 Model

Simulations of the TEVES Project have been performed using a version of the TOUGH2 computer program (Pruess, 1991). TOUGH2 simulates fluid flow and heat transport in porous and fractured media, including unsaturated conditions. TOUGH2 and its predecessors have been used in a wide variety of applications including geothermal and nuclear waste repository performance evaluation as exemplified by the papers given in Pruess (1990). In addition, model comparisons to a number of analytical solutions and experimental data for single and

two-phase fluid flow and heat transfer in porous media have been reported by Moridis and Pruess (1992) with favorable results.

The original TOUGH2 program evaluates fluid flow and heat transport for water and air fluids. Recent modifications to the code include the capability to simulate a single-component NAPL in addition to the water and air components already present (Finsterle and Pruess, 1993), and the addition of a conjugate gradient solver package to improve the numerical performance (Moridis and Pruess, 1993). Test versions of these modifications were provided to the author for testing and evaluation. The assistance and cooperation of Lawrence Berkeley Laboratory in providing these versions is gratefully acknowledged.

The single-component NAPL capability in TOUGH2 is based on the work of Falta et al. (1992a, 1992b) and the STMVOC computer program (Falta and Pruess, 1991). STMVOC is a modification of TOUGH (Pruess, 1987), the predecessor to TOUGH2. The formulation is restricted in that the gas and aqueous phases can never totally disappear; this effect is noted in the present results. This restriction does not apply to the NAPL phase which may or may not be present. The current study uses the single-component NAPL version of TOUGH2 with the conjugate gradient solver. More recently, further improvements have been made in the NAPL simulation capability to include multicomponent capability in the M^2NOTS code (Adenekan et al., 1993), which is based on the TOUGH2 code. The multi-component NAPL formulation is planned to be used in future analyses to address multi-component issues.

Three-dimensional models of TEVES have been used to determine the system performance for variations in borehole vacuum pressure, borehole locations, and soil permeability. Temperature, water and NAPL saturation profiles, and gas velocity vectors are presented and compared for different conditions. Separate TOUGH2 models were employed for vapor extraction through the vapor extraction wells (inside extraction) and through the guard electrodes (outside extraction). In both cases, quarter symmetry was employed to simplify the model. The borehole vacuum is assumed to be constant. The ambient pressure used in these calculations is 83.5 kPa (12.1 psia) based on local (Albuquerque) conditions.

The x, y, and z dimensions of both models (inside and outside extraction) are listed in Table 2-2; over 2200 elements were used in each case. In both cases, the models cover a surface equivalent to 36.6 m x 45.7 m (120 ft by 150 ft). For the case of inside extraction, the model depth is 19.1 m (62.5 ft). Because the wells used for outside extraction are deeper, the depth of this model is greater and is 22.9 m (75 ft).

Table 2-2
Element Dimensions (m)

Inside Venting Model

X-dimension (11 total)

0.610, 0.610, 0.914, 0.914 (heating ends), 0.914, 0.914 (insulation ends), 0.914 (vapor barrier ends), 1.524, 2.438, 3.658, 4.877

Y-dimension (16 total)

0.914, 0.914, 0.610, 0.610, 0.610, 0.610, 0.914, 1.219, 1.219 (heating ends), 0.914, 0.914 (insulation ends), 0.914 (vapor barrier ends), 1.524, 2.438, 3.658, 4.877

Z-dimension (13 total)

ambient air, insulation and vapor barrier, 0.610, 0.914, 1.219, 1.219, 0.914, 0.762 (heating and venting ends), 0.914, 1.524, 2.438, 3.658, 4.877

Outside Venting Model

X-dimension (10 total)

1.219, 0.914, 0.914 (heating ends), 0.914, 0.914 (insulation ends), 0.914 (vapor barrier ends), 1.524, 2.438, 3.658, 4.877

Y-dimension (15 total)

1.219, 1.067, 0.914, 0.914, 0.914, 0.914, 0.914, 0.762 (heating ends), 0.914, 0.914 (insulation ends), 0.914 (vapor barrier ends), 1.524, 2.438, 3.658, 4.877

Z-dimension (16 total)

ambient air, insulation and vapor barrier, 0.610, 0.914, 1.219, 1.219, 0.914, 0.762 (heating ends), 0.762, 1.067, 1.067 (venting ends), 1.067, 1.676, 2.438, 3.658, 5.486

The boundary conditions at the sides and bottom of the model are specified as no flow; therefore, all the air that is drawn into the borehole comes through the top of the model. Gas velocity vector plots shown later indicate that the model boundaries are sufficient. These side and bottom boundaries are also insulated such that no heat can be transferred out the sides or the bottom; temperature contours shown later also indicate that the model domain is adequate.

The top boundary is connected to the atmosphere, which serves as the source of the air drawn into the borehole through the soil. The atmosphere is modeled as vapor-saturated air at constant conditions of 83.5 kPa and 20°C. No flow through the top boundary is specified for the vapor blanket and insulation areas. Heat transfer between the soil and the atmosphere is allowed considering an effective heat transfer coefficient of 20 W/m^2-°C as mitigated by the insulation and vapor blanket where appropriate.

The soil is assumed to be initially at ambient conditions of 83.5 kPa and 20°C, and the heating and the venting occur simultaneously. As time proceeds, the soil heats up, and liquid water and NAPL are vaporized and generally transported toward the borehole due to the air sweep. At 60 days, heating is stopped but venting continues. The soil in the heated zone cools down due to heat losses to the unheated soil and to the atmosphere.

The Parker et al. three-phase characteristic curves (Parker et al., 1987) have been used in the model based on actual soil measurements (D.B. Stephens, 1989), although with an initial water saturation of 0.20 and an assumed initial o-xylene saturation of 0.05, both liquid phases are initially immobile since the liquid residual saturation is 0.2845. In the present model, liquid transport only occurs due to evaporation and condensation phenomena, not due to transport of the liquid phase unless evaporation and condensation processes increase the local saturation sufficiently to mobilize the liquid. Diffusion was not included in these calculations.

The borehole consists of a series of elements connected to the appropriate soil elements. Flow resistances from the surrounding soil elements to the borehole elements were modified to reflect the borehole geometry. The borehole is specified as a constant pressure and temperature boundary condition. Initial simulations, such as those given by Phelan and Webb (1994) as discussed in Appendix A, specified heat transfer between the borehole and the soil. Upon examination of the results, the heat loss to the borehole was not realistic and affected the results. Therefore, the simulations were redone with an insulated boundary condition at the borehole, thereby eliminating the heat loss from the soil to the borehole. The resulting temperature and saturation profiles look more reasonable as discussed in Appendix A. The insulated boundary condition for the borehole was used for all the simulations presented in the main report.

2.3 TOUGH2 Simulations

Inside and outside extraction results for various borehole vacuums are presented in Sections 3.0 and 4.0, respectively. The borehole vacuum was decreased from the nominal value of 2.5 kPa until NAPL migration into the unheated soil surrounding the heated zone occurred. Even in these cases, the NAPL migration percentage was small compared to the total inventory, and the NAPL quickly re-evaporated and was transported to the vapor extraction location as time went on. Nevertheless, migration into the unheated zone represents a loss of containment of the NAPL within the heated zone. Values of the borehole vacuum investigated are 2.5, 1.0, and 0.5 kPa for inside extraction, and 2.5 and 1.0 kPa for outside extraction.

In addition to the extraction location and borehole vacuum variations, the permeability of the soil was varied for inside extraction. For the nominal borehole vacuum of 2.5 kPa, the soil permeability was reduced by a factor of 5 from 50 darcies to 10 darcies. Based on Darcy's law, the gas velocity is a function of the product of the intrinsic permeability and the imposed pressure difference. Therefore, the case with a reduction in soil permeability by a factor of 5, should be similar to a reduction in the borehole vacuum by a factor of 5, or 0.5 kPa. These results will be compared to evaluate the potential for scaling and are shown in Section 5.0.

3.0 Simulation Results - Inside Extraction

The results in this section are for vapor extraction from the 2 inside wells, or inside extraction. Figure 3-1 gives a schematic of the model. Symmetry planes are noted in Figure 3-1a for the top view. Figures 3-1b and c give the side views for the model looking at the long and short side of the heated zone, respectively. Due to the symmetry, 1/4 of the domain is modeled including 1/2 of a well. The results presented in this section have been scaled to reflect the entire heated zone. Therefore, when masses or flow rates are given, they refer to the entire heated zone or to the 2 wells, not to the results from the quarter symmetry model.

Figure 3-2 shows the nodalization relative to the various features of the model. This figure shows the size and location of the elements. As discussed earlier, no flow boundary conditions are specified on the sides and bottom of the model. The top boundary condition is ambient air at constant conditions, while the borehole boundary is also constant conditions at the desired borehole vacuum. Plots are given in this report for parameters at the center of each element. The planes are labelled for reference to the plots. The K=1 plane is the insulation and the vapor barrier and is not included in the figures.

3.1 2.5 kPa Borehole Vacuum

The 2.5 kPa borehole vacuum case was simulated for a total time period of 180 days. Venting occurs during the entire time period due to the imposed borehole vacuum. The heated zone soil is heated for the first 60 days of the simulation. During the time period 60 to 180 days, the heated zone cools down due to heat losses to the unheated soil, to the atmosphere, to the air flowing through the soil, and to the evaporation of water and NAPL in the soil.

The time variation of the soil temperature in the heated zone (average, minimum, and maximum) out to 180 days is shown in Figure 3-3a, while the maximum soil temperature in the unheated zone is given in Figure 3-3b. The temperature in the heated zone increases over the first 10 days and then begins to level out as the liquid water evaporates. The temperature then starts to increase again at about 18 days. After 60 days, the average heated zone temperature is about 246°C; at this time, the minimum and maximum heated zone temperatures are 122 and 361 °C, respectively. The wide variation in temperatures is due to heat conduction to the unheated soil and to the overlying atmosphere, cooling by the air flowing through the soil, and evaporation. After the heating is stopped, the temperatures rapidly decrease, and the average heated zone temperature is 41°C at 180 days; the temperature range is 26 to 55°C. For the unheated zone, the maximum soil temperature is 138°C at 60 days and continues to increase even when the heating is stopped, reaching a maximum of 143°C at 64 days. At 180 days, the maximum unheated zone soil temperature is 46°C.

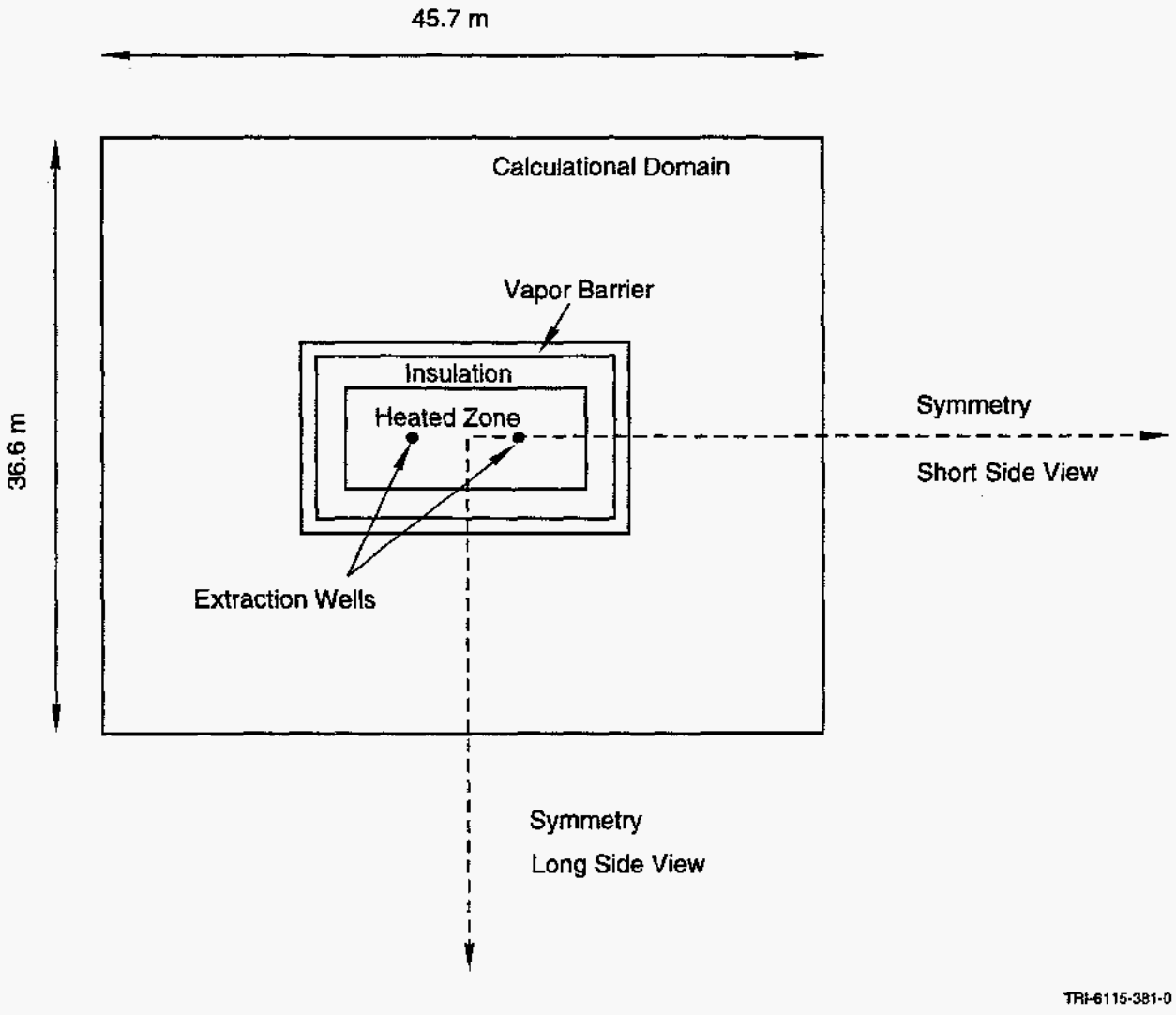

(a) Top view

Figure 3-1. Inside extraction schematic

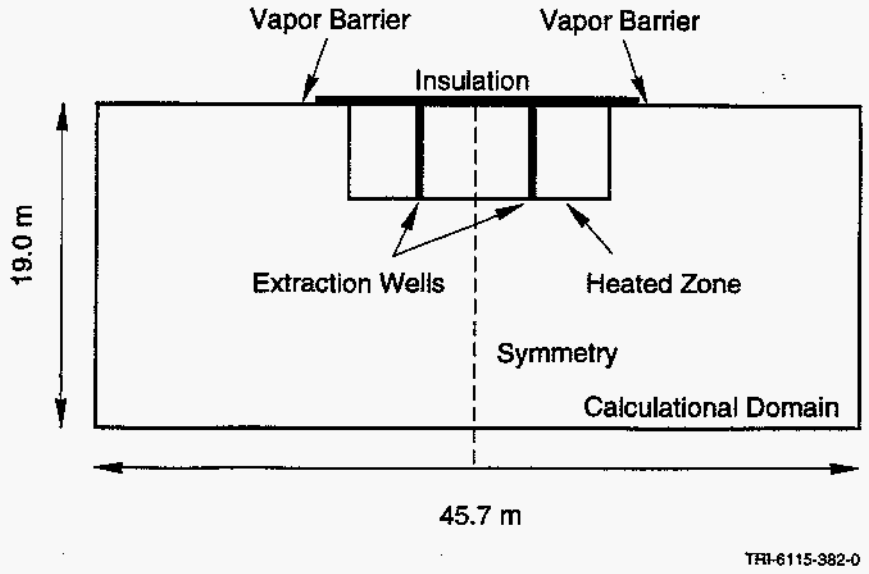

(b) Long-side view

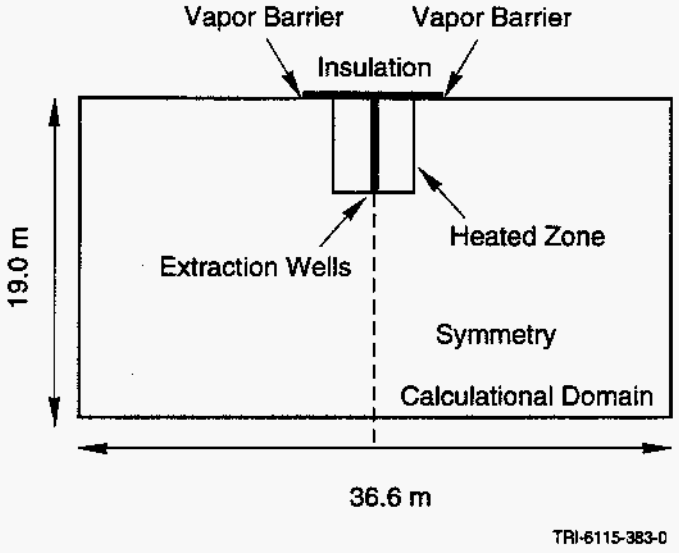

(c) Short-side view.

Figure 3-1. Inside extraction schematic, continued.

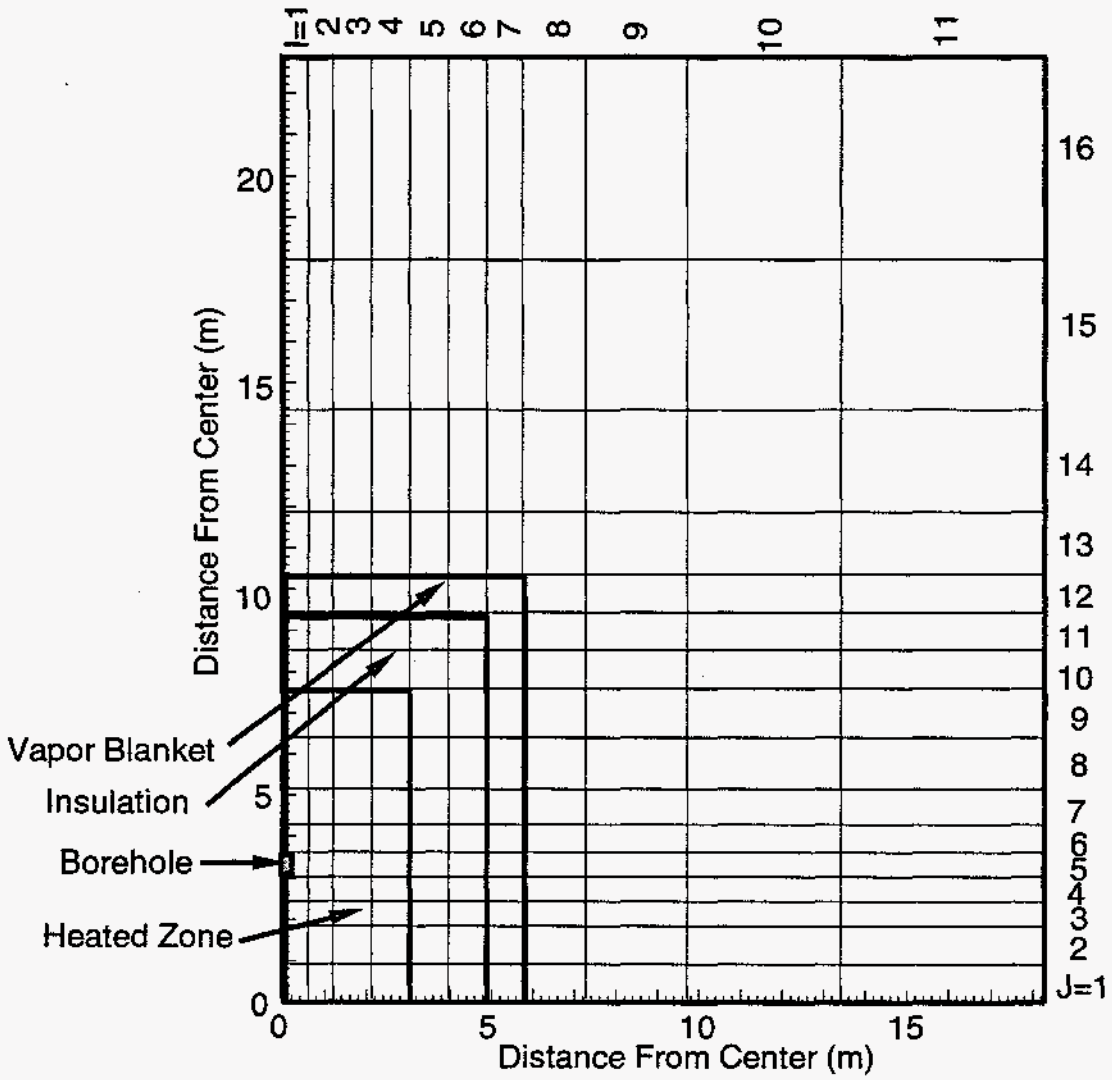

(a) Top view

Figure 3-2. Inside extraction nodalization

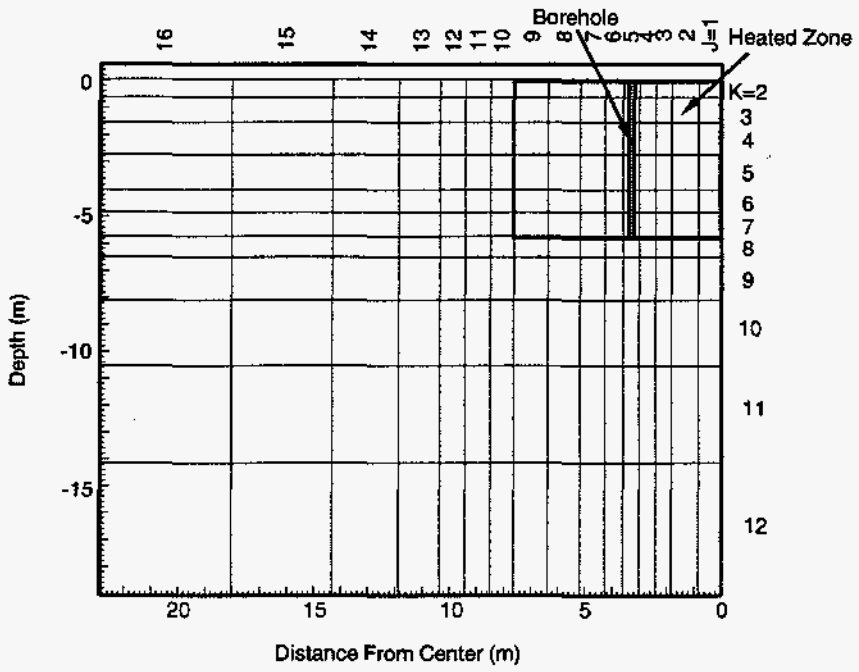

(b) Long-side view

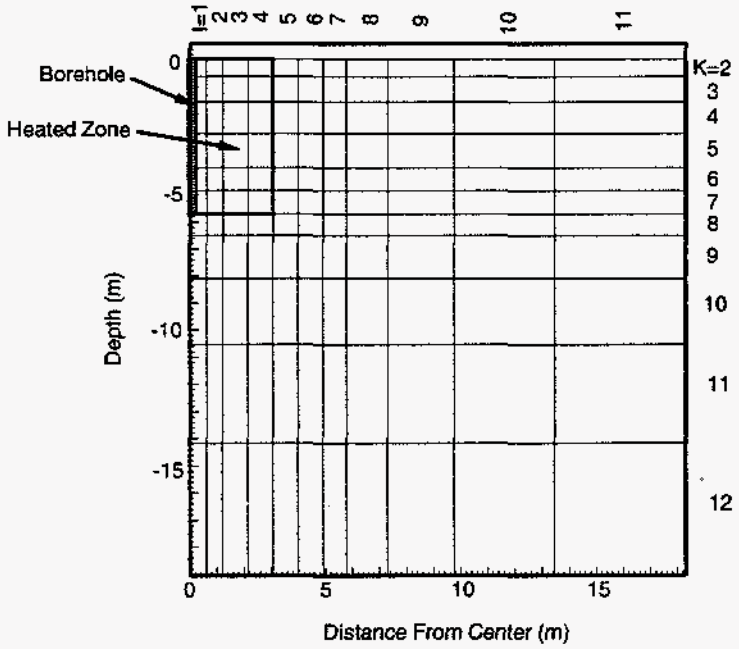

(c) Short-side view

Figure 3-2. Inside extraction nodalization, continued

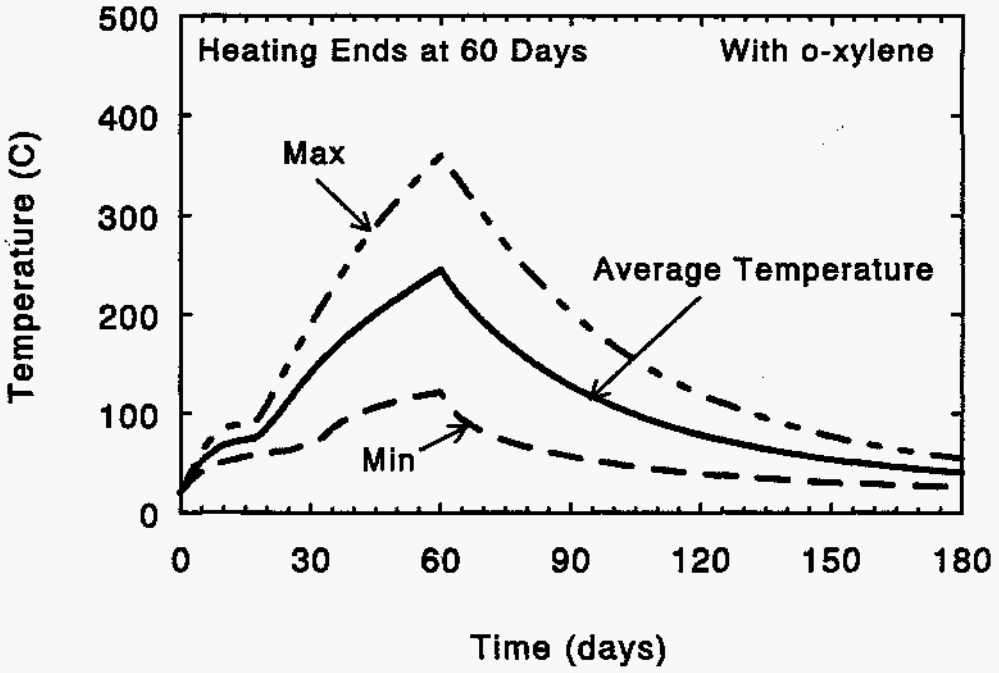

(a) Heated zone temperatures

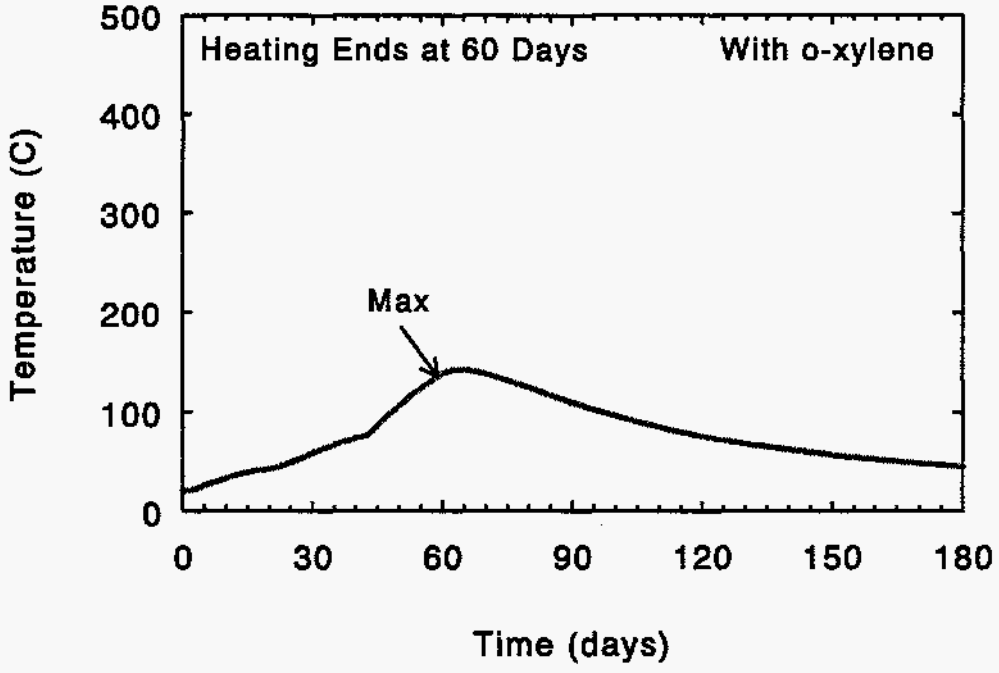

(b) Maximum unheated zone temperatures

Figure 3-3. Heated and unheated zone temperatures, inside extraction; 100 kW - 2.5 kPa (10" water) borehole (BH) vacuum

Figures 3-4 through 3-6 show temperature contours at 30, 60, 90, and 180 days looking from the top and sides of the model. Figure 3-4 gives the top view, while the long-side and short-side views are shown in Figures 3-5 and 3-6, respectively. Only one slice or plane is shown for each direction which is indicated on the figures. For the exact location of the planes, refer to Figure 3-2. For the top view, the layer is just above the center of the heated zone. For the long and short side views, the plane is that nearest the planes of symmetry. The temperatures generally increase outward from the center of the heated zone. The temperature contour levels are consistent for all the plots. Heating of the soil not only increases the soil temperature in the heated zone but increases the temperature in the unheated soil as well.

Figure 3-7a gives the time variation of the water and NAPL liquid masses in the heated zone for the first 60 days. The liquid water in the heated zone decreases from an initial mass of 35,000 kg to less than 700 kg in 60 days. This decrease to a non-zero value is due to an assumption in the VOC version of TOUGH2 that the aqueous phase may not completely disappear as discussed above and does not reflect water that would be expected to remain in the actual situation. Figure 3-7a also shows the o-xylene liquid mass variation, which decreases from an initial mass of 8000 kg. The NAPL is completely gone in less than 9 days. In the present case, there is no migration of o-xylene from the heated zone to the unheated soil; all the o-xylene is evaporated and transported to the vapor extraction wells. Figure 3-7b shows the variation in the heated zone water mass for the entire 180 day transient. When the soil is heated, water evaporates, and the liquid mass in the heated zone decreases. After heating is discontinued, the water mass in the heated zone increases slightly due to condensation of some of the water vapor as the soil cools down.

Early-time liquid water and NAPL saturation contours are given in Figures 3-8 to 3-10. Plots at 1.2 days (10^5 seconds) and 4.5 days are given. As shown in Figure 3-7a, the NAPL (o-xylene) mass is essentially gone at 7 days. The 4.5 day time corresponds to about half of the NAPL remaining. At 1.2 days, the liquid water saturation is essentially uniform; the contours indicated on the figures are only due to small numerical differences of 0.001 in liquid saturation between the indicated regions. The NAPL contours are also uniform; the discrete contours at the boundaries of the heated zone are primarily due to interpolation since NAPL is only initially present in the heated zone. At 4.5 days, the liquid water and NAPL saturations generally decrease from the edge of the heated zone towards the borehole as expected. A lower flow, or "dead", zone exists at the center of the model where the symmetry planes intersect as will be noted in the gas velocity vectors shown later in this section. Figure 3-8d shows the effect of asymmetric flow due to the vapor blanket. As shown later in Figure 3-15a, the gas flow rate is higher from the right edge of the heated zone than from the top edge as seen from the top view. Thus, the NAPL concentration is preferentially lowered where the gas velocity is the highest, and the concentration contours are not symmetrical. The water saturation contours probably do not show the same behavior since the air entering the soil is initially vapor saturated and liquid water is present in all the soil, not just in the heated zone.

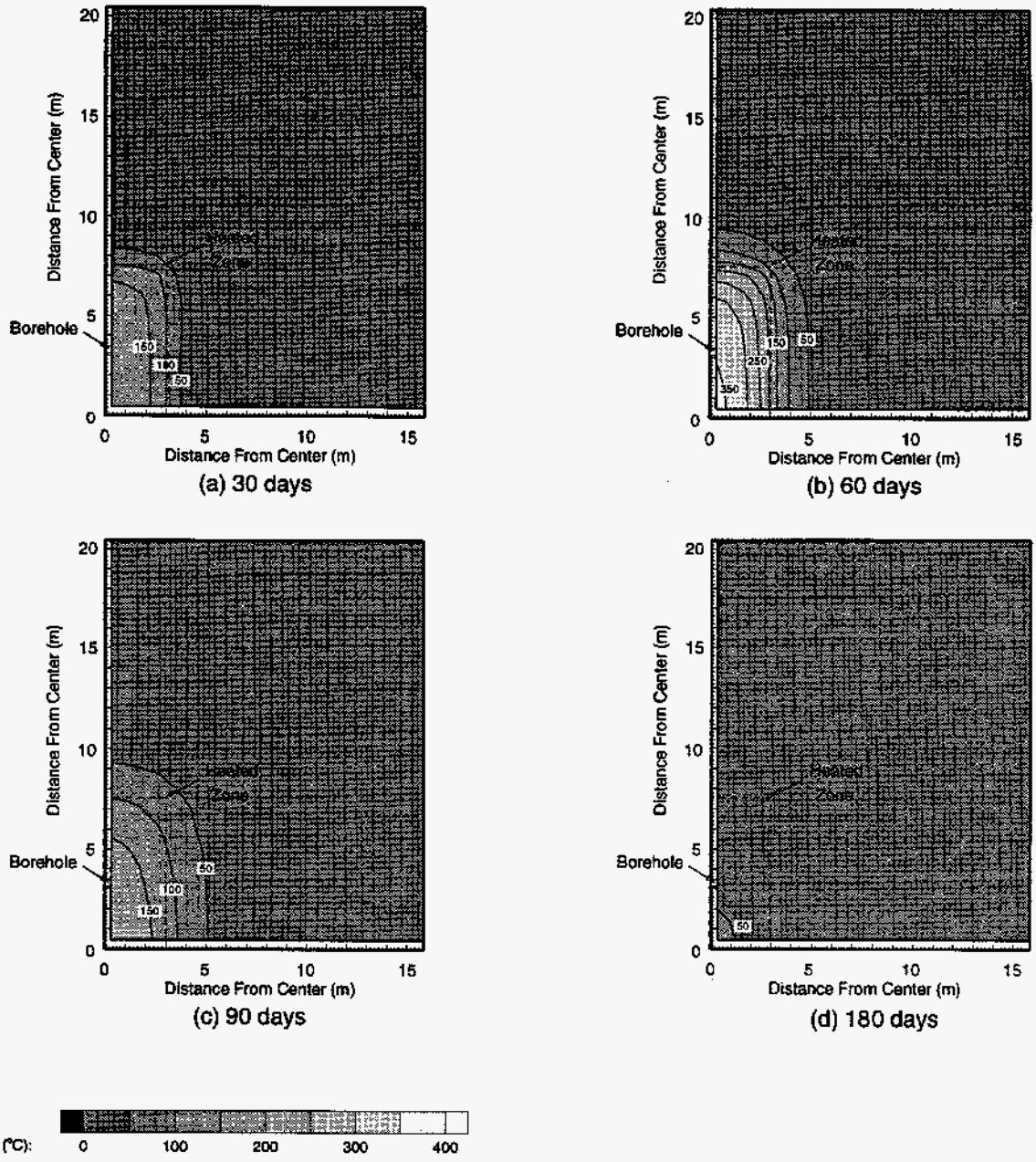

Figure 3-4. Temperature contours, top view, inside extraction, 2.5 kPA vacuum, K=4 plane

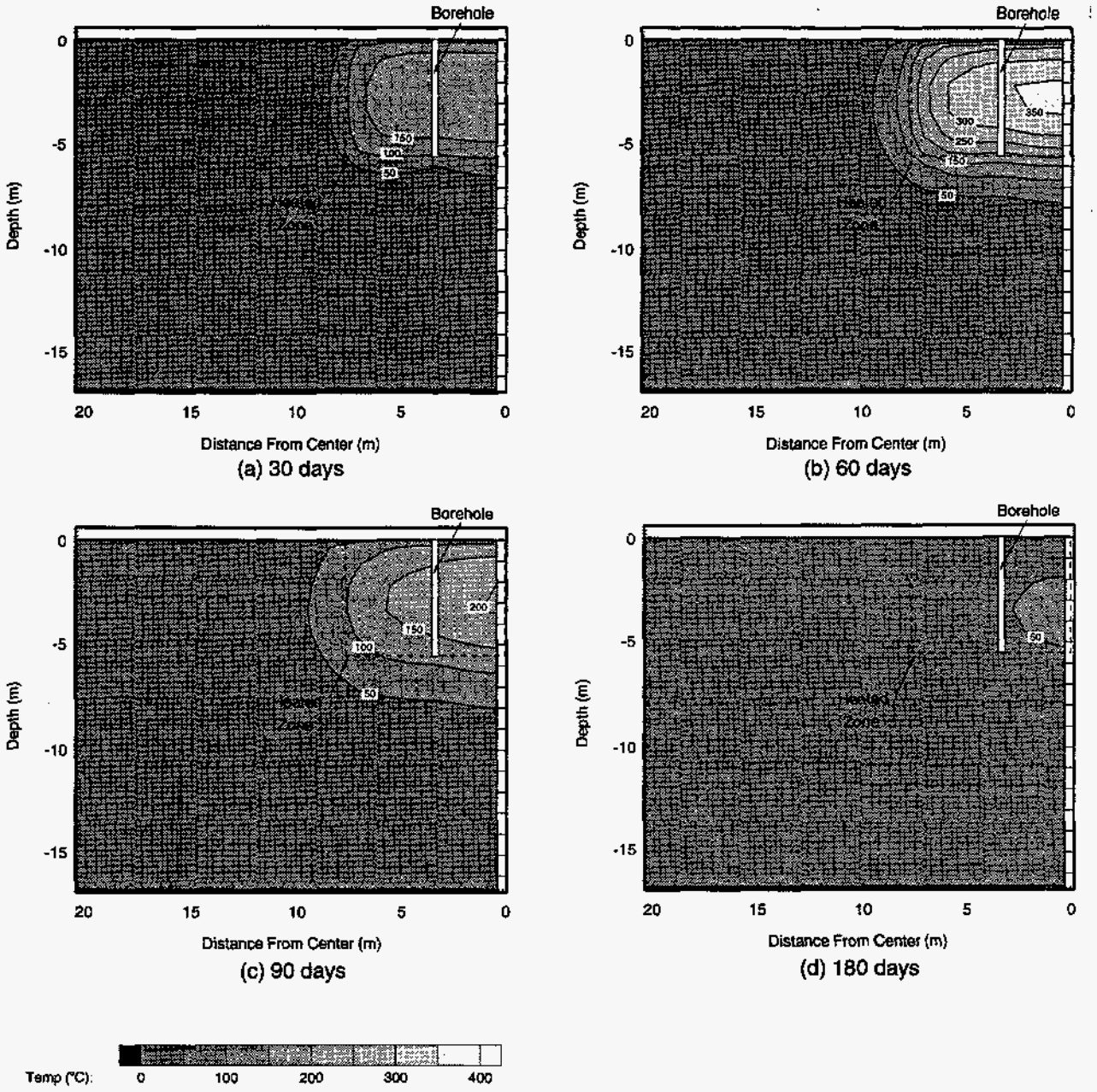

Figure 3-5. Temperature contours, long-side view, inside extraction, 2.5 kPA vacuum, I=1 plane

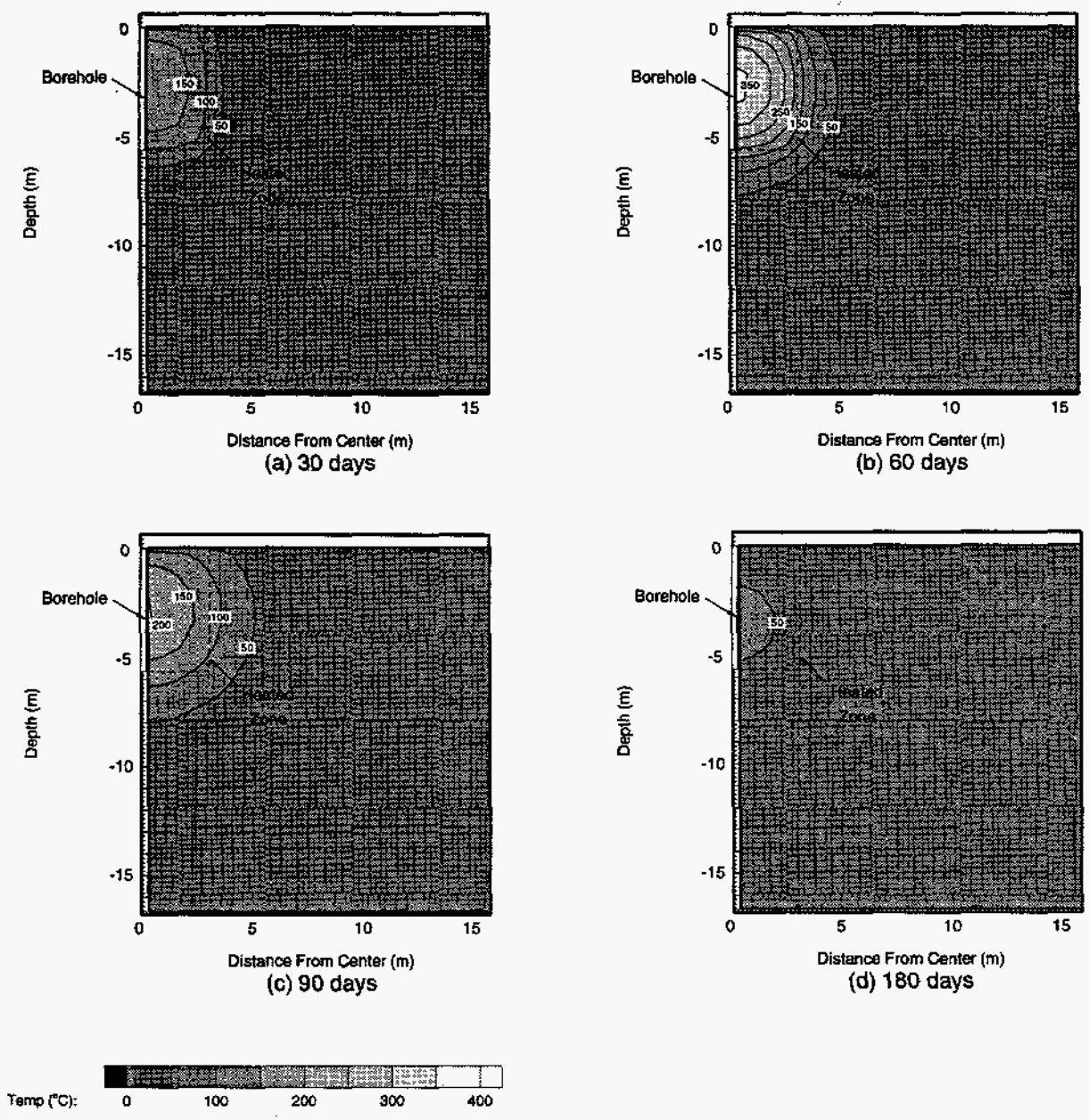

Figure 3-6. Temperature contours, short-side view, inside extraction, 2.5 kPA BH vacuum, J=1 plane

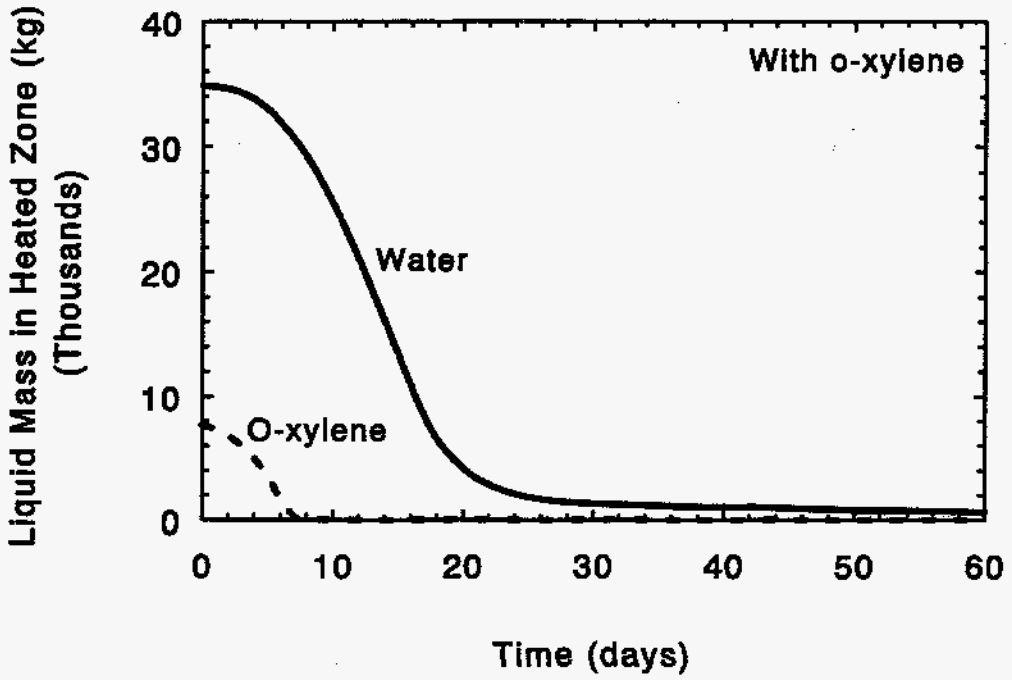

(a) Heated zone fluid masses - 0 to 60 days

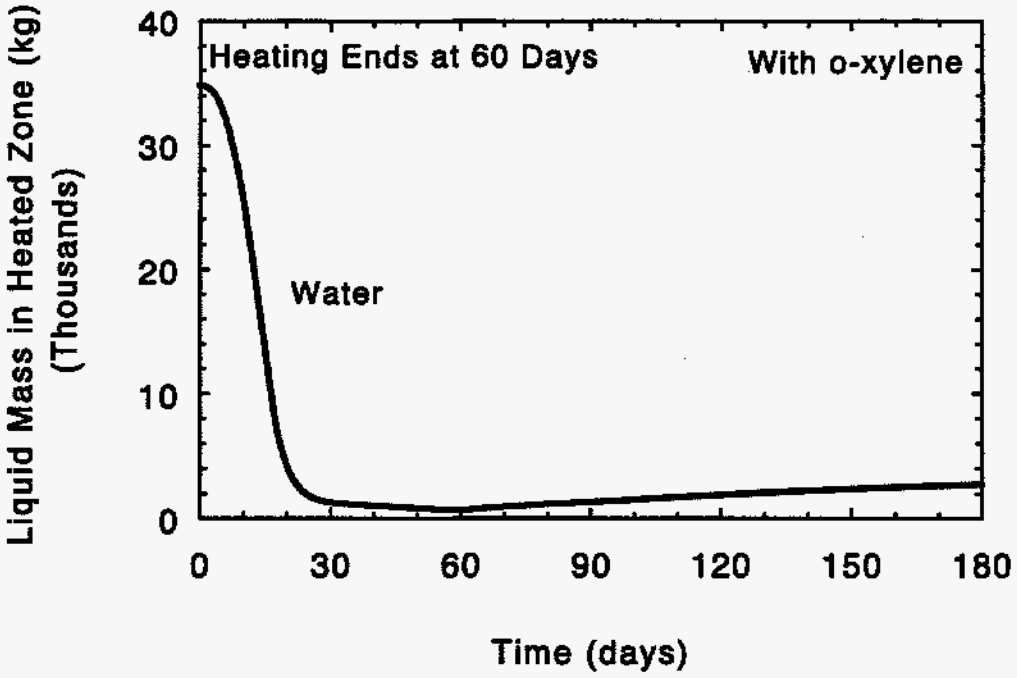

(b) Heated zone water mass - 0 to 180 days

Figure 3-7. Heated zone fluid and water mass - inside extraction; 100 kW 2.5 kPa (10" water) BH vacuum

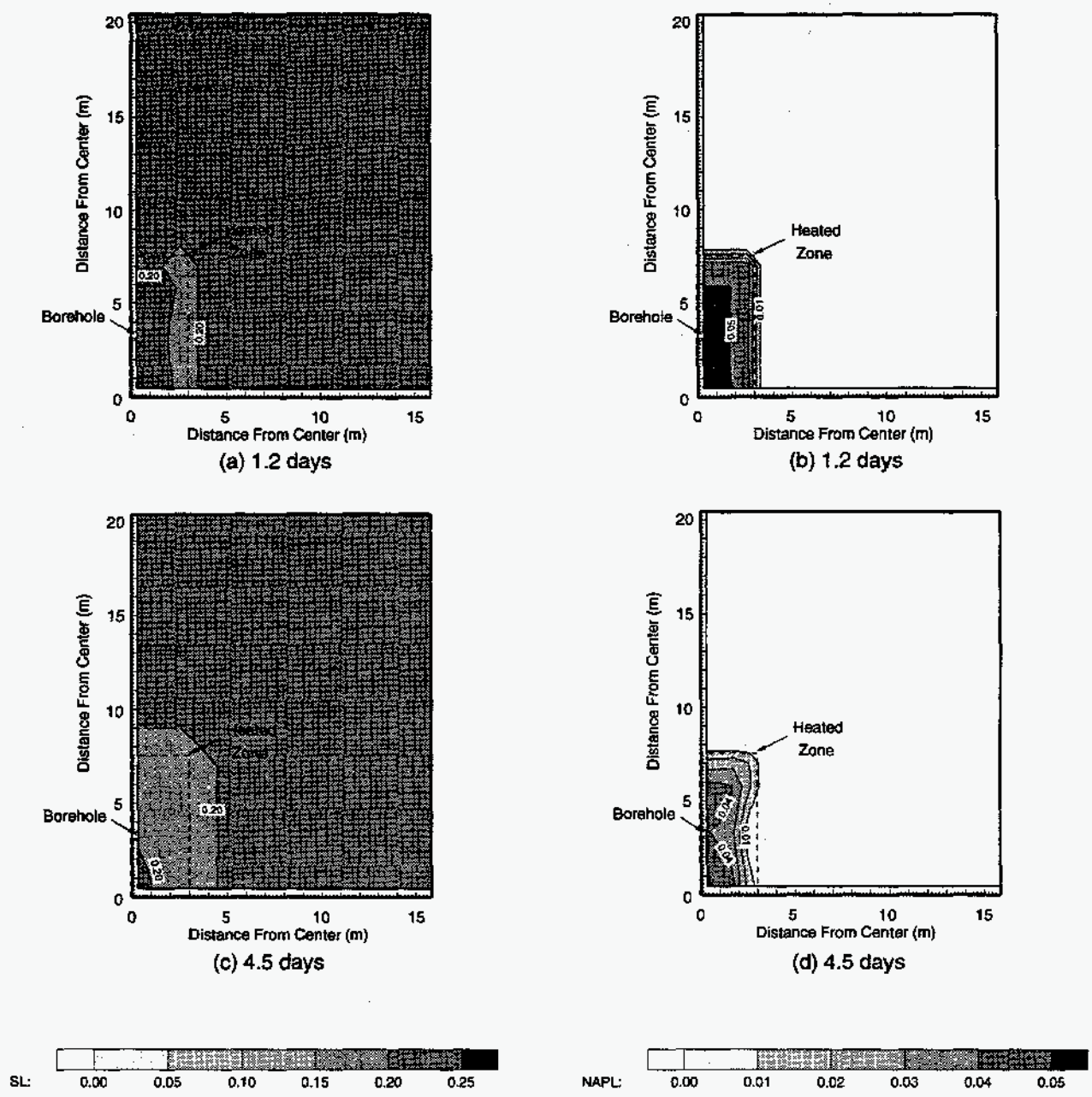

Figure 3-8. Early-time water (left diagram) and NAPL (right diagram) saturation contours, 2.5 PA vacuum, top view, inside extraction, K=4 plane

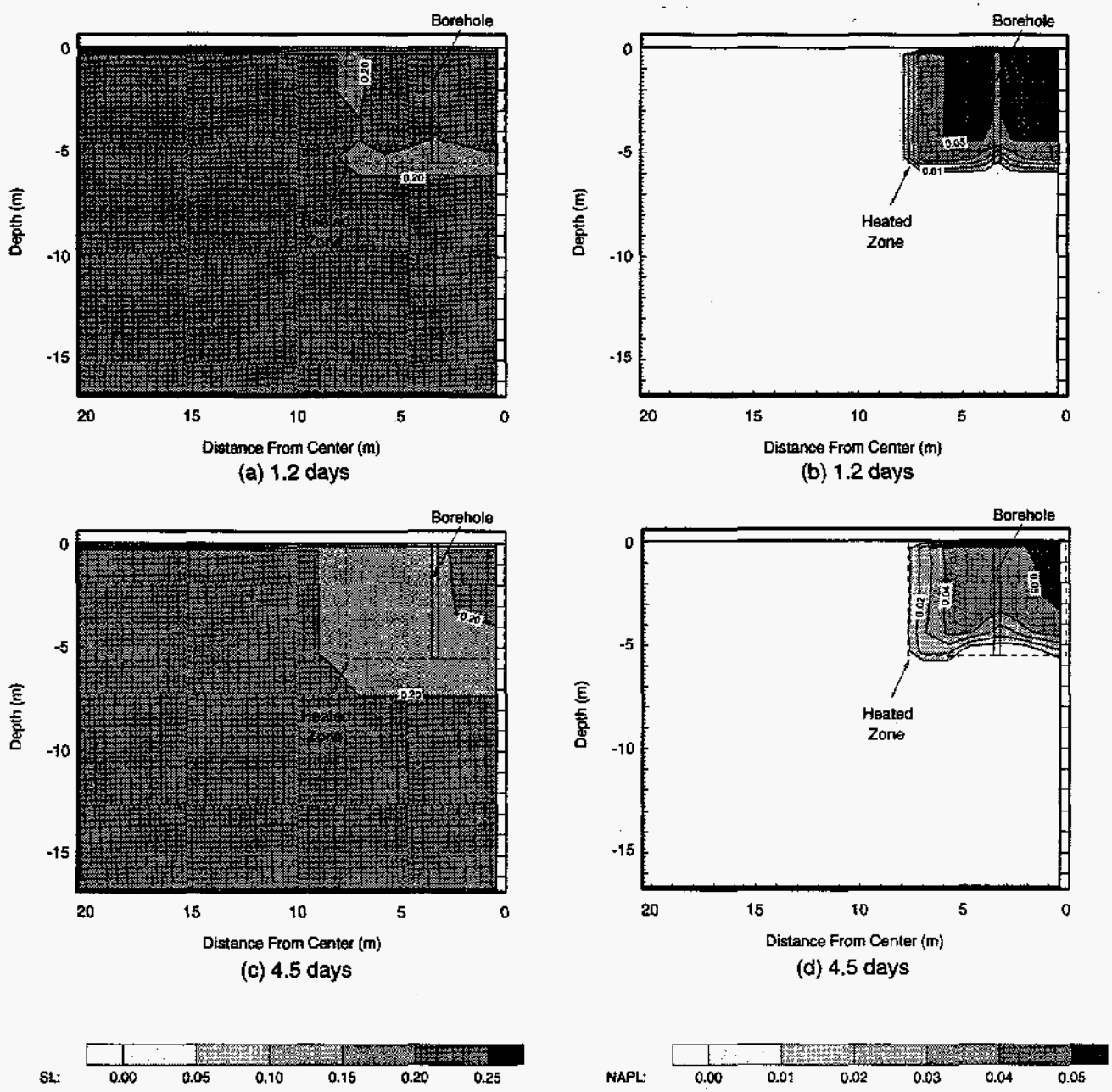

Figure 3-9. Early-time water (left diagram) and NAPL (right diagram) saturation contours, 2.5 kPA vacuum, long-side view, inside extraction, I=1 plane

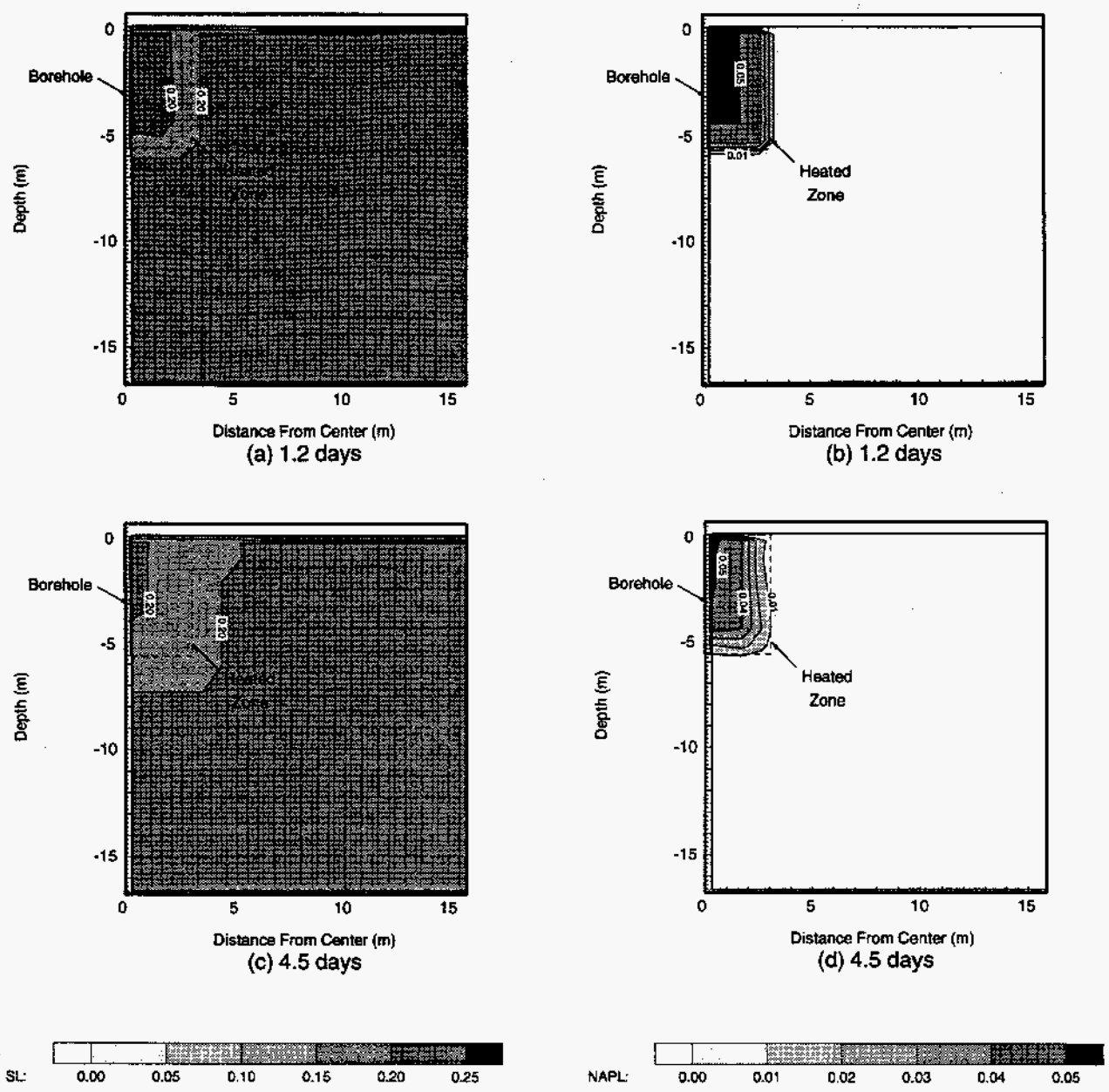

Figure 3-10. Early-time water (left diagram) and NAPL (right diagram) saturation contours, 2.5 kPA vacuum, short-side view, inside extraction, J=1 plane

Liquid water saturation contours for the same views and times as the temperature contours are shown in Figures 3-11 to 3-13 for water; no NAPL is left at any of these times as shown in Figure 3-7a. As in the temperature contours, the zone of influence for liquid water saturation is much larger than just the heated zone. After heating is stopped, the liquid saturation in the heated zone increases slightly due to condensation as shown earlier in Figure 3-7b, although the contour plots do not show it. The liquid saturation in the unheated zone, however, continues to decrease due to evaporation into the air flowing to the borehole. Therefore, the liquid water saturation zone of influence increases with time even without heating.

Water continues to evaporate partially due to the increase in the air temperature towards the borehole and due to the gas pressure drop. As the air temperature increases, the vapor pressure will also increase. In addition, due to the pressure drop in the soil, the air pressure decreases in the soil. Even if the temperature were constant, this decrease in air pressure would increase the vapor mole (and mass) fraction in the gas phase as it flows toward the borehole.

Figure 3-14a shows the various mass flow rates into the borehole. The total mass flow rate into the borehole increases in the early stages of heating primarily due to the evaporation of the NAPL (VOC) component in the heated soil. For the duration of the simulation, the borehole mass flow rate is predominantly air. After heating is stopped, the air flow rate into the borehole increases as the soil and air temperatures decrease. This increase in flow rate is due to an increase in air density and a decrease in air viscosity resulting in a higher mass flow rate for the same pressure drop. Figure 3-14b shows the average evaporation rate in the heated and unheated zones along with the vapor flow rate into the borehole. Early in the transient, the heated zone evaporation rate dominates, while the unheated zone evaporation is the major source of vapor later in the transient. The vapor flow rate into the borehole is essentially the same as the heated zone evaporation rate in the early stages. During the later stages, the vapor flow rate is greater than the heated zone evaporation rate. The heated zone evaporation rate is negative after heating is stopped since condensation is occurring. The unheated zone evaporation rate is always positive, indicating no migration of water from the heated soil into the unheated zone. The vapor flow rate into the borehole is always slightly greater than the sum of the evaporation rates due to vapor in the ambient air.

Gas flow velocity vectors are given in Figure 3-15. The gas flow pattern does not vary significantly during the transient; only the magnitude changes as indicated by Figure 3-14. Therefore, only the gas velocity vectors at 60 days are given in Figure 3-15. For velocities, the side view vertical plane is approximately in the middle of the heated zone, not near the plane of symmetry as in the temperature and saturation figures. The effect of the vapor blanket on the flow velocities is obvious, as flow from the atmosphere into the soil only occurs outside the vapor blanket zone. In both side views, gas flow is vertically upward in the entire heated zone and extends well below the borehole. The top view indicates gas velocities directed toward the borehole. The lower flow rate under the insulation near the symmetry planes can be seen clearly.

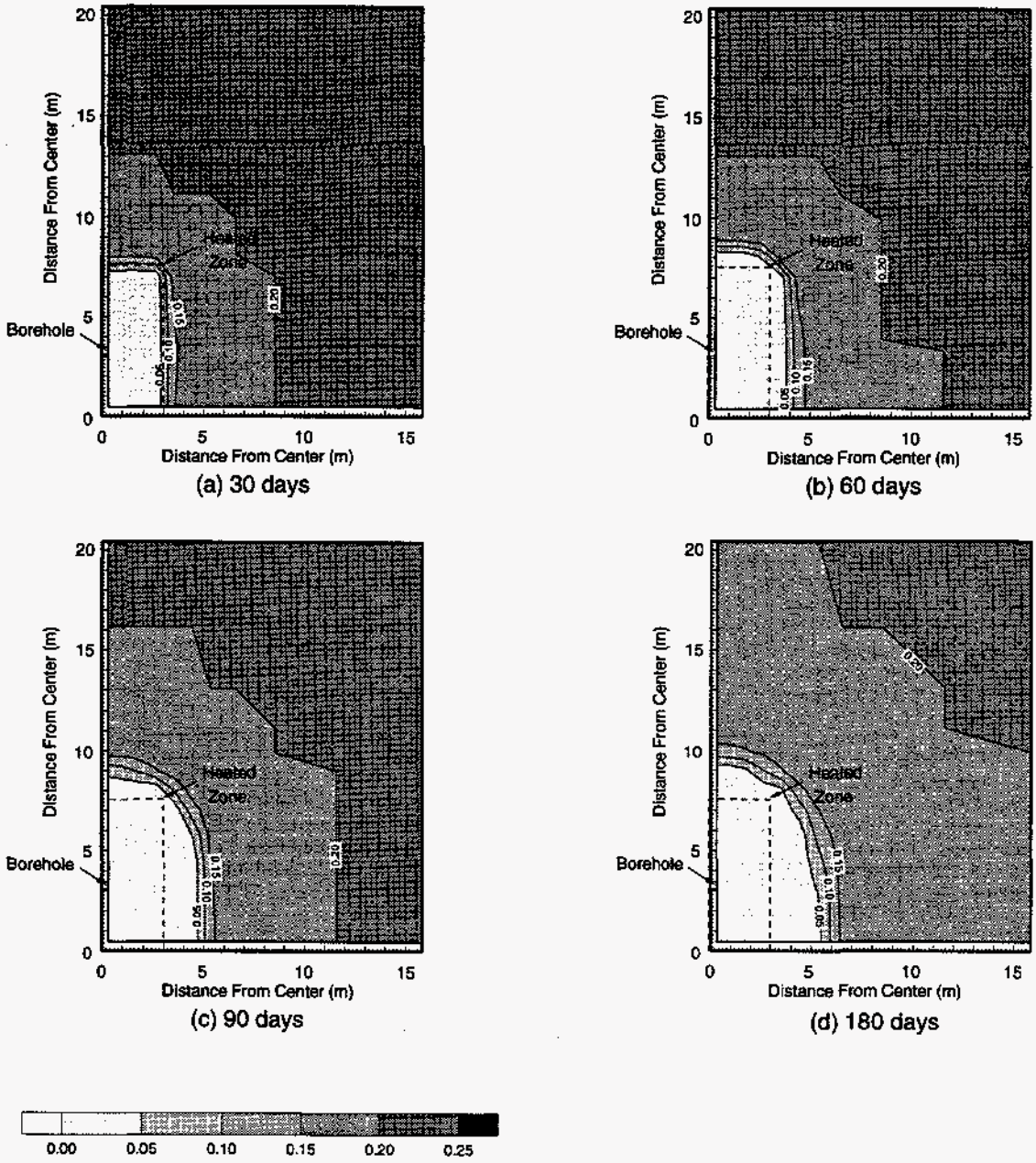

Figure 3-11. Late-time water saturation contours, 2.5 kPA vacuum, inside extraction, top view, K=4 plane

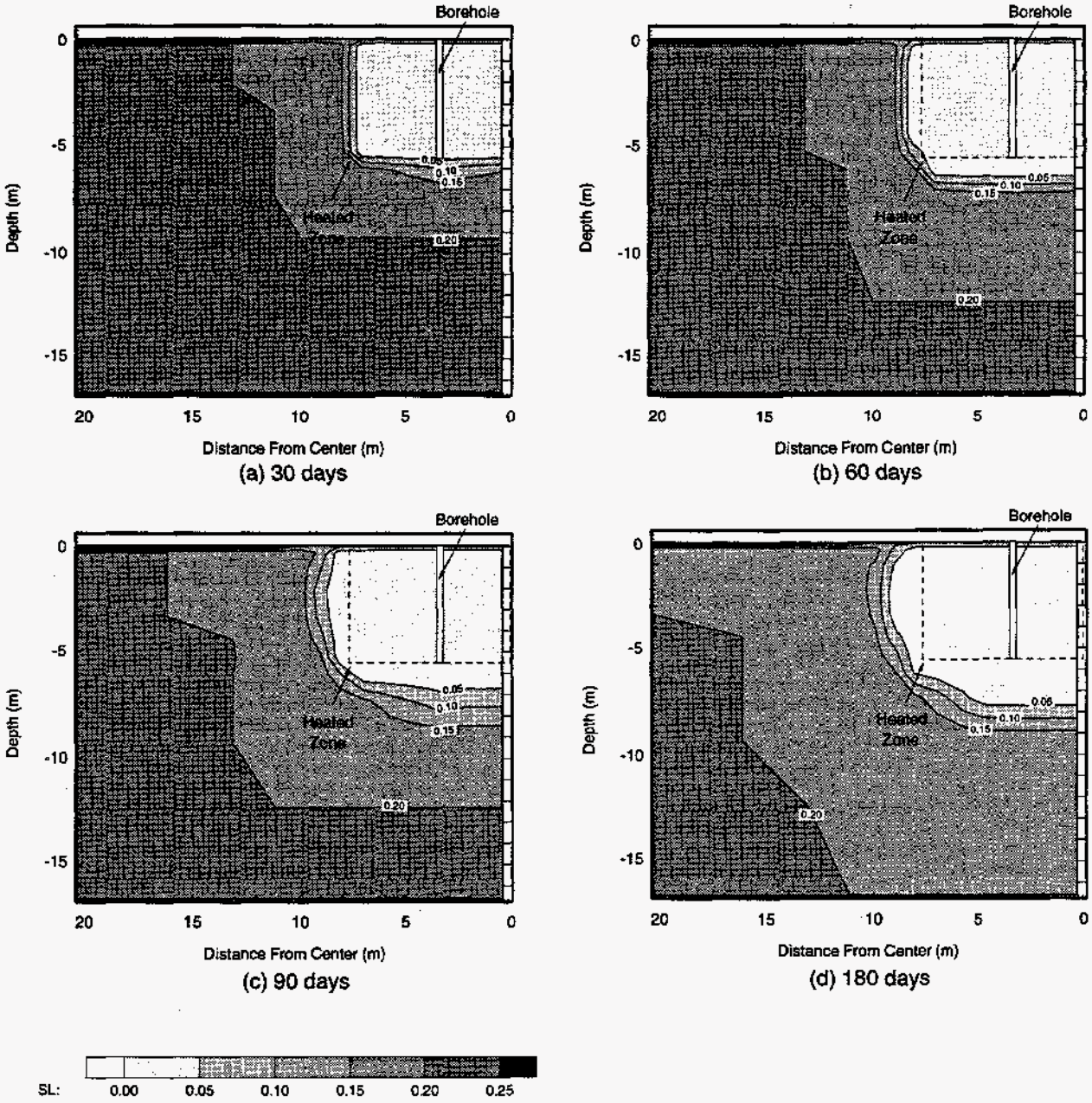

Figure 3-12. Late-time water saturation contours, 2.5 kPA vacuum, inside extraction, long-side view, I=1 plane

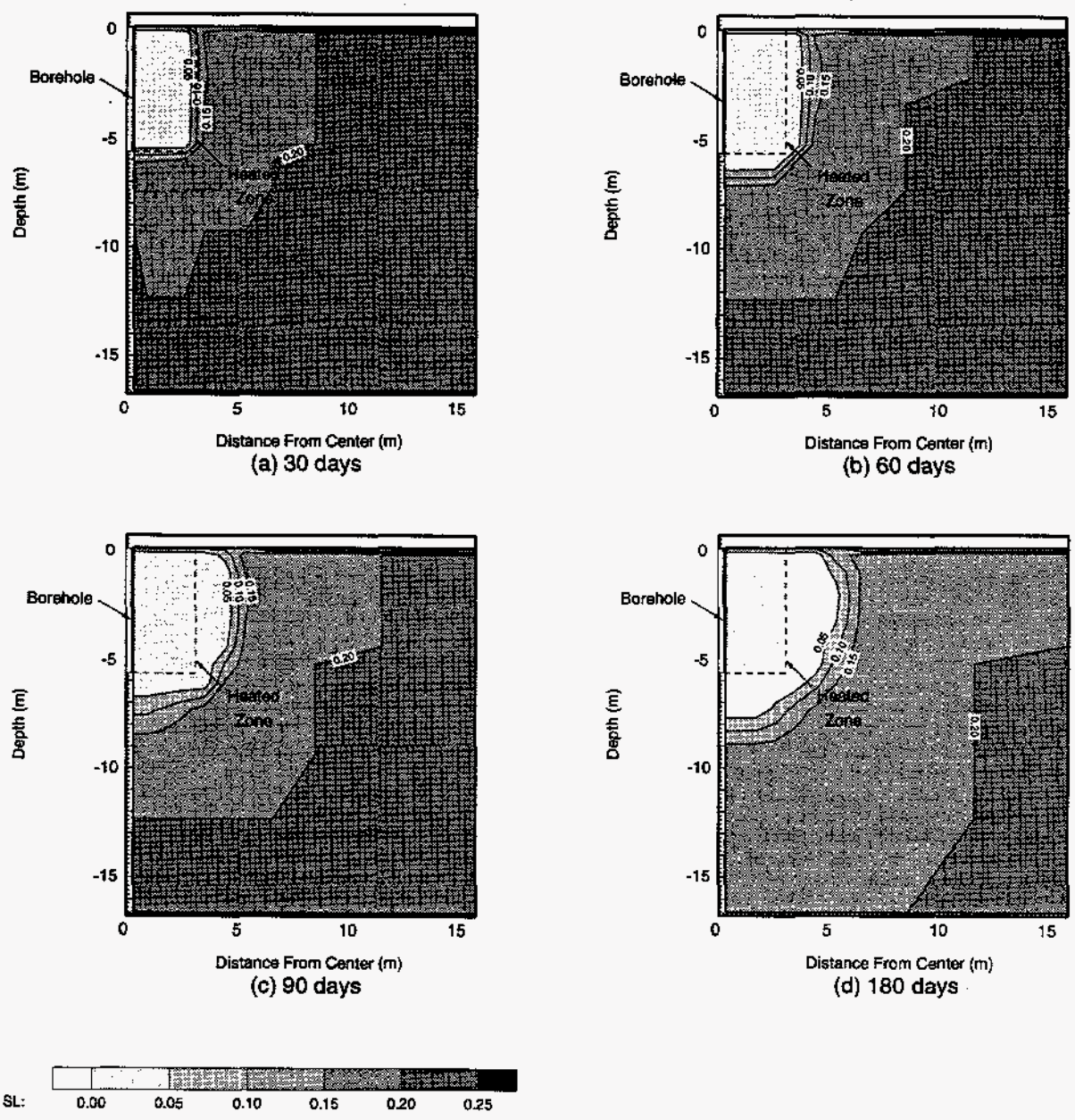

Figure 3-13. Late-time water saturation contours, 2.5 kPA vacuum, inside extraction, short-side view, J=1 plane

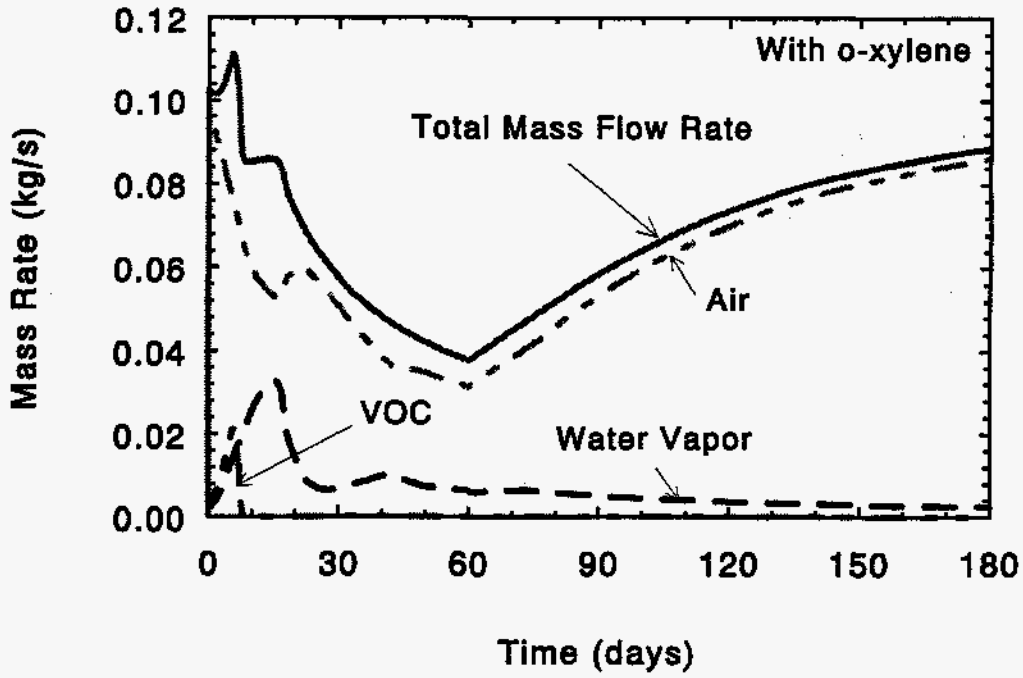

(a) Mass flow rates into boreholes

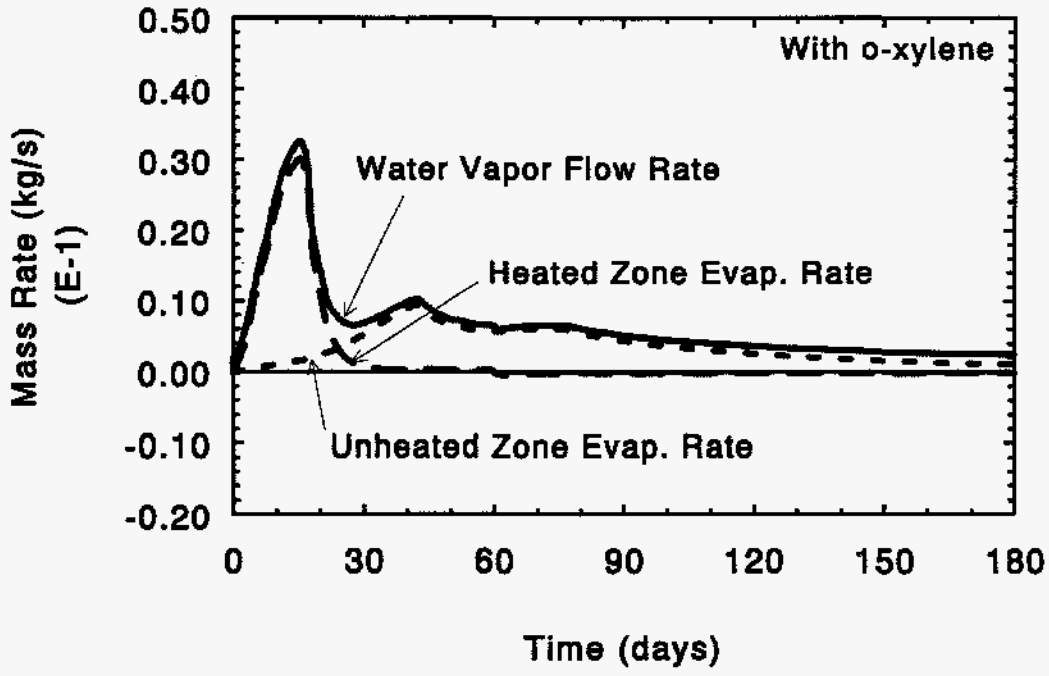

(b) Evaporation and water vapor mass rates

Figure 3-14. Mass rates, inside extraction, 100 kW - 2.5 kPA (10" water) BH vacuum

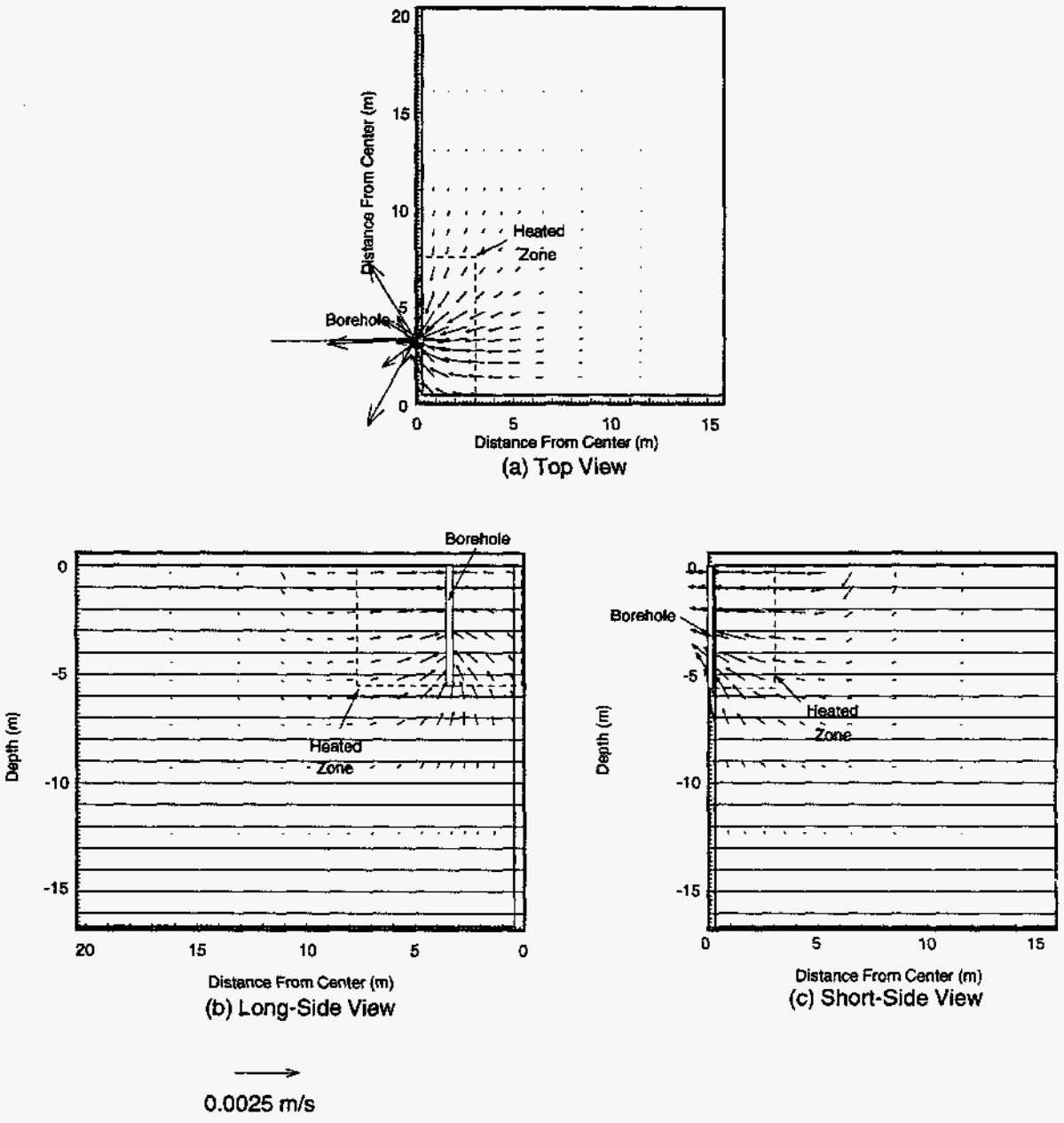

Figure 3-15. Gas velocity vectors at 60 days, 2.5 kPa vacuum, inside extraction
(a) Top view: K=4 plane
(b) Long-side view: I=3 plane
(c) Short-side view: J=3 plane

3.2 1.0 kPa Borehole Vacuum

Results for a borehole vacuum of 1.0 kPa (4 in. of water) for inside extraction are given in this section. Unlike the 2.5 kPa case, only the heatup phase of 60 days was simulated. The cooldown behavior is expected to be similar to the 2.5 kPa borehole vacuum case.

The time variation of the soil temperature in the heated zone out to 60 days is shown in Figure 3-16 as is the maximum soil temperature in the unheated zone. The time variation is very similar to that for a 2.5 kPa borehole vacuum. After 60 days, the heated zone average temperature is about 258°C with a range of 131 to 371 °C; the values for the 2.5 kPa vacuum case are an average of 246°C with a range of 122°C to 361°C. The maximum unheated zone temperature is 148°C compared to 138°C for the 2.5 kPa case. Thus, the temperature increases are about 10°C higher than for the 2.5 kPa case due to the lower air flow rate through the soil. The temperature contour plots are very similar to those for 2.5 kPa vacuum. The contour plots at 60 days for all three planes are given in Figure 3-17.

Figure 3-18 shows the time variation of the water and NAPL liquid masses in the heated zone. The evaporation rate of the water and NAPL is similar to that given earlier for 2.5 kPa vacuum although slightly slower due to the decreased air flow rate due to the lower vacuum. The NAPL mass is essentially depleted within 10 days for 1.0 kPa vacuum compared to 7 days for the 2.5 kPa case. The approximate time when half of the NAPL remains is about 7 days.

Early-time liquid water and NAPL saturation contours are given in Figures 3-19 to 3-21. Plots at 1.2 days (10^5 seconds) and 7 days are shown. Both the liquid water and NAPL saturation contours look generally similar to the 2.5 kPa case. In both cases, the NAPL saturations generally decrease away from the borehole. For 1.0 kPa vacuum, these contours are not as crisp. As noted in the top and long-side views at 7 days, removal of NAPL at some of the edges of the heated zone lags behind the general removal trend, indicating possible low air flow regions. Liquid water saturation contours for later times are also essentially the same as for 2.5 kPa; the three views at 60 days are given in Figure 3-22.

Figure 3-23a shows the various mass flow rates into the borehole. The total mass flow rate into the borehole increases in the early stages of heating due to the evaporation of the NAPL (VOC) component in the heated soil. For much of the simulation, the mass fractions of air and water vapor are comparable; in contrast, for 2.5 kPa, the mass flow was predominantly air. The air flow rate is much smaller than for 2.5 kPa while the vapor flow rate is about the same. Figure 3-23b shows the evaporation rate in the heated and unheated zones along with the vapor flow rate into the borehole. The heated zone evaporation rate dominates early, while the unheated zone evaporation is the major source of vapor later in the transient.

Gas flow velocity vectors are similar to the 2.5 kPa case as flow is generally directly toward the borehole. The vectors at 60 days are given in Figure 3-24; the vector length has been linearly scaled with the inverse of the borehole vacuum for comparison to other vector plots.

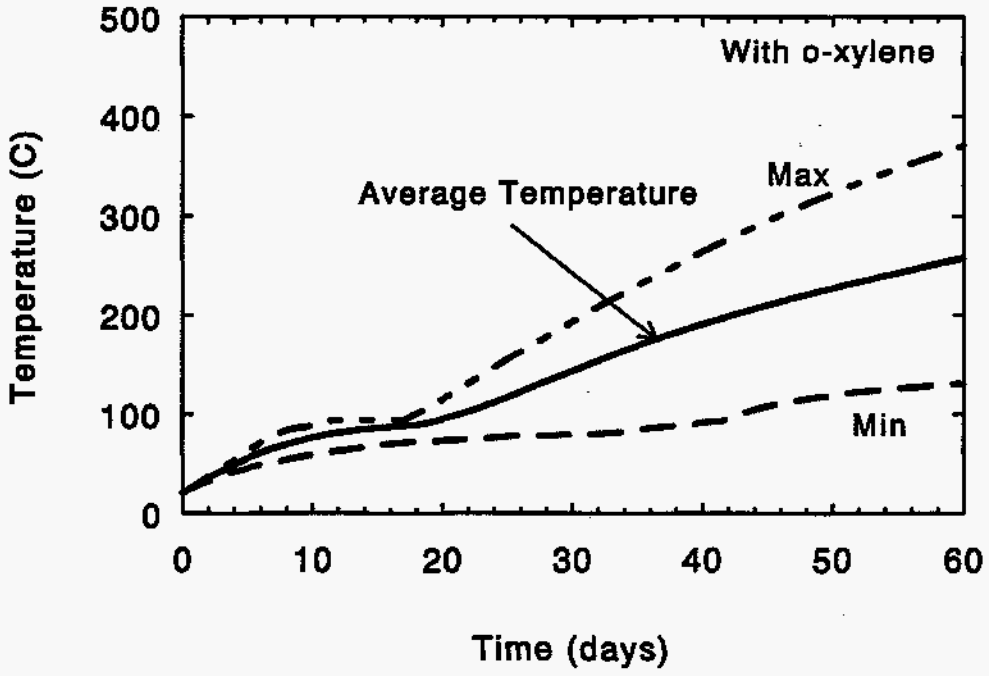

(a) Heated zone temperatures

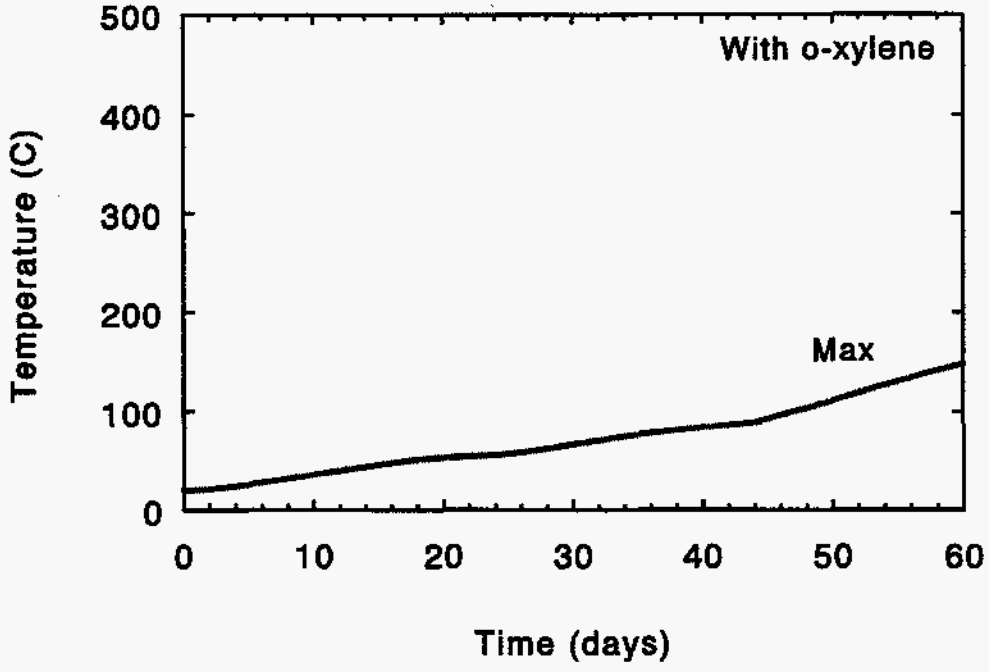

(b) Maximum unheated zone temperatures

Figure 3-16. Heated and unheated zone temperatures, inside extraction; 100 kW - 1.0 kPa (4" water) BH vacuum

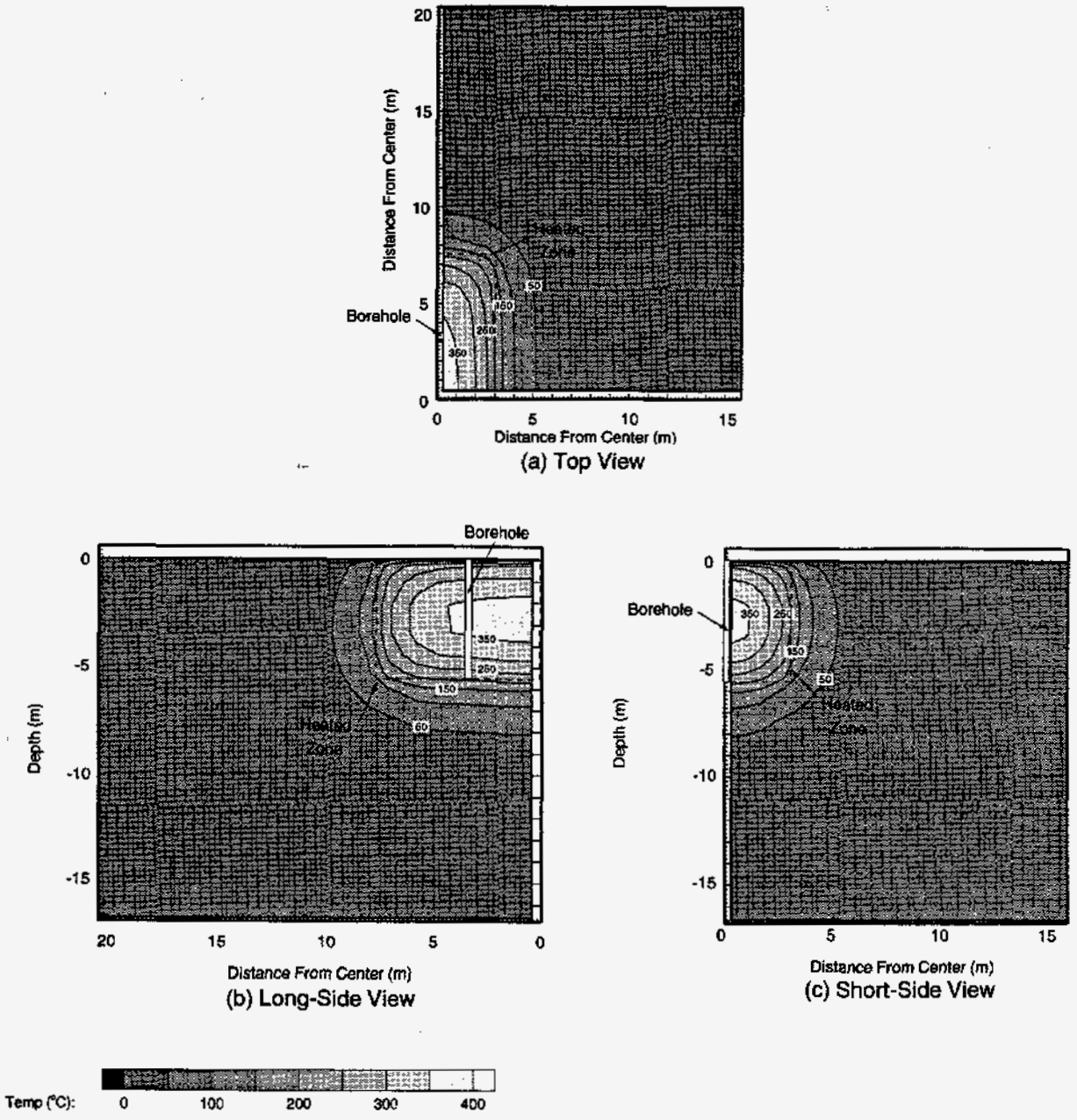

Figure 3-17. Temperature contours at 60 days, inside extraction, 1.0 kPa BH vacuum
(a) Top view: K=4 plane
(b) Long-side view: I=3 plane
(c) Short-side view: J=3 plane

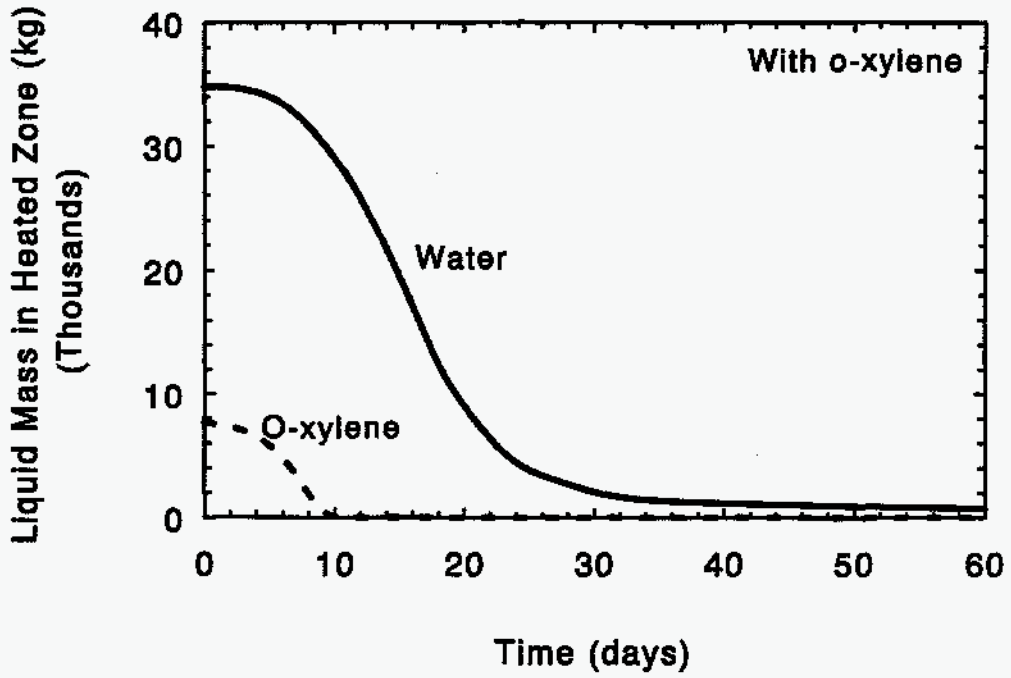

Figure 3-18. Heated zone fluid masses, inside extraction, 100 kW - 1.0 kPa (4" water) BH vacuum, 0-60 days

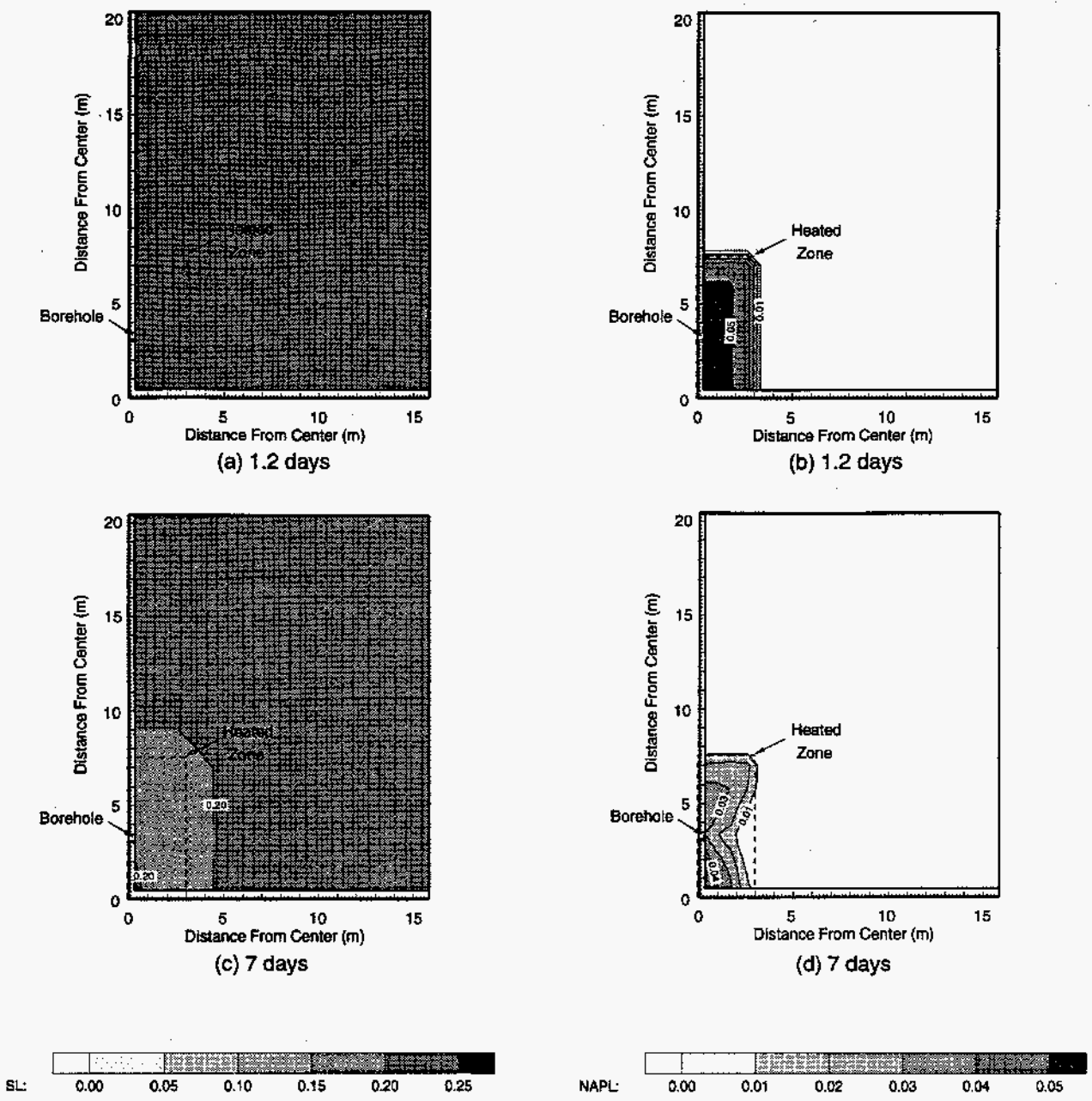

Figure 3-19. Early-time water (left diagram) and NAPL (right diagram) saturation contours, 1.0 kPa vacuum, top view, inside extraction, K=4 plane

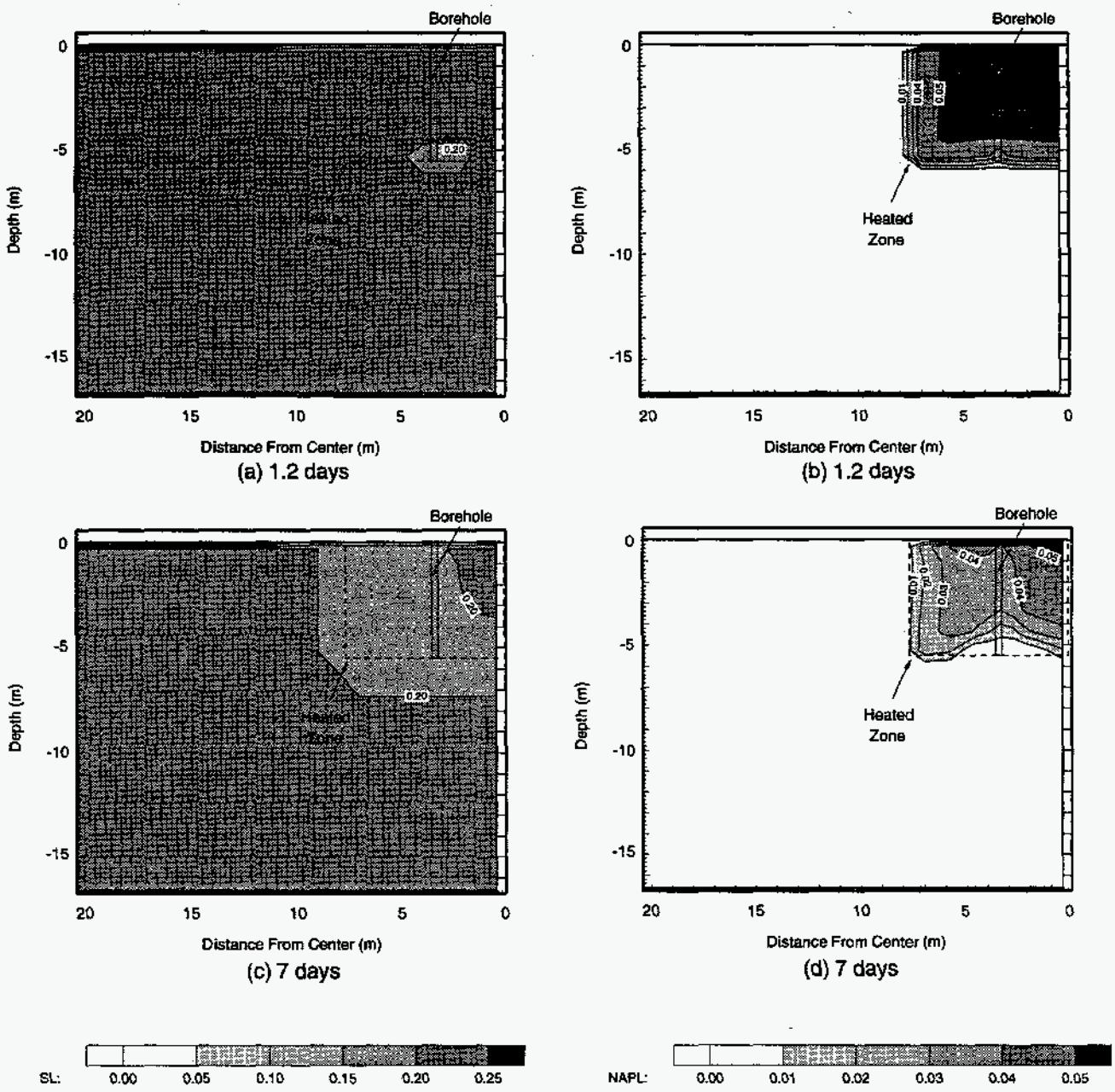

Figure 3-20. Early-time water (left diagram) and NAPL (right diagram) saturation contours, long-side view, 1.0 kPa vacuum, inside extraction, I=1 plane

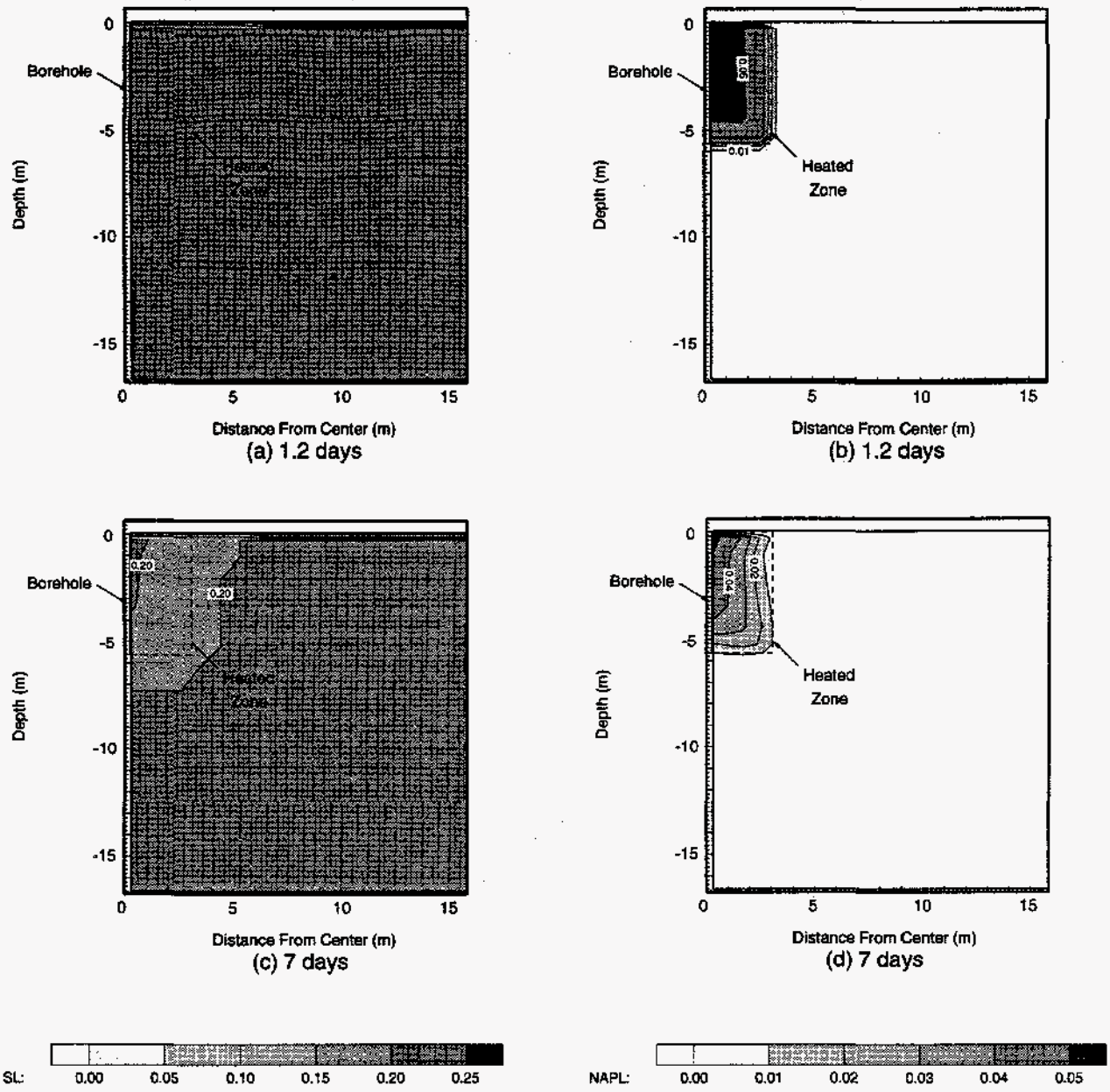

Figure 3-21. Early-time water (left diagram) and NAPL (right diagram) saturation contours, short-side view, 1.0 kPa vacuum, inside extraction, J=1 plane

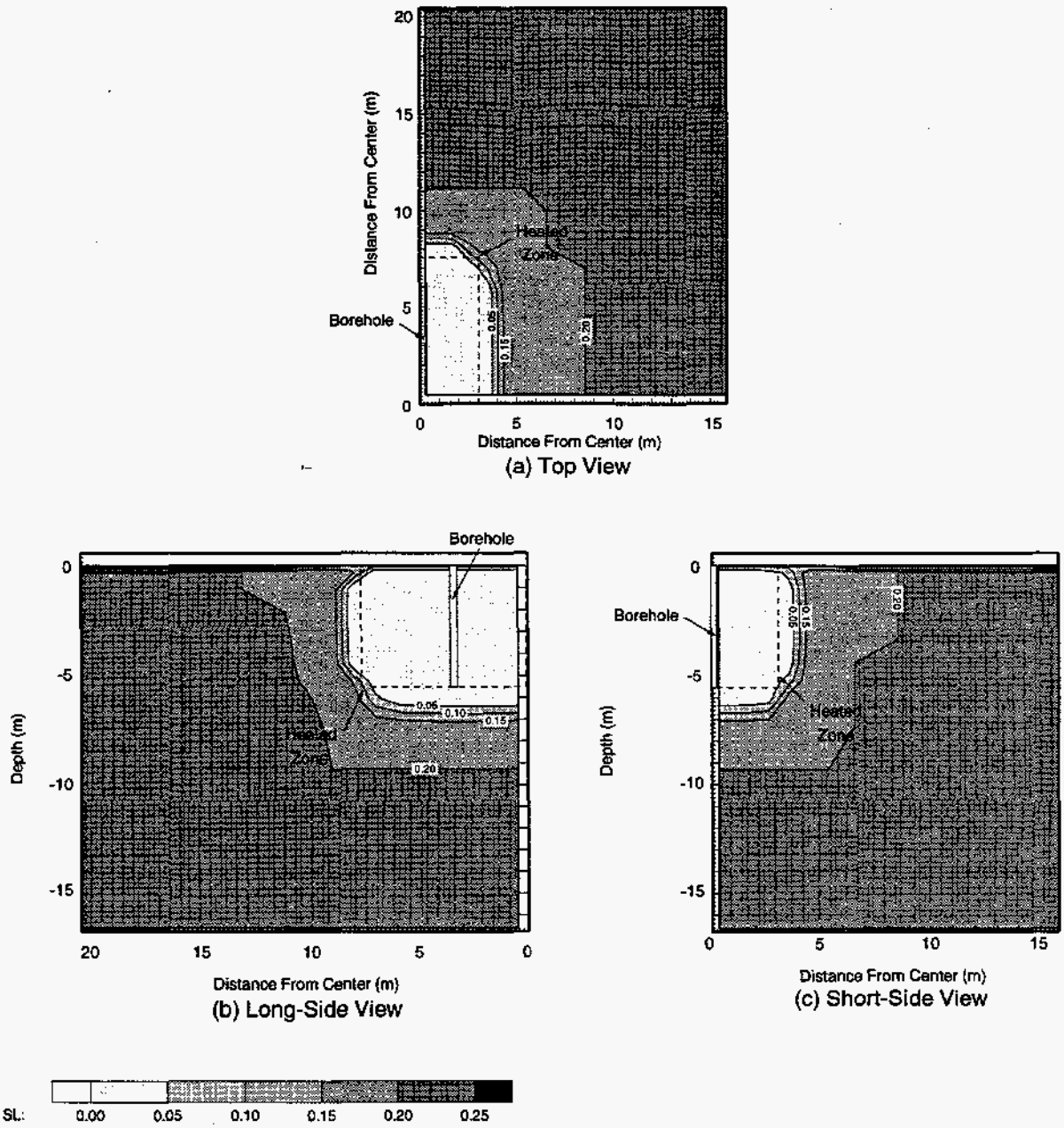

Figure 3-22. Late-time water saturation contours at 60 days 1.0 kPa vacuum, inside extraction
(a) Top view: K=4 plane
(b) Long-side view: I=1 plane
(c) Short-side view: J=1 plane

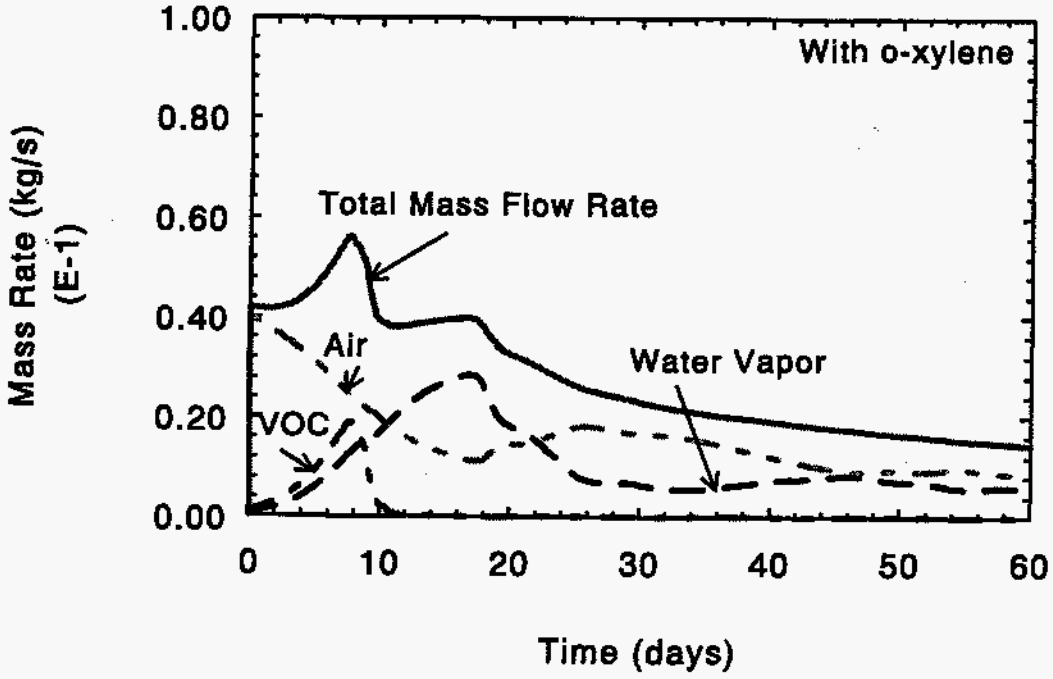

(a) Mass flow rates into boreholes

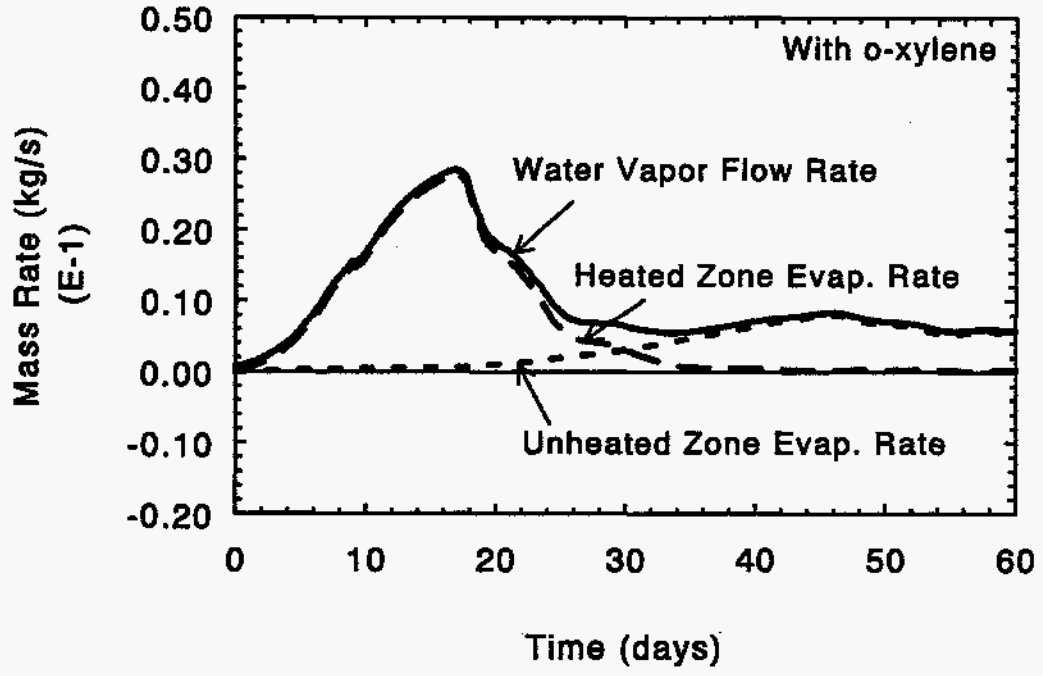

(b) Evaporation and water vapor mass rates

Figure 3-23. Mass rates, inside extraction, 100 kW - 1.0 kPa (4" water) BH vacuum

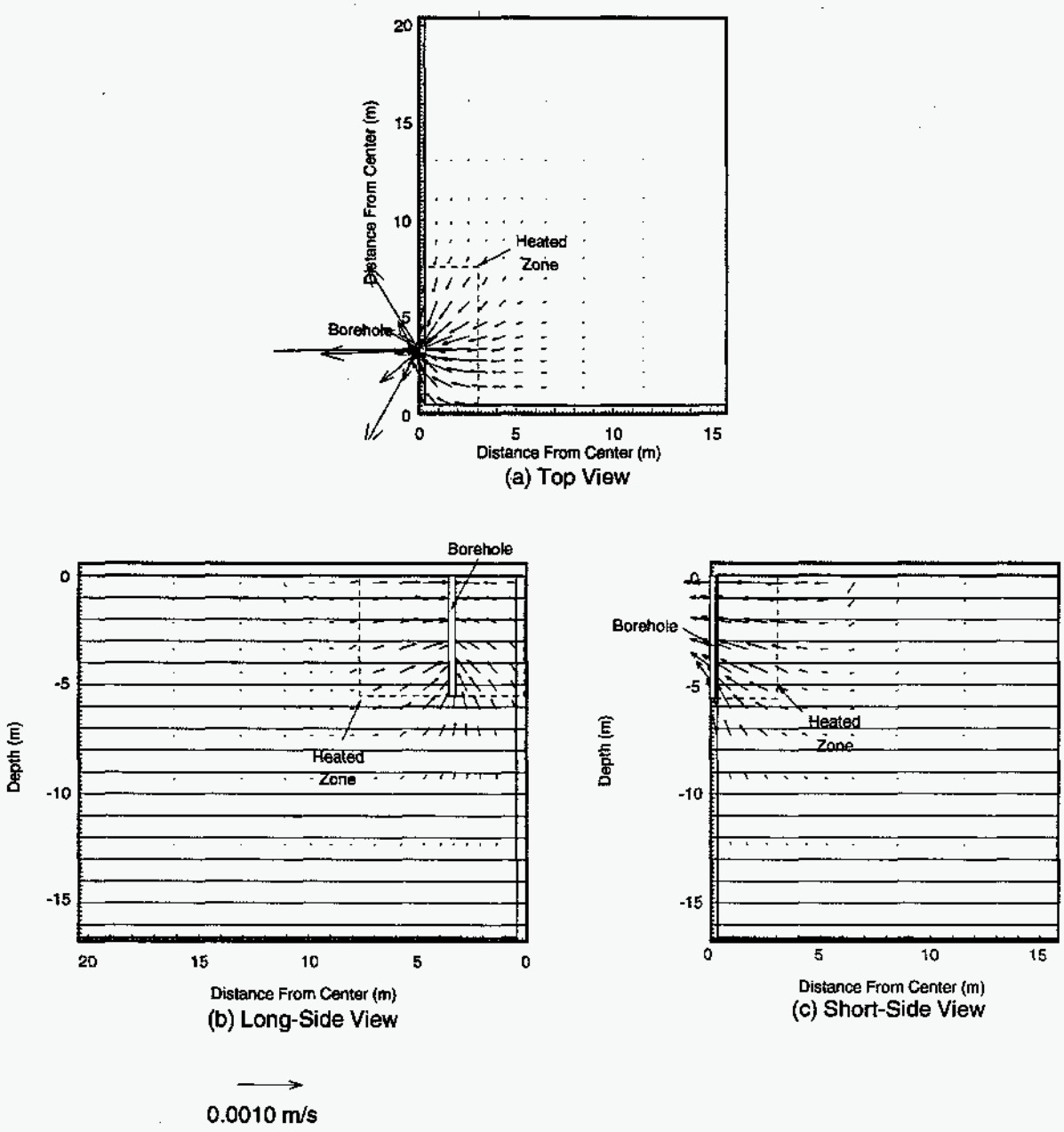

Figure 3-24. Gas velocity vectors at 60 days - 1.0 kPa vacuum, inside extraction
(a) Top view: K=4 plane
(b) Long-side view: I=3 plane
(c) Short-side view: J=3 plane

3.3 0.5 kPa Borehole Vacuum

Results for a borehole vacuum of 0.5 kPa (2 in. of water) for inside extraction are given in this section. Similar to the 1.0 kPa case, only the heatup phase of 60 days was simulated. The cooldown behavior is expected to be similar to the 2.5 kPa borehole vacuum case.

The time variation of the soil temperature in the heated zone (average, minimum, and maximum) out to 60 days is shown in Figure 3-25a, while the maximum soil temperature in the unheated zone is given in Figure 3-25b. The time variation is very similar to the other two cases. After 60 days, the heated zone average temperature is about 264°C with a range of 137 to 375 °C; these values for the 1.0 kPa vacuum case are an average of 258°C with a range of 131°C to 371°C. The maximum unheated zone temperature is 149°C compared to 148°C for the 1.0 kPa case. Thus, the temperature rise is about 5°C higher for 0.5 kPa than for 1.0 kPa. The temperature contour plots are very similar to those for the other two cases. The contour plots for all three planes are given in Figure 3-26 at 60 days only.

Figure 3-27a gives the time variation of the water and NAPL liquid masses in the heated zone. The evaporation rate of the water and NAPL is slower than for the other two cases due to the smaller air flow rate through the soil. The NAPL mass in the heated zone is mostly depleted within about 16 days compared to about 10 days for the 1.0 kPa case and 7 days for 2.5 kPa. The approximate time when half of the NAPL remains in the heated zone is about 8 days. Figure 3-27b shows the NAPL mass variation in the heated and unheated zones. At about 14 days, just before all the NAPL in the heated zone disappears, NAPL starts to migrate to the unheated soil. The NAPL in the unheated soil continues to increase until about 20 days, when it starts to decrease as the unheated soil temperature increases and due to evaporation into the incoming air stream. Some NAPL is still present in the unheated zone at the end of the simulation at 60 days. The maximum NAPL mass in the unheated soil is about 200 kg compared to an initial mass of almost 8000 kg in the heated zone, or less than 3% of the initial mass. While this migrated NAPL will eventually be evaporated and transported to the borehole, the migration into the unheated soil represents undesirable contaminant migration caused by insufficient air sweep.

Early-time liquid water and NAPL saturation contours are given in Figures 3-28 to 3-30. Plots at 1.2 days (10^5 seconds), 8 days, and 11.6 days (10^6 seconds) are given. The liquid water and NAPL saturation contours look generally similar to the 1.0 kPa case except that a zone of NAPL is left behind on the edges of the heated zone as shown at 11.6 days; these "pockets" are areas that lagged behind in the 1.0 kPa case. Transport into the unheated zone is due to evaporation in the heated zone, convective flow into the unheated soil, and condensation in the cooler unheated soil.

Liquid water saturation contours also indicate an insufficient air sweep as shown in Figures 3-31 to 3-33 for 30 and 60 days. Water evaporates in the heated zone and is

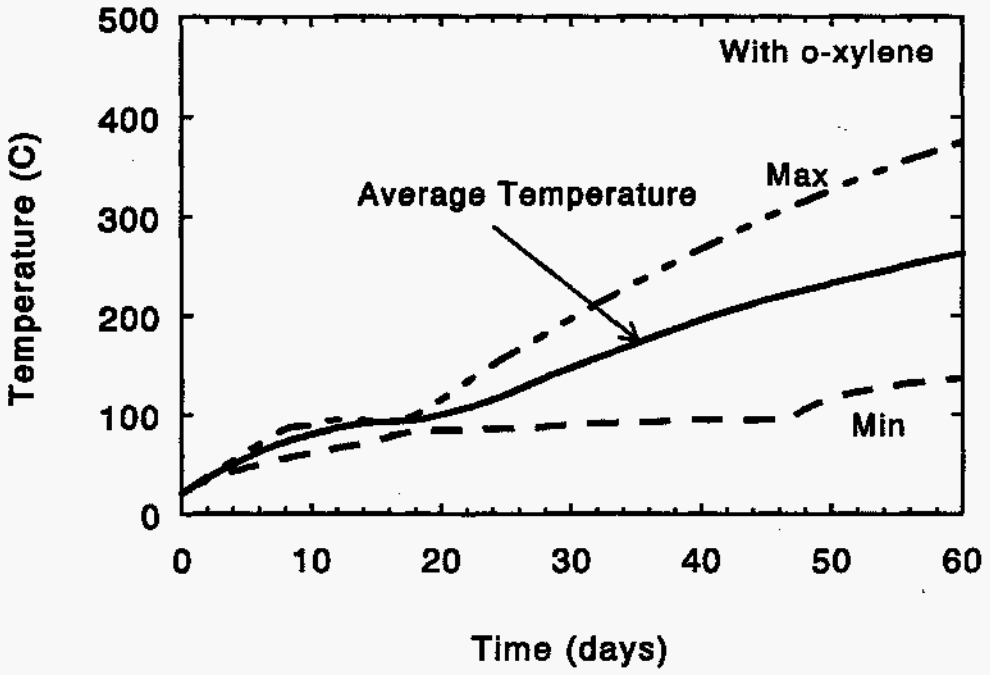

(a) Heated zone temperatures

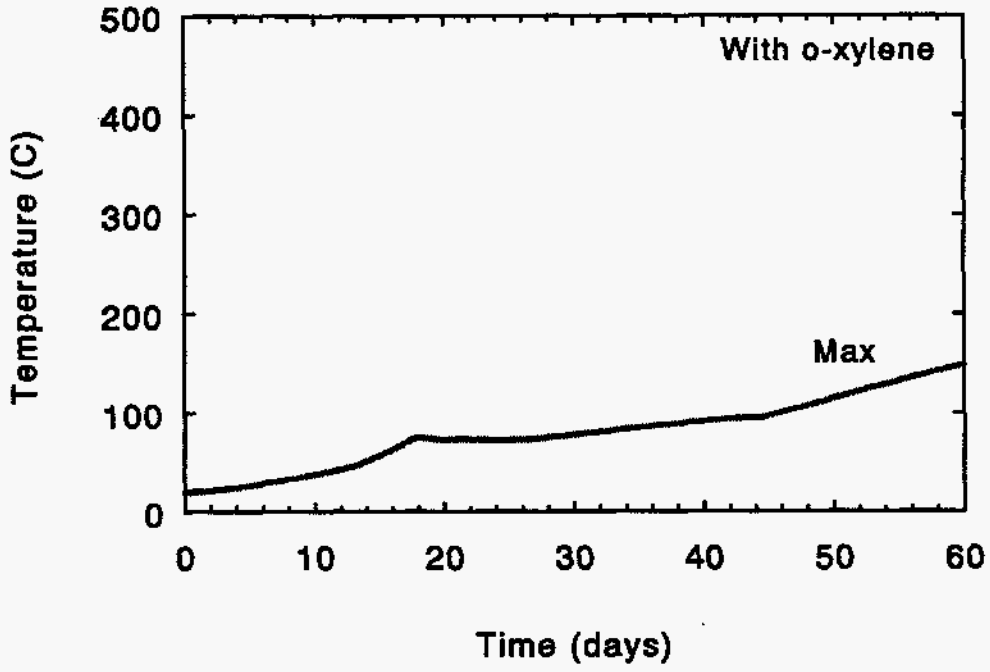

(b) Maximum unheated zone temperatures

Figure 3-25. Heated and unheated zone temperatures, inside extraction; 100 kW - 0.5 kPa (2" water) BH vacuum

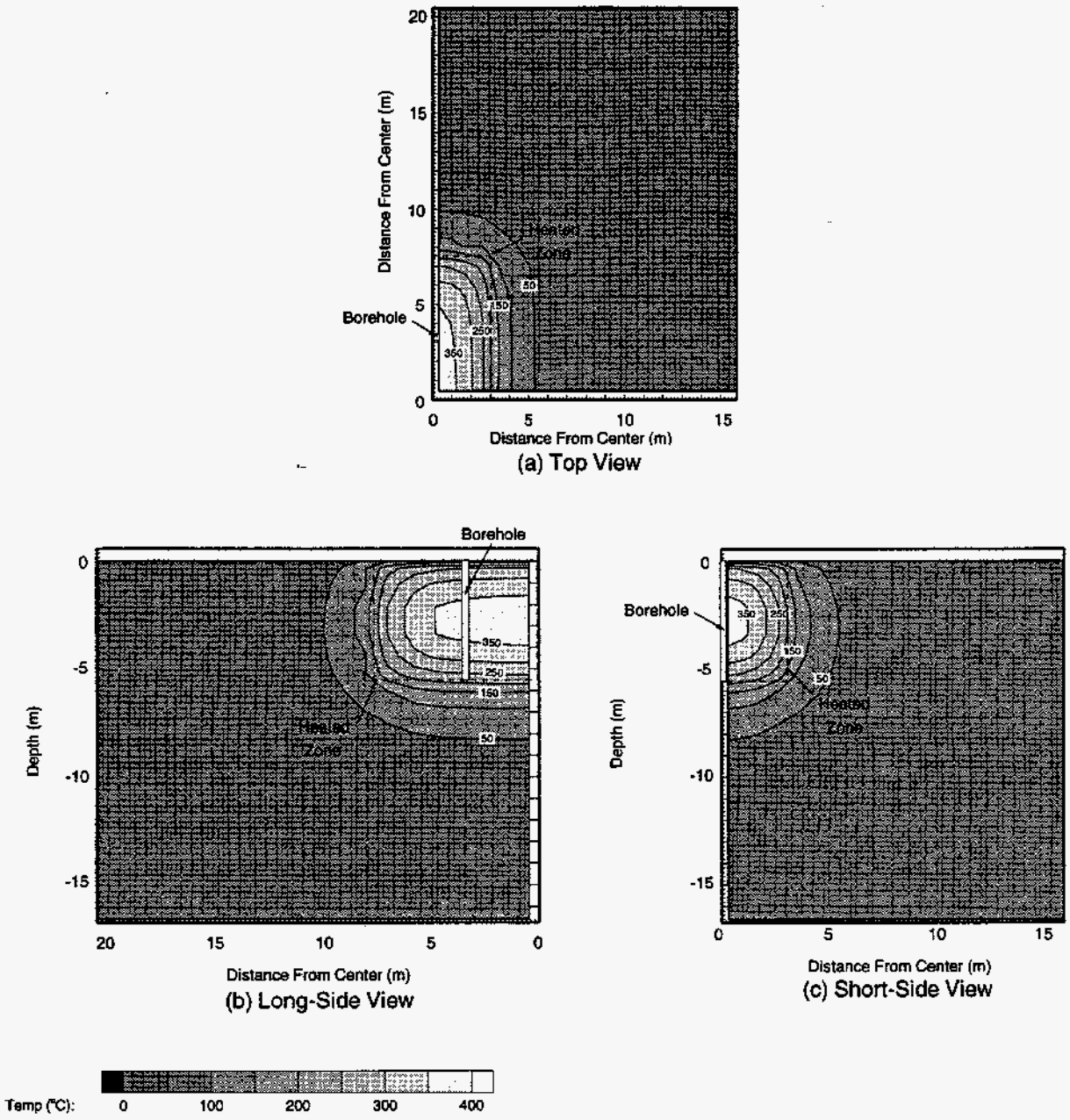

Figure 3-26. Temperature contours at 60 days, inside extraction, 0.5 kPa vacuum
(a) Top view: K=4 plane
(b) Long-side view: I=1 plane
(c) Short-side view: J=1 plane

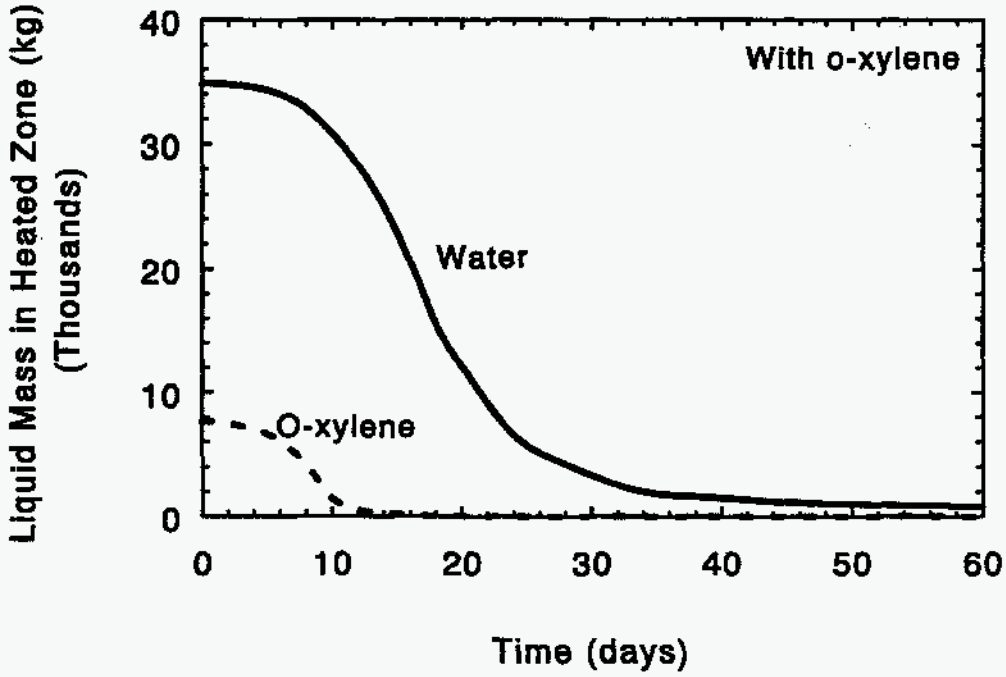

(a) Heated zone fluid masses

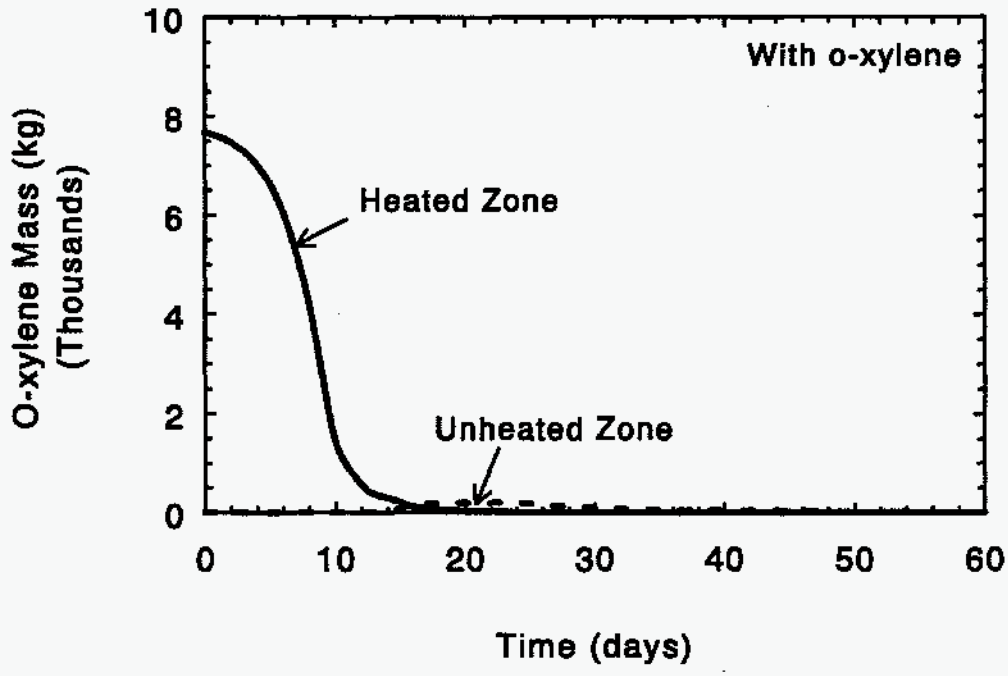

(b) O-xylene mass variation

Figure 3-27. Heated zone fluid masses and O-xylene mass variation, inside extraction, 100 kW, 0.5 kPa (2" water) BH vacuum

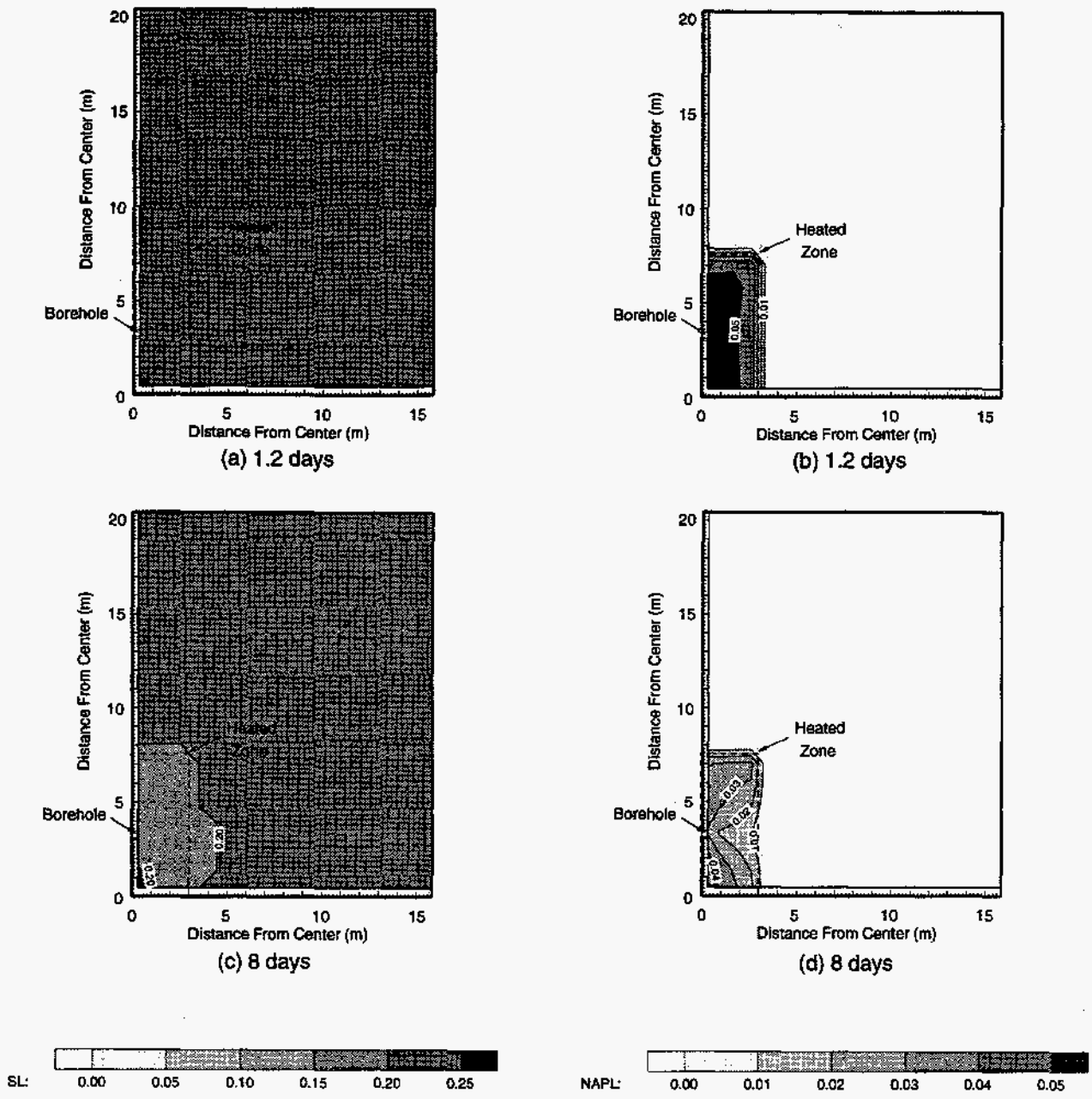

Figure 3-28. Early-time water (left diagram) and NAPL (right diagram) saturation contours, 0.5 kPa vacuum, top view, inside extraction, K=4 plane

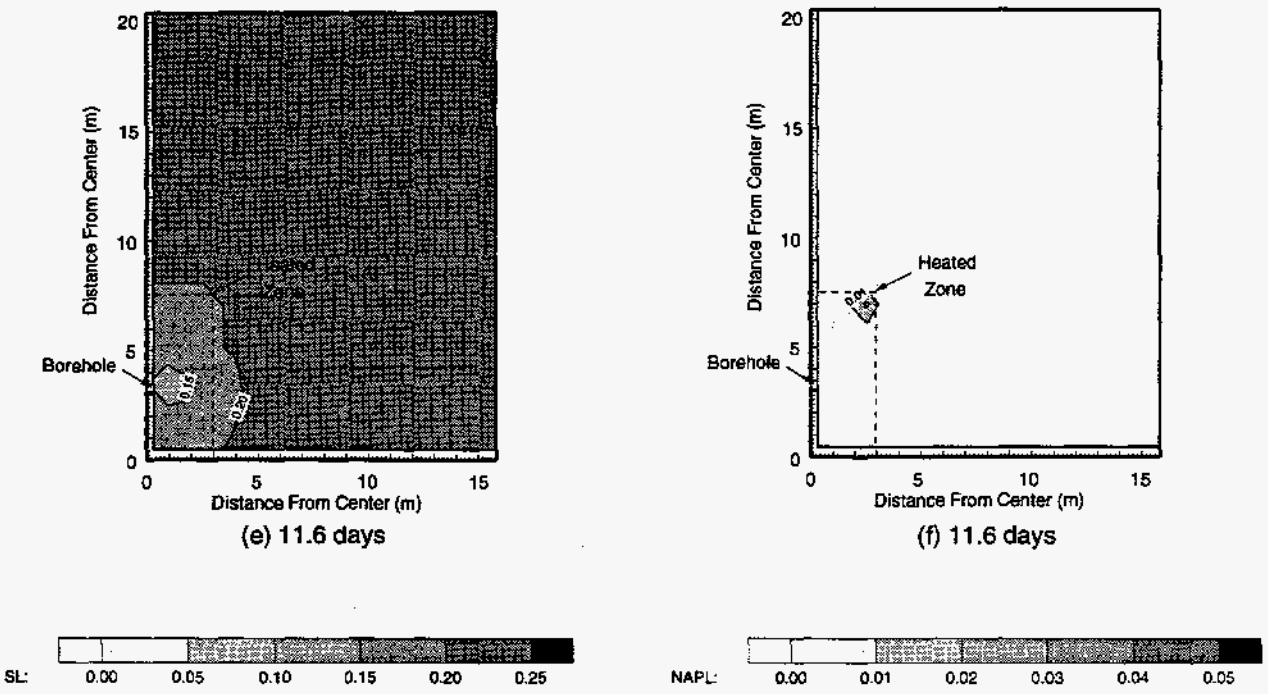

Figure 3-28. Early-time water (left diagram) and NAPL (right diagram) saturation contours, 0.5 kPa vacuum, top view, inside extraction, K=4 plane, continued

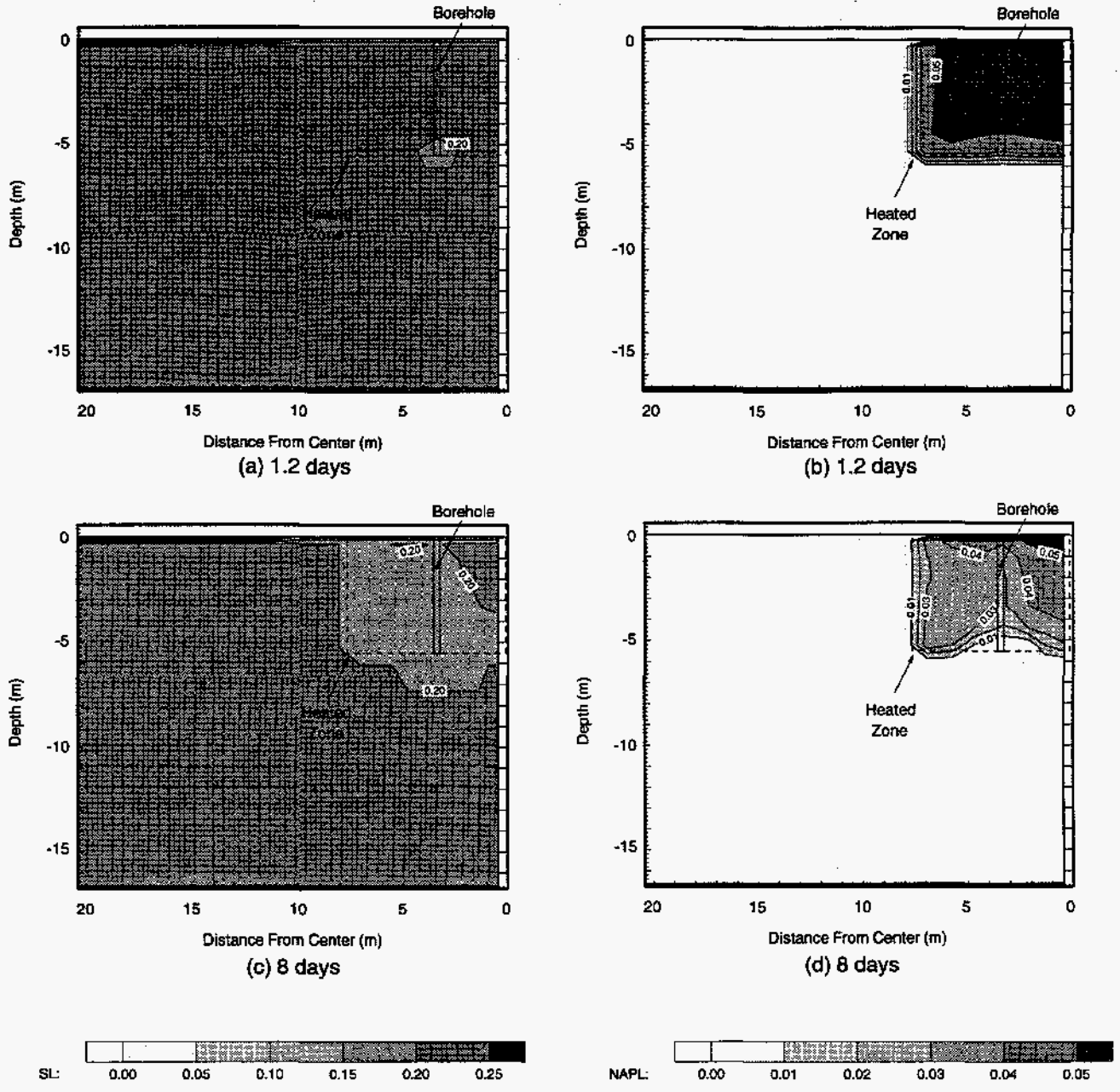

Figure 3-29. Early-time water (left diagram) and NAPL (right diagram) saturation contours, 0.5 kPa vacuum, long-side view, inside extraction, I=1 plane

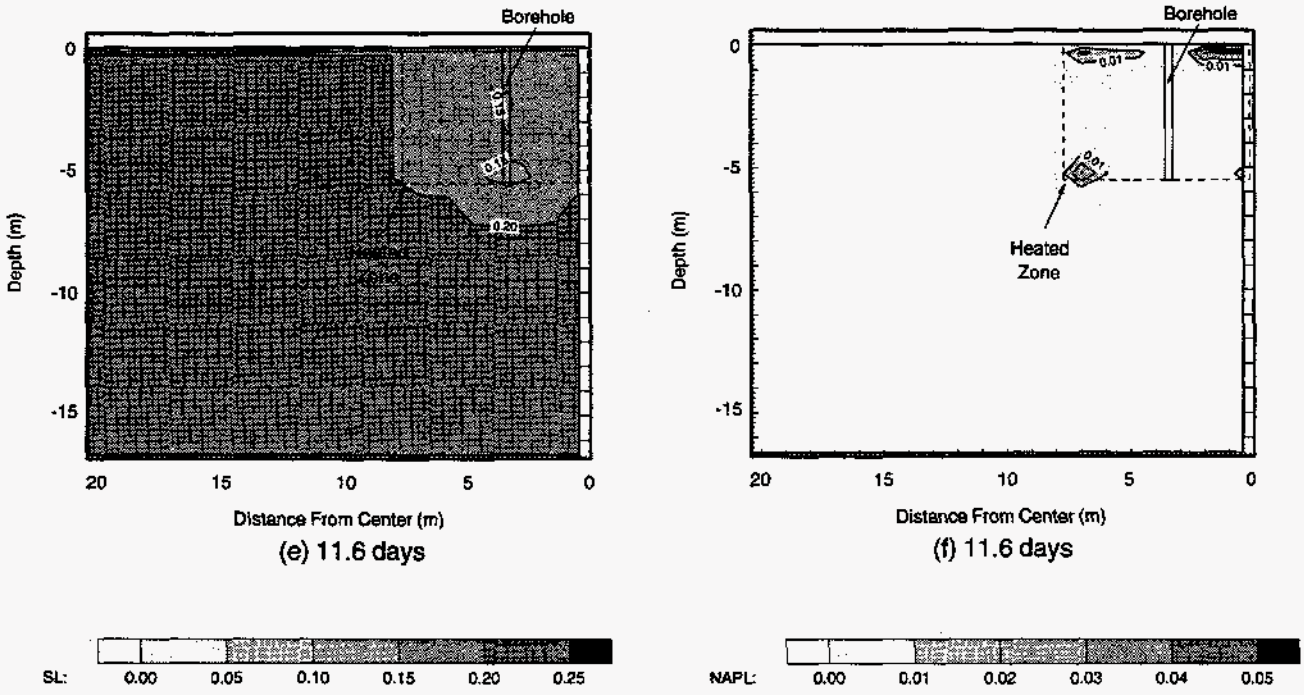

Figure 3-29. Early-time water (left diagram) and NAPL (right diagram) saturation contours, 0.5 kPa vacuum, long-side view, inside extraction, I=1 plane, continued

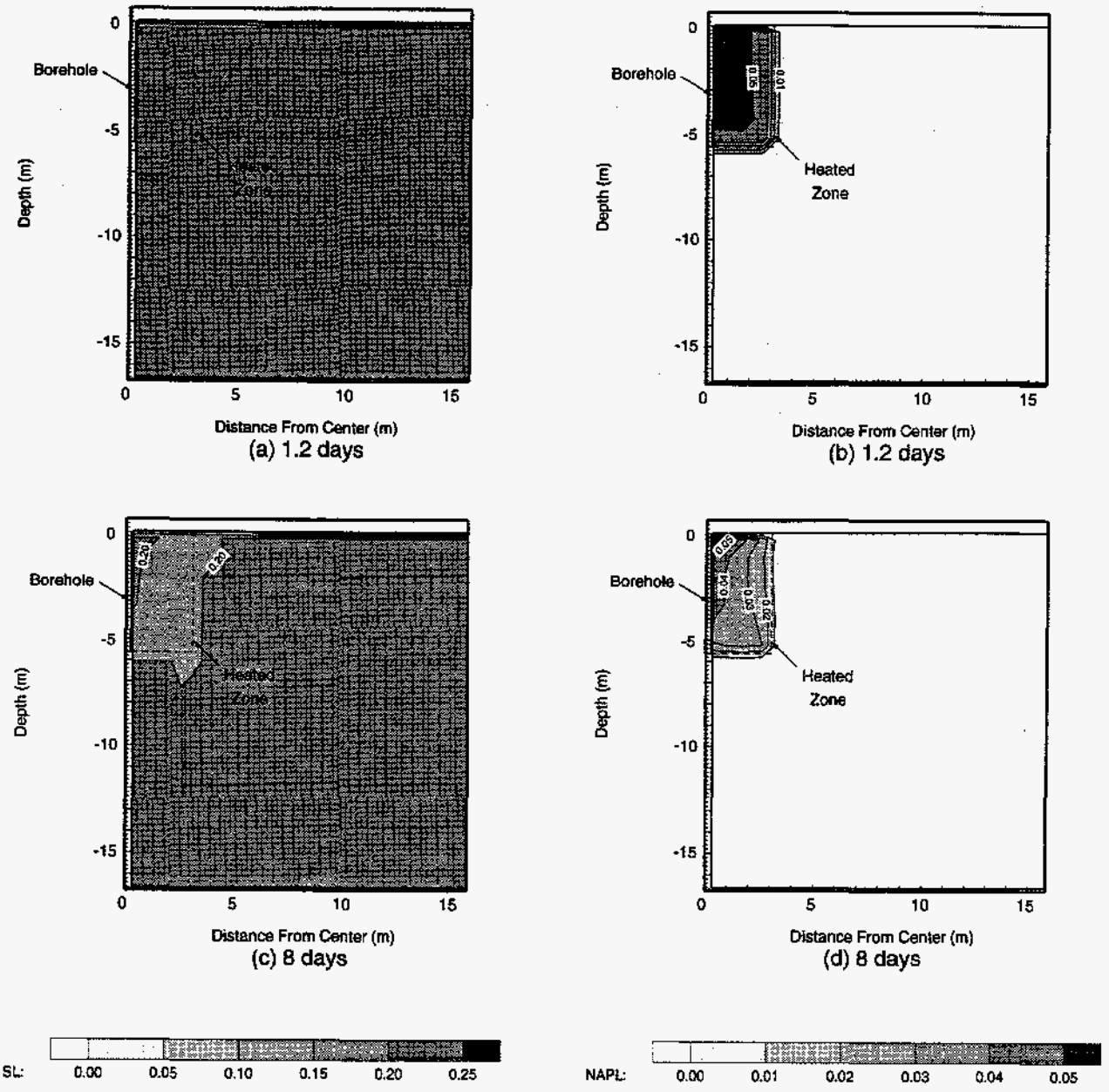

Figure 3-30. Early-time water (left diagram) and NAPL (right diagram) saturation contours, 0.5 kPa vacuum, short-side view, inside extraction, J=1 plane

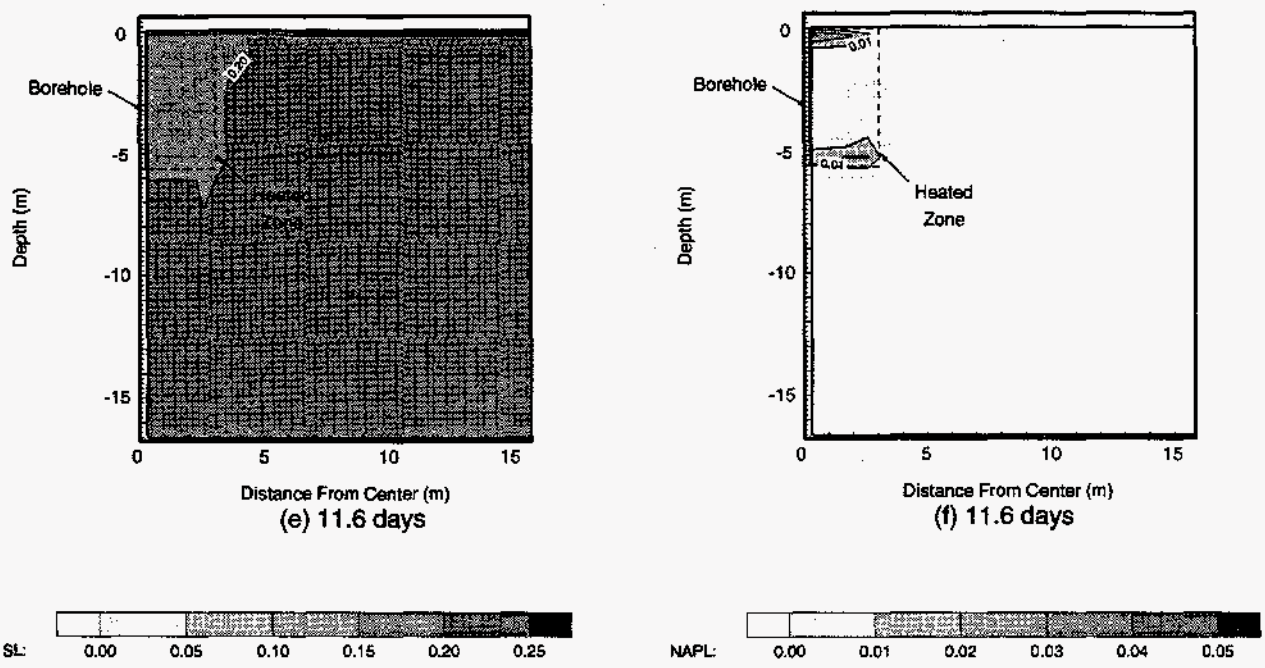

Figure 3-30. Early-time water (left diagram) and NAPL (right diagram) saturation contours, 0.5 kPa vacuum, short-side view, inside extraction, J=1 plane, continued

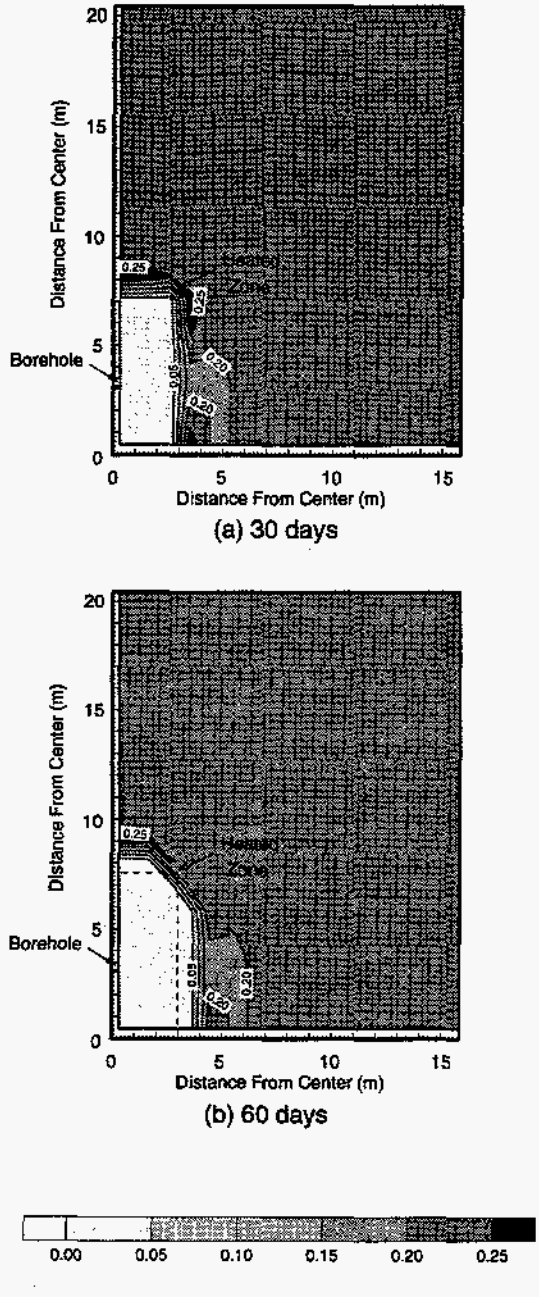

Figure 3-31. Late-time water saturation contours, 0.5 kPa vacuum, inside extraction, top view, K=4 plane

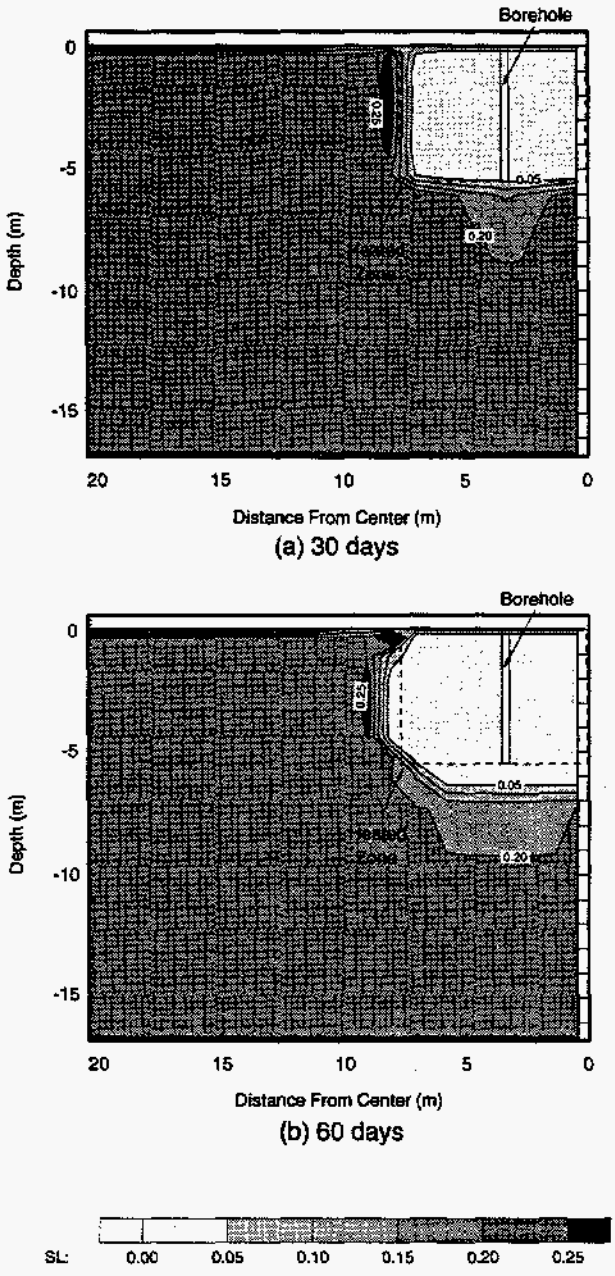

Figure 3-32. Late-time water saturation contours, 0.5 kPa vacuum, inside extraction, long-side view, I=1 plane

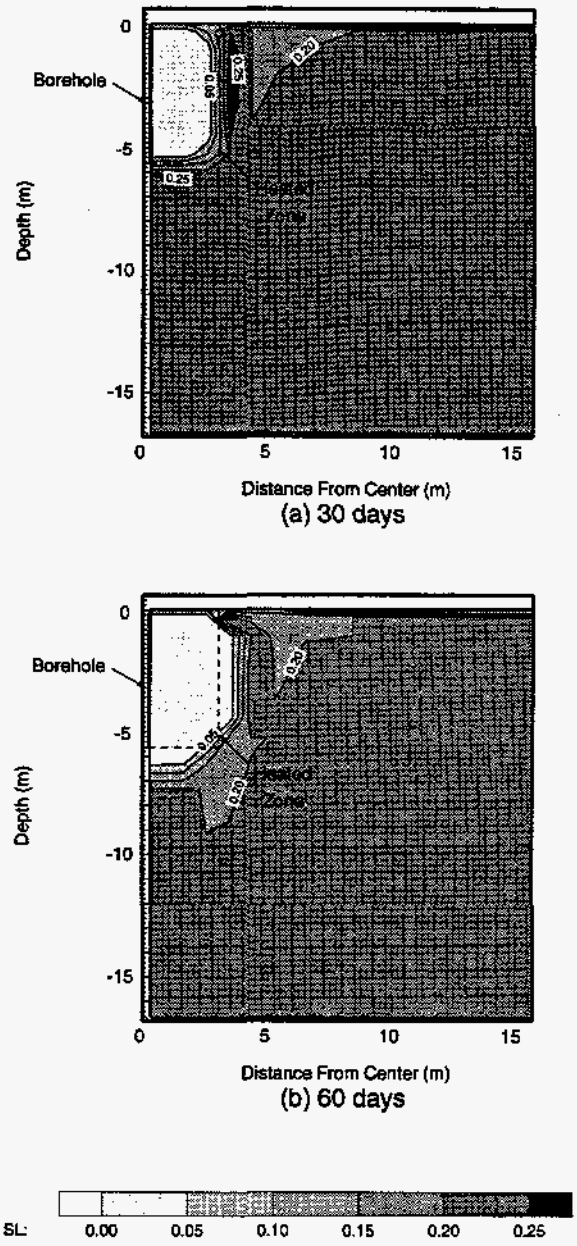

Figure 3-33. Late-time water saturation contours, 0.5 kPa vacuum, inside extraction, short-side view, J=1 plane

subsequently transported and condensed in the unheated soil as indicated by liquid saturations higher than 0.20 along some of the edges of the heated zone including directly under the borehole.

Figure 3-34a shows the various mass flow rates into the borehole. The total mass flow rate into the borehole increases in the early stages of heating due to the evaporation of the NAPL (VOC) component in the heated soil. For much of the simulation, the mass fraction is predominantly water vapor. Figure 3-34b shows the evaporation rate in the heated and unheated zones along with the water vapor flow rate into the borehole. The unheated zone evaporation rate becomes negative at about 13 days indicating condensation in the unheated zone as was seen in the liquid water saturation plots shown earlier.

Gas flow velocity vectors are essentially constant with time; the various view at 60 days are shown in Figure 3-35. The length of the vectors has been linearly scaled with the inverse of the borehole vacuum for comparison with earlier vector plots. The vectors are generally directed toward the borehole, although other directions including away from the borehole are indicated near the edges of the heated zone. In fact, some vectors in Figures 3-35a and 3-35b in the unheated soil are directly away from the borehole. In general, the velocity vectors pattern is much less structured than for higher borehole vacuums.

Figure 3-36 shows details of the NAPL migration into the unheated soil; the results are given for 15 days, which corresponds to the maximum rate of NAPL flow into the unheated zone. Figure 3-36a shows the top view of the pressure difference compared to the far-field value; dark areas indicate gas pressures less than the far-field, while light areas indicate higher gas pressures. At the top of the heated zone, the gas pressure is significantly higher than the far-field value. Figure 3-36b shows the resulting gas velocity vectors indicating significant convective gas flow from the heated zone into the unheated soil. As shown in Figure 3-36c, this region corresponds to NAPL migration into the unheated soil.

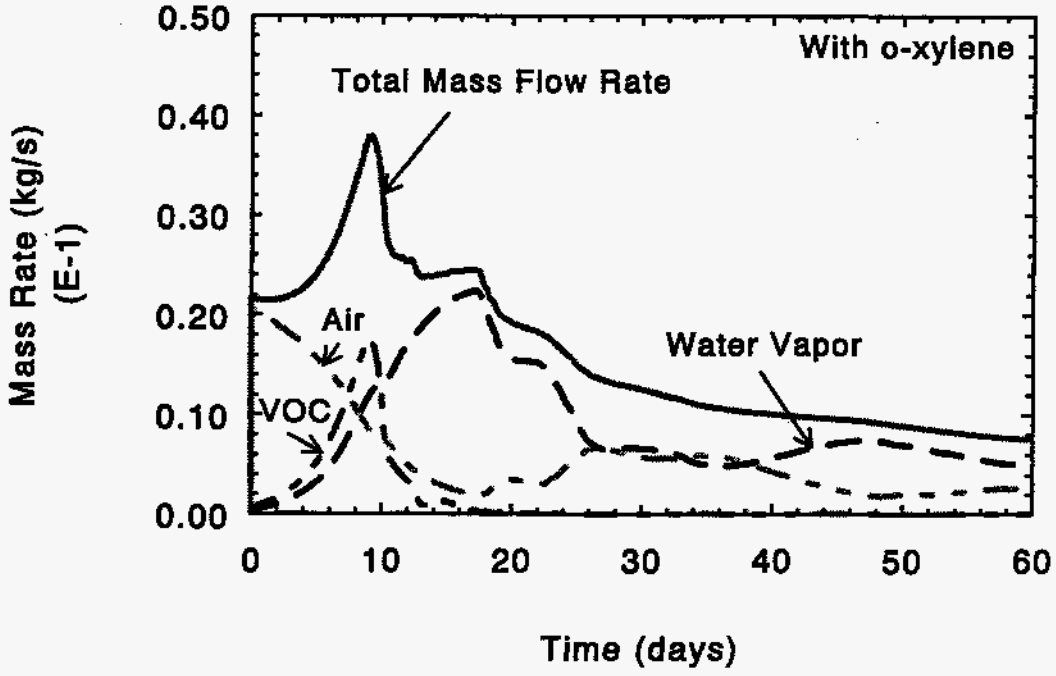

(a) Mass flow rates into boreholes

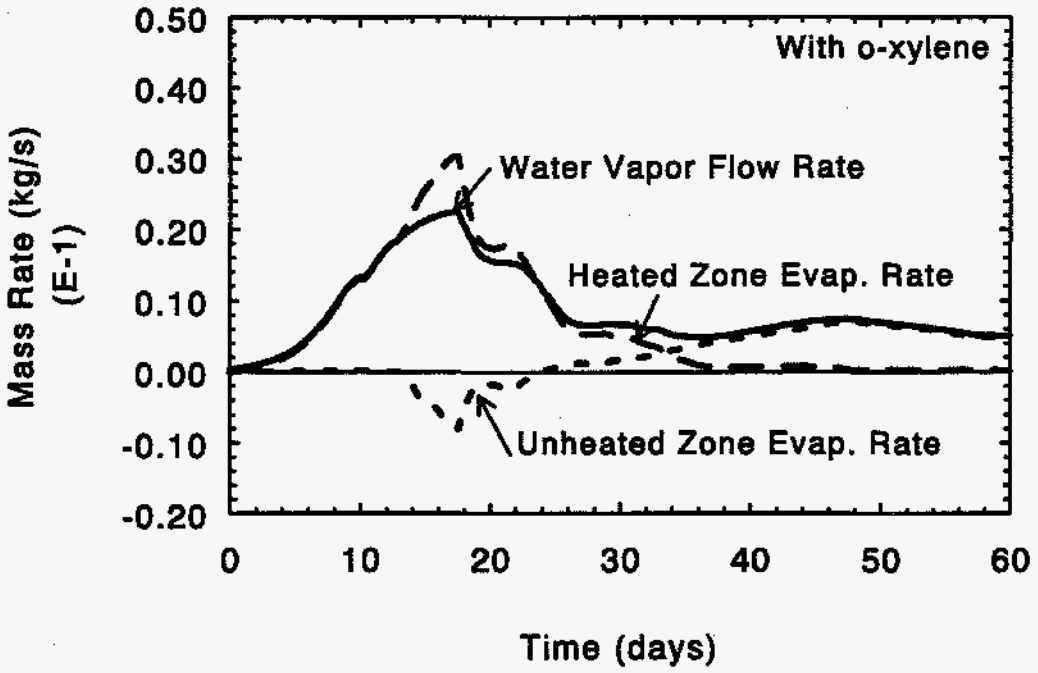

(b) Evaporation and water vapor mass rates

Figure 3-34. Mass rates, inside extraction, 100 kW - 0.5 kPa (2" water) BH vacuum

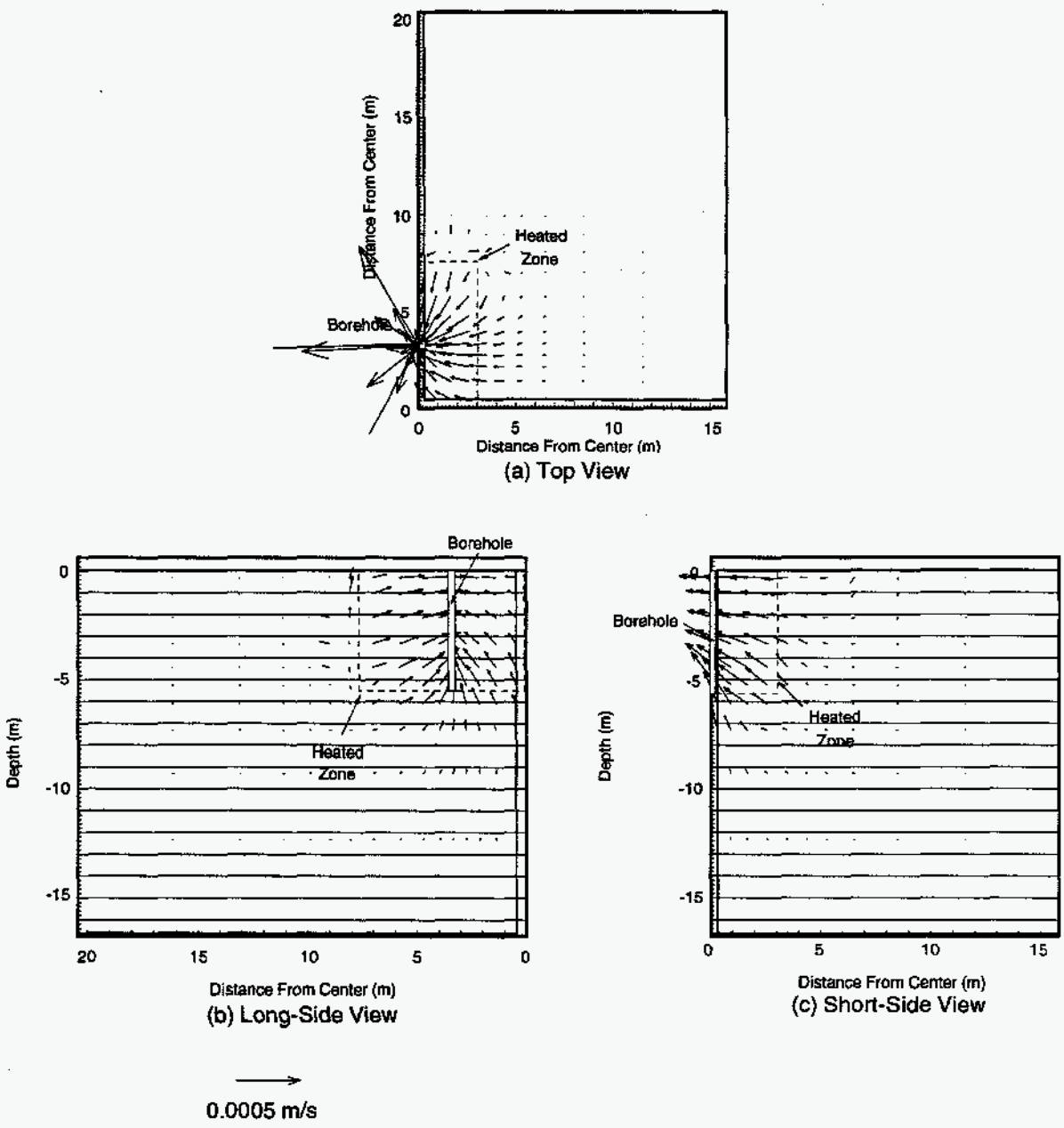

Figure 3-35. Gas velocity vectors at 60 days, 0.5 kPa vacuum, inside extraction
(a) Top view: K=4 plane
(b) Long-side view: I=3 plane
(c) Short-side view: J=3 plane

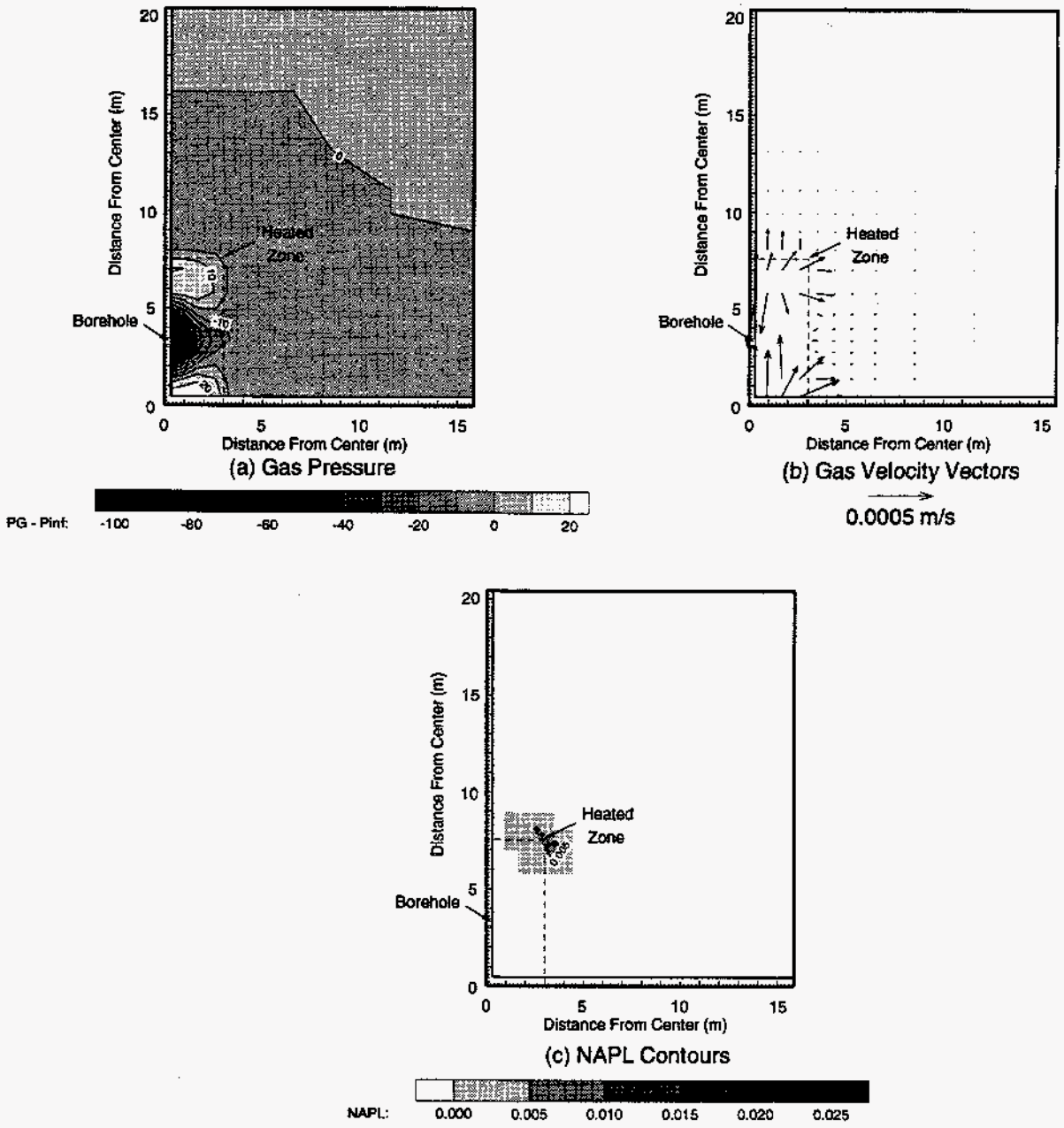

Figure 3-36. Details of NAPL migration into unheated zone at 15 days, 0.5 kPa vacuum, inside extraction, K=4 plane

Intentionally Left Blank

4.0 Simulation Results - Outside Extraction

The results in this section are for vapor extraction from the 4 outside vapor extraction wells. Figure 4-1 gives a schematic of the outside extraction model. Symmetry planes are noted in Figure 4-1a for the top view. Figures 4-1b and 4-1c give the side views for the model looking at the long and short side of the heated zone, respectively. Note that the wells in the outside extraction case are much deeper than for inside extraction as they extend below the heated zone. Due to quarter symmetry, only a single well is included in the present model. The results given in this section have been scaled to reflect the entire heated zone. Therefore, when masses or flow rates are given, they refer to the entire heated zone or to the 4 wells, not the results from the quarter symmetry model.

Figure 4-2 shows the model nodalization relative to the various features of the model. This figure shows the size and location of the elements. Boundary conditions are the same as for inside extraction. Plots are given for parameters at the center of each element, and the planes shown in the plots are labelled on Figure 4-2 for reference. Again, the K=1 plane is the insulation and vapor barrier and is not indicated on the figures.

4.1 2.5 kPa Borehole Vacuum

The time variation of the soil temperature in the heated zone (average, minimum, and maximum) out to 180 days is shown in Figure 4-3. Also included is the maximum soil temperature in the unheated zone. The maximum soil temperature in the heated zone increases over the first 10 days and then begins to level out as the liquid water evaporates. The temperature then starts to increase again at about 18 days. After 60 days, the heated zone average temperature is about 250°C; this temperature is just slightly higher than for the inside extraction case (246°C). At this time, the minimum and maximum heated zone temperatures are 98°C and 365 °C, respectively. The variation in temperatures is much greater for outside extraction then for inside extraction. After heating is stopped, temperatures rapidly decrease, and the average heated zone temperature is 41°C at 180 days. For the unheated zone, the maximum temperature is 147°C at 60 days, which continues to increase even when the heating is stopped, reaching a maximum of 151°C at 63 days. The maximum unheated zone temperature at 180 days is 48°C. All these unheated soil temperatures are slightly greater than for inside extraction. The differences between inside and outside extraction are reasonably small considering the large difference in gas flow rates, velocities, and flow patterns, indicating that heat losses to the air flowing through the soil is a minor factor in the overall heat balance.

Figures 4-4 through 4-6 show the temperature contours at 30, 60, 90, and 180 days looking from the top and sides of the model for the same planes as shown for the inside extraction model. The temperature contours are very similar to those given earlier for inside extraction.

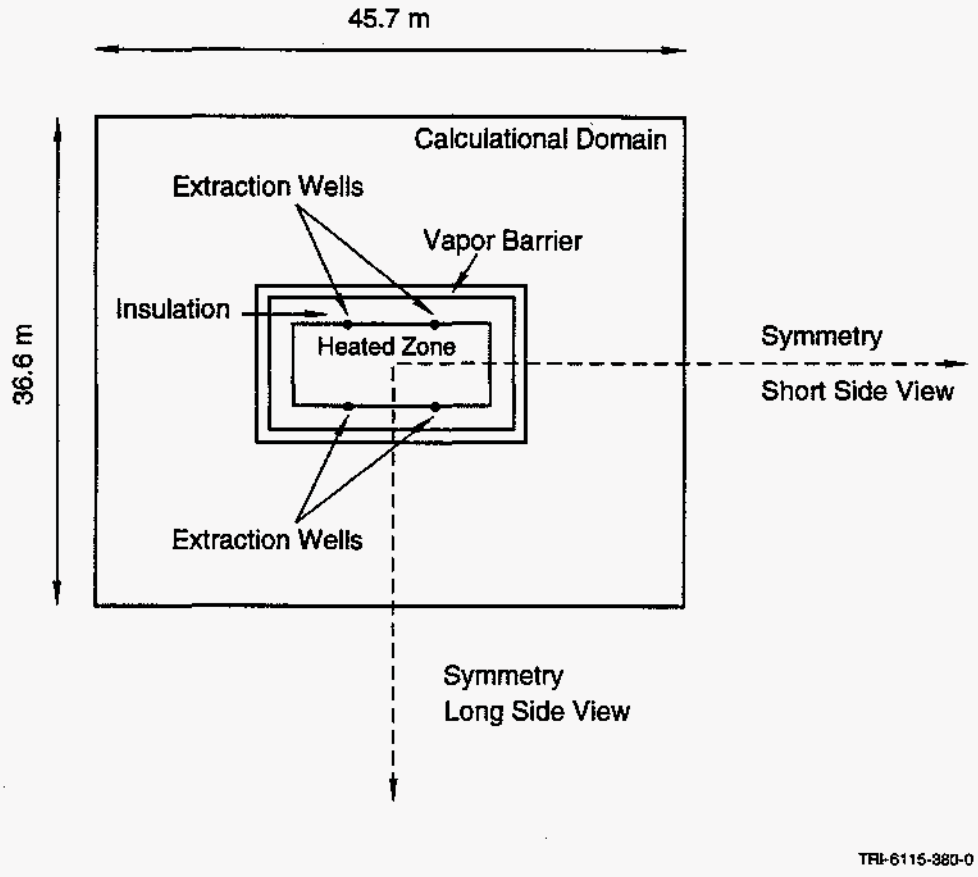

(a) top view

Figure 4-1. Outside extraction schematic

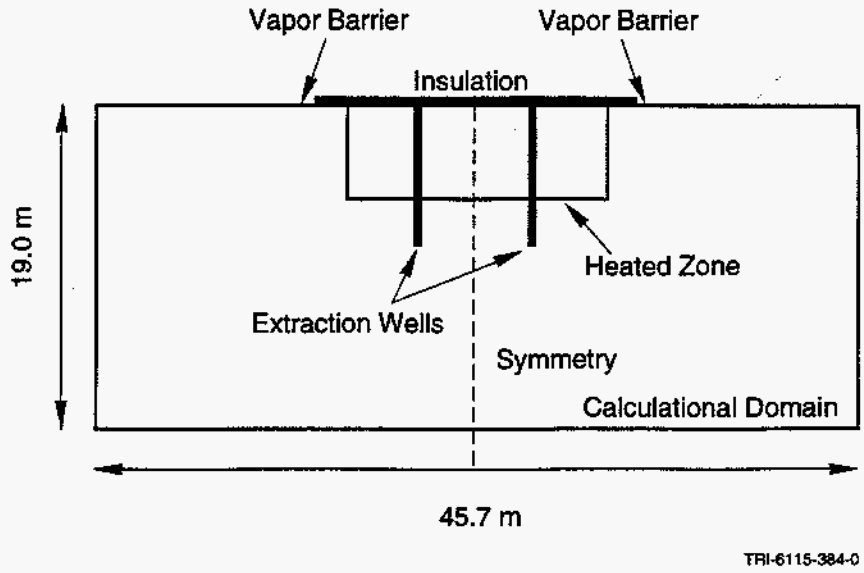

(b) long-side view

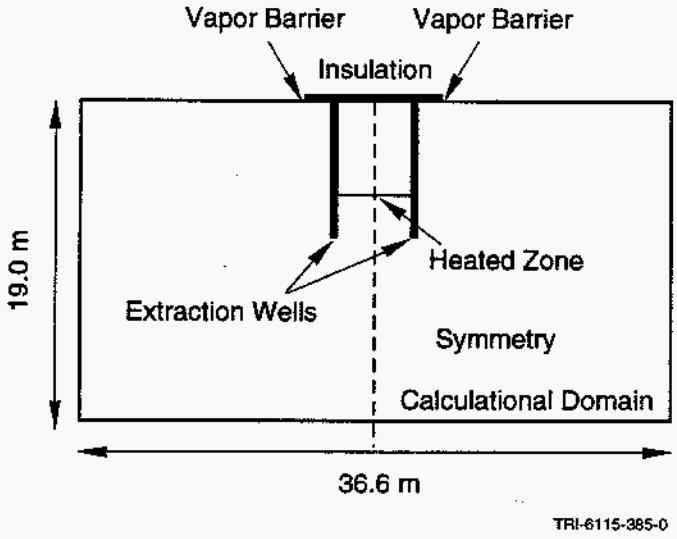

(c) short-side view

Figure 4-1. Outside extraction schematic, continued

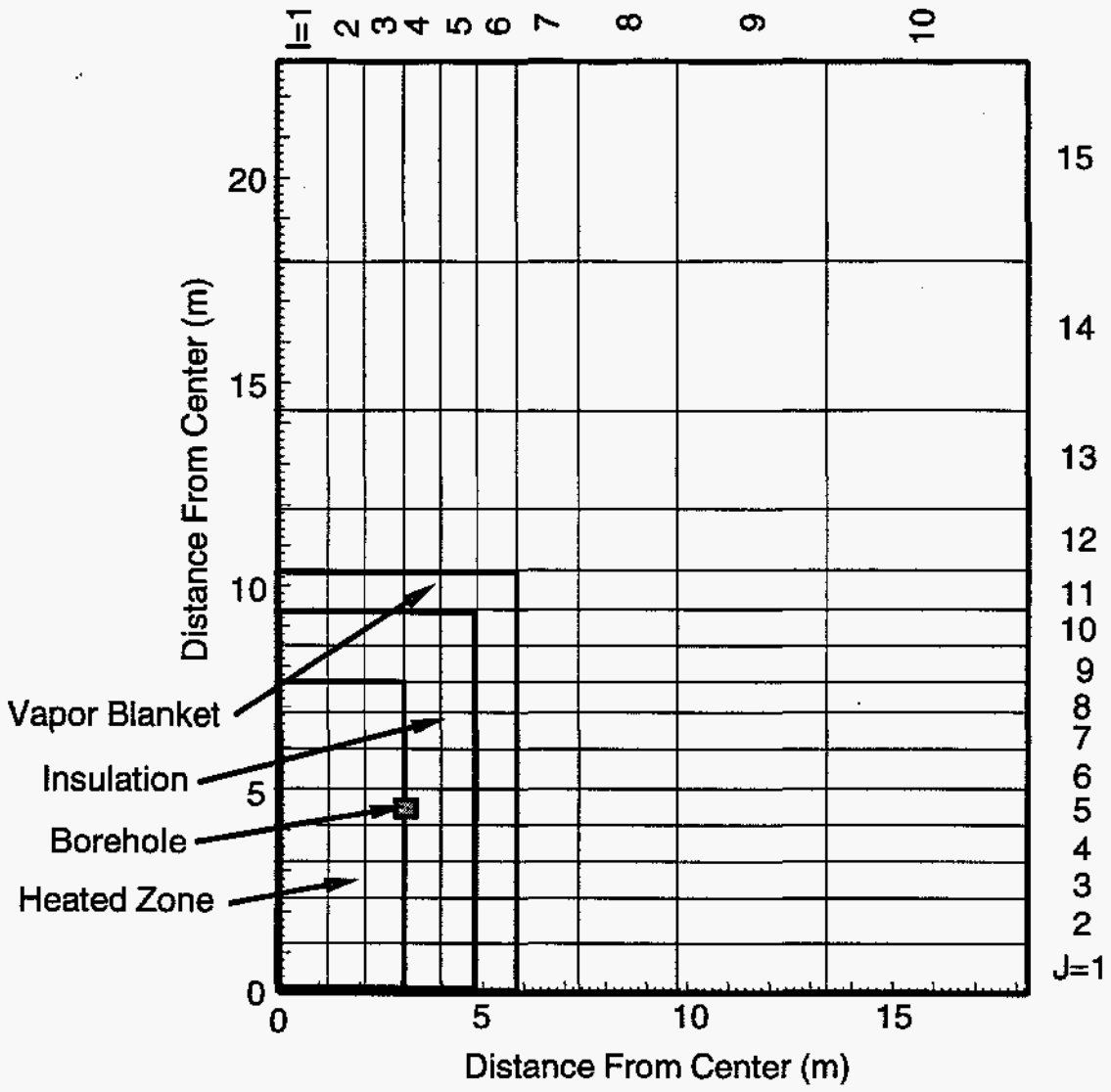

(a) top view

Figure 4-2. Outside extraction nodalization

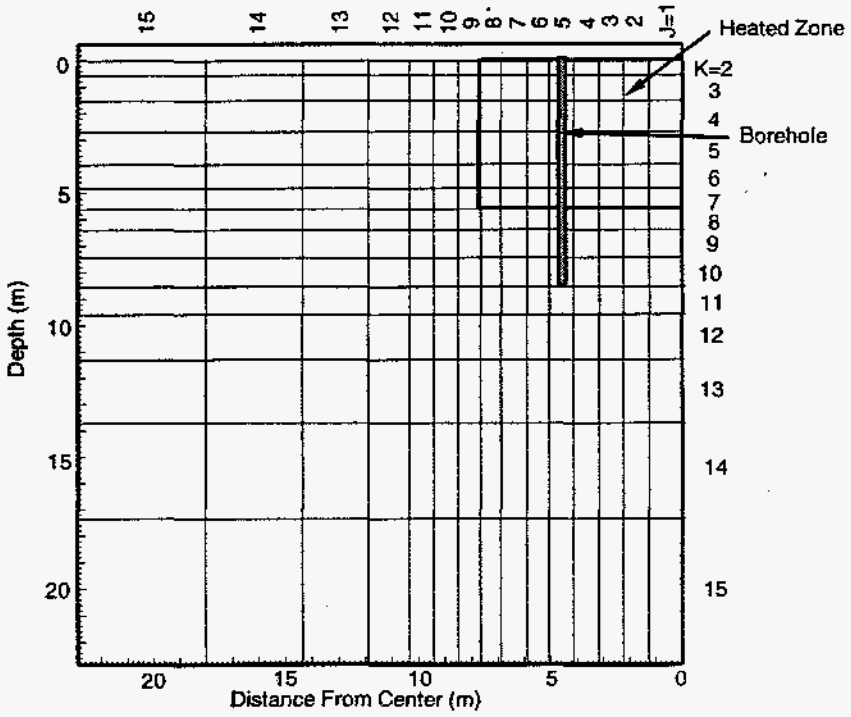

(b) long-side view

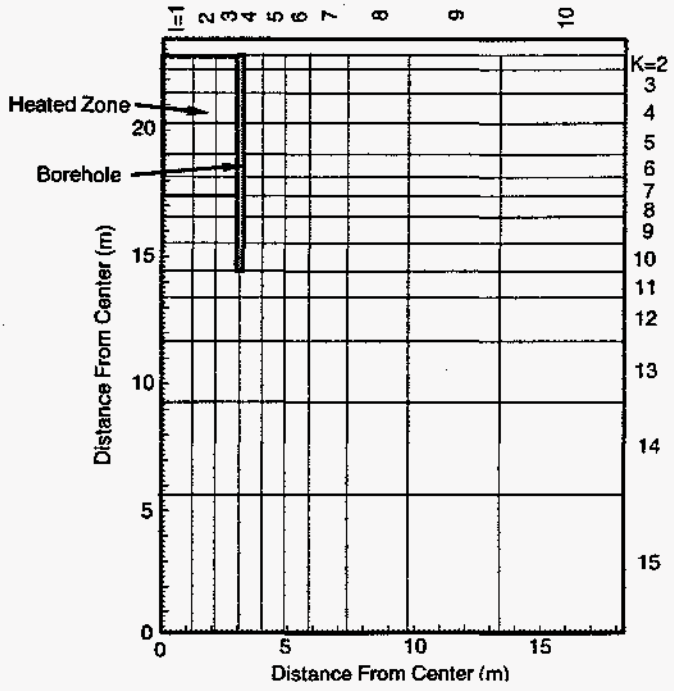

(c) short-side view

Figure 4-2. Outside extraction nodalization, continued

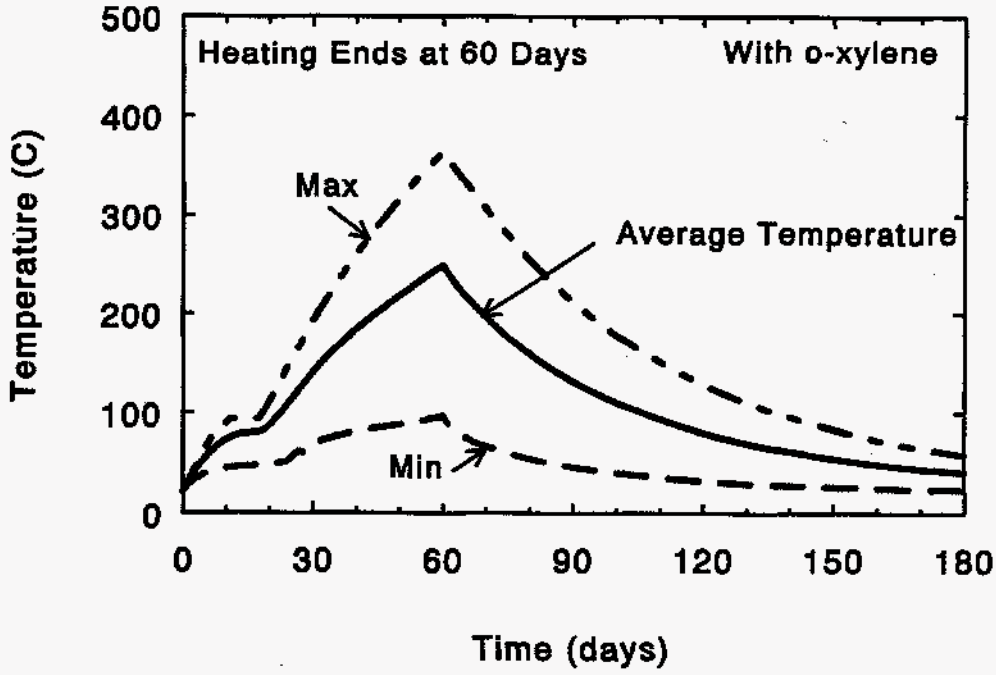

(a) Heated zone temperatures

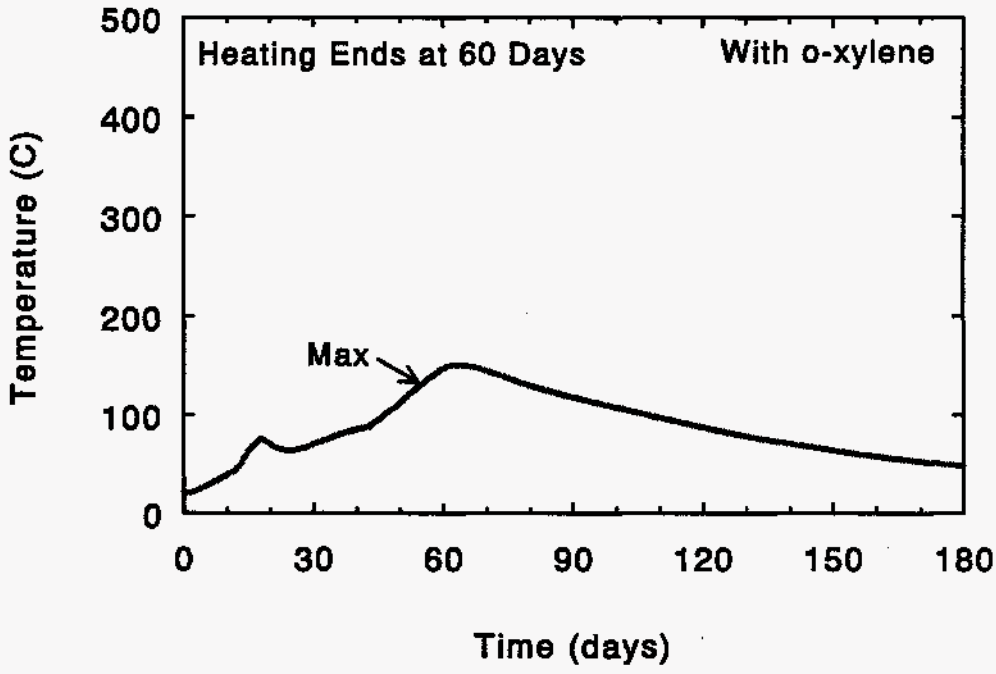

(b) Maximum unheated zone temperatures

Figure 4-3. Heated and unheated zone temperatures, outside extraction; 100 kW - 2.5 kPa (10" water) BH vacuum

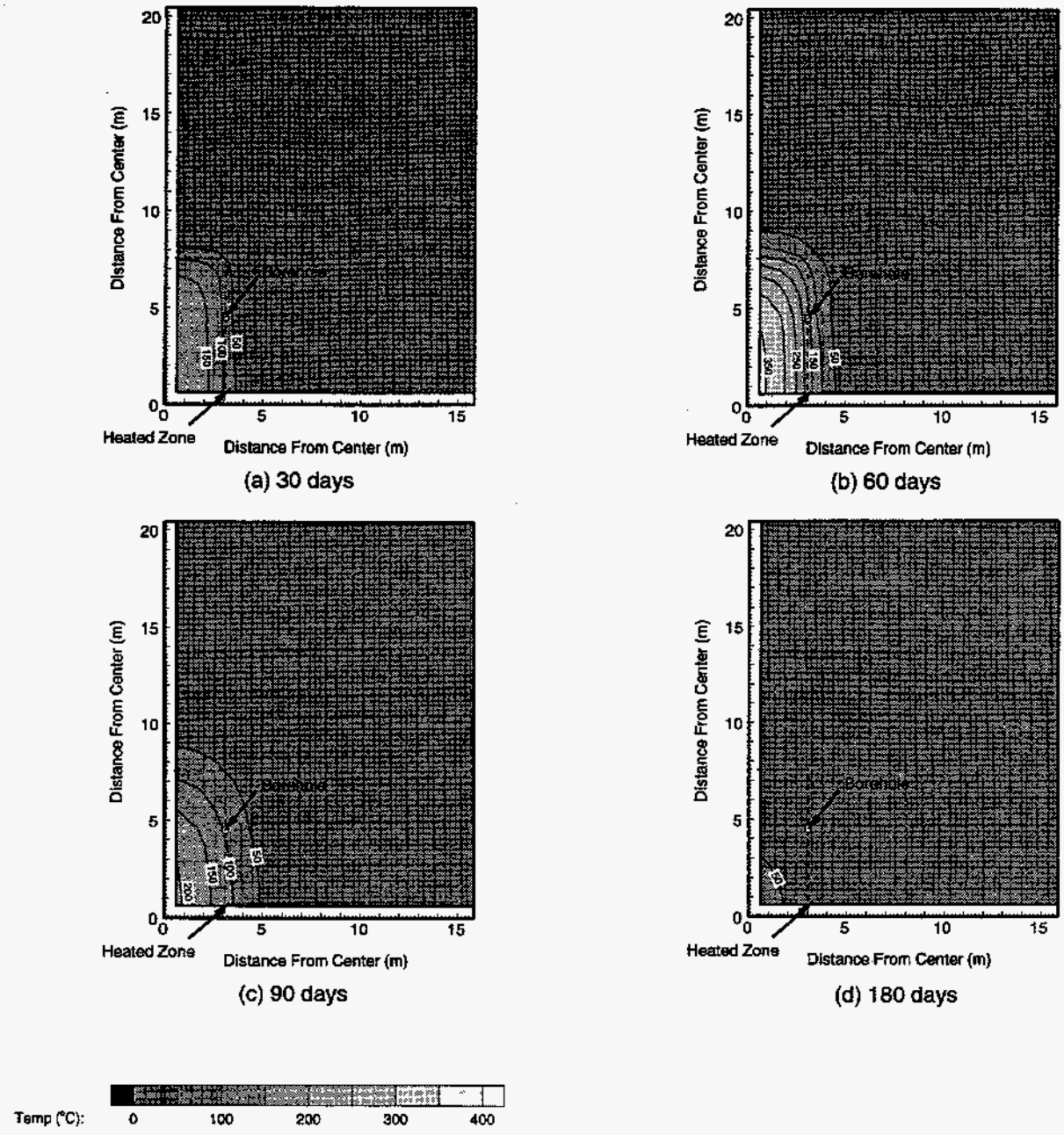

Figure 4-4. Temperature contours, top view, outside extraction 2.5 kPa vacuum, K=4 plane

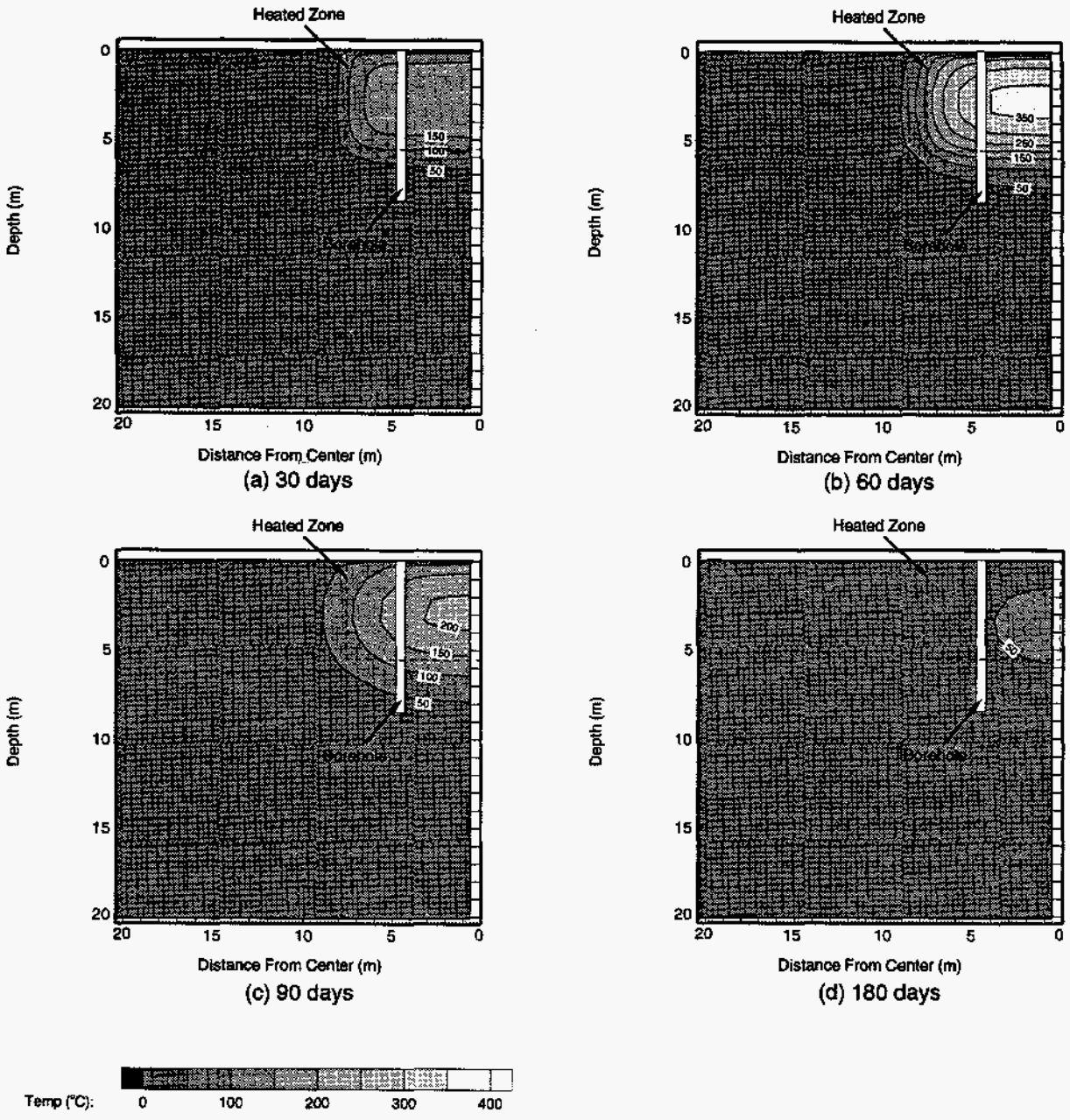

Figure 4-5. Temperature contours, long-side view, outside extraction 2.5 kPa vacuum, I=1 plane

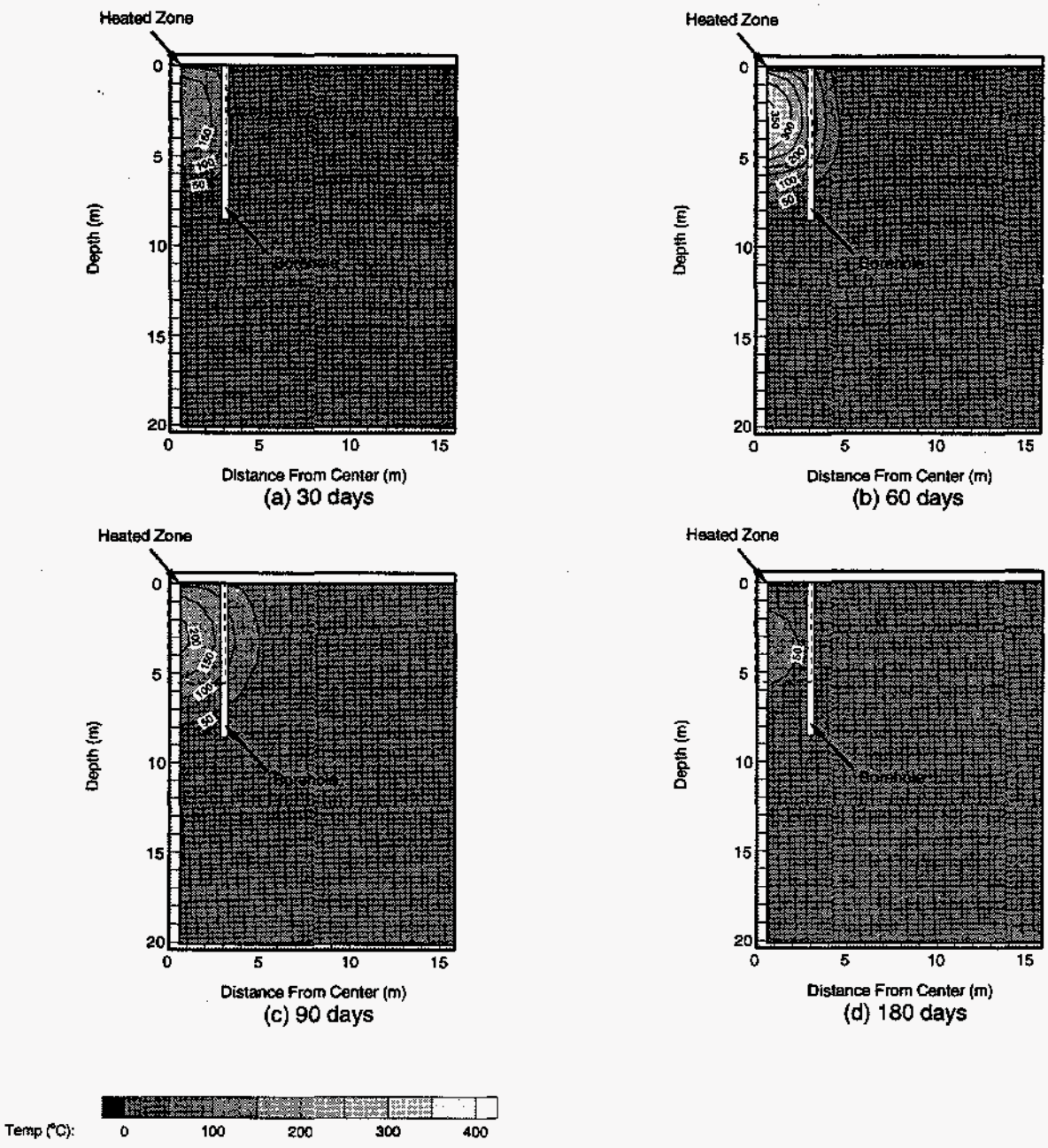

Figure 4-6. Temperature contours, short-side view, outside extraction 2.5 kPa vacuum, J=1 plane

Figure 4-7a shows the time variation of the water and NAPL liquid masses in the heated zone for the first 60 days. The liquid water in the heated zone decreases from an initial mass of 35,000 kg to 500 kg at 60 days; the rate of decrease is lower than for inside extraction probably due to differences in the flow rate through the heated zone. The value at 60 days in slightly lower than for inside extraction probably due to higher heated zone temperatures. Again, this water is due to an assumption in the VOC version of TOUGH2 and is not expected to be there in the actual situation. Figure 4-7a also shows the o-xylene liquid mass variation, which decreases from an initial 8000 kg and essentially disappears by 10 days. This slower evaporation rate for outside extraction is similar to the liquid water mass behavior. There is no migration of o-xylene from the heated zone to the unheated soil in the present case; all the o-xylene is evaporated and transported to the vapor extraction wells. Figure 4-7b shows the variation in the heated zone water mass for the entire transient. As with inside extraction, after heating is discontinued, the water mass in the heated zone increases slightly due to condensation of some of water vapor. As with temperatures, differences in the liquid masses are relatively small considering the significant difference in extraction location.

Early-time liquid water and NAPL saturation contours are shown in Figures 4-8 to 4-10 at 1.2 days (10^5 seconds) and 5 days. A low-flow zone exists between the borehole and the symmetry planes. Low air flow rates are expected in this region due to the symmetry of the problem. Figures 4-11 to 4-13 show later time liquid saturation contours at 11.6, 30, 60, and 180 days; the NAPL has disappeared at these later times. In general, the saturation contours for outside extraction are very similar to inside extraction with the exception of localized behavior between the borehole and the symmetry planes. The liquid saturation in the unheated zone continues to decrease even after heating is stopped due to evaporation into the air flowing to the borehole.

Figure 4-14a shows the various mass flow rates into the borehole. The total mass flow rate into the wells is considerably higher than for inside extraction due to the larger borehole surface area in the model and the borehole location. In the present model, the borehole pressure is held constant, so the flow is proportional to the borehole surface area. For outside extraction, the borehole is 8.5 m (28 ft) deep, and the total surface area is 5.7 m^2, while the inside wells are 5.6 m (18.5 ft) deep with a total surface area of 3.6 m^2. In addition, the outside wells are closer to the edge of the vapor blanket, so there is less resistance to flow for outside extraction than inside extraction. The result is than the flow rate is up to 4 times higher for outside extraction. Figure 4-14b shows the evaporation rate in the heated and unheated zones along with the water vapor flow rate into the borehole. The water vapor flow rate into the borehole is higher than for inside extraction due to the higher air flow rate in the unheated zone and the resulting evaporation. As in the case of inside extraction, the heated zone evaporation rate is negative after heating is stopped since condensation is occurring. The unheated zone evaporation rate is always positive, indicating no migration of water from the heated soil into the unheated zone.

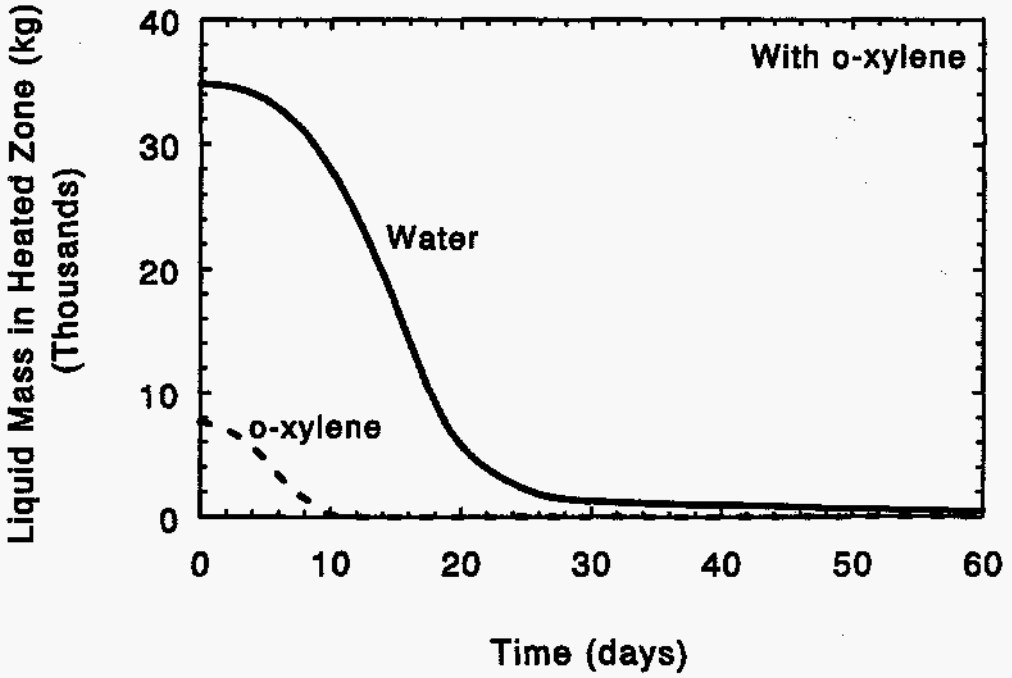

(a) Heated zone fluid masses - 0 to 60 days

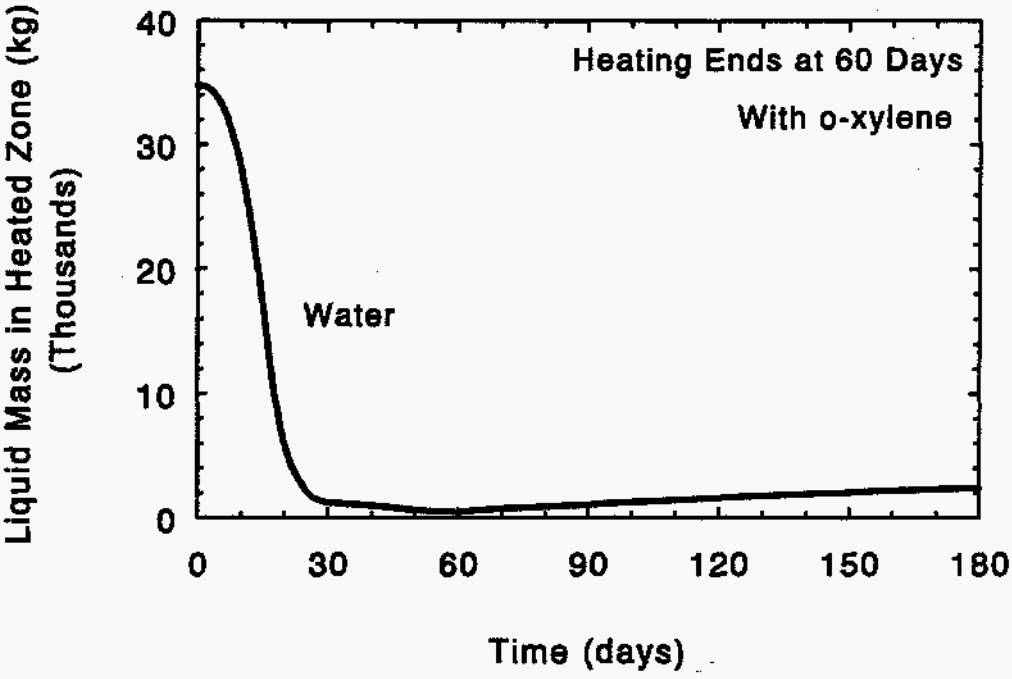

(b) Heated zone water mass

Figure 4-7. Heated zone fluid and water masses, outside extraction, 100 kW, 2.5 kPa (10" water) BH vacuum

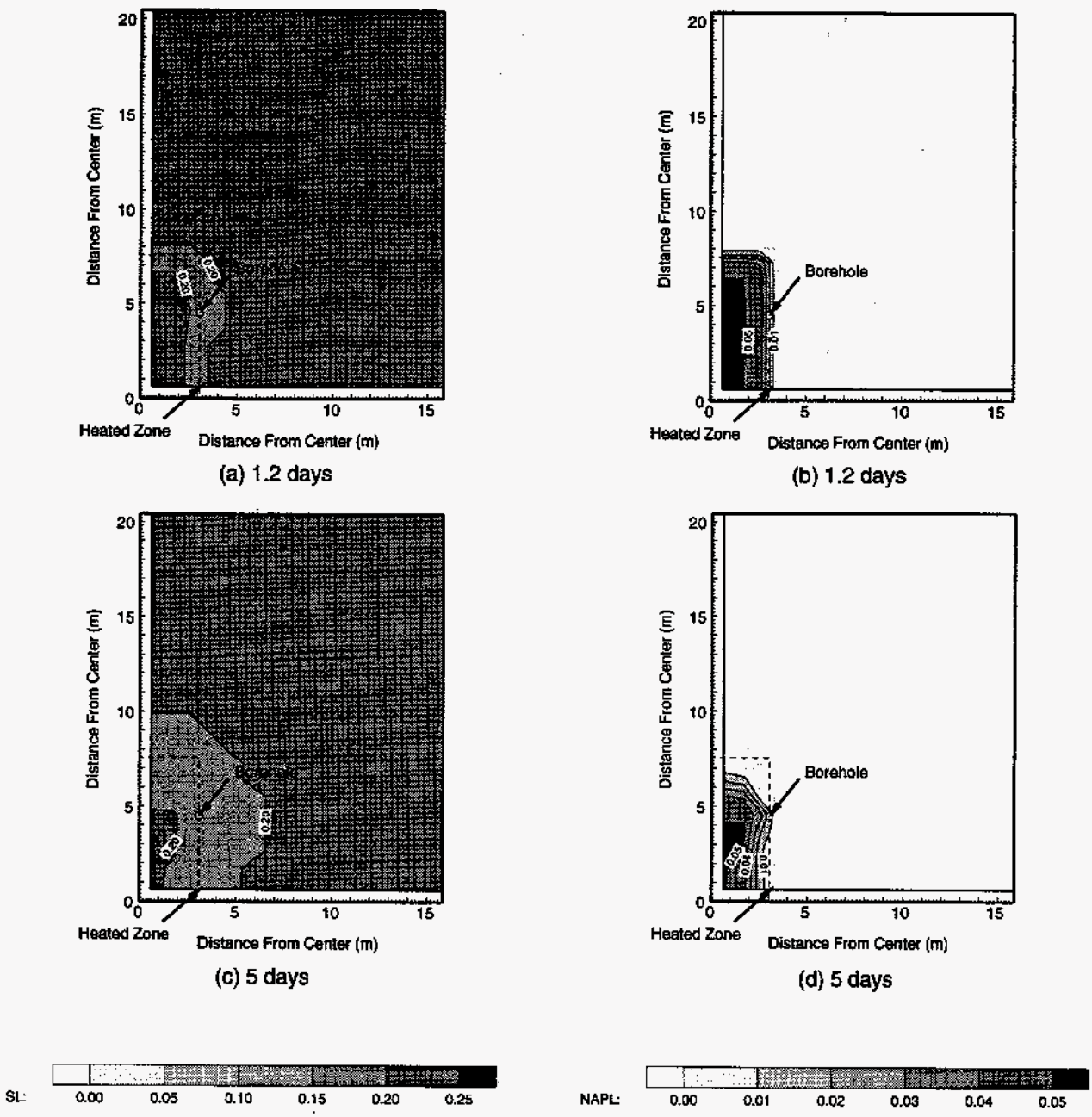

Figure 4-8. Early-time water (left diagram) and NAPL (right diagram) saturation contours, 2.5 kPa vacuum, top view, outside extraction, K=4 plane

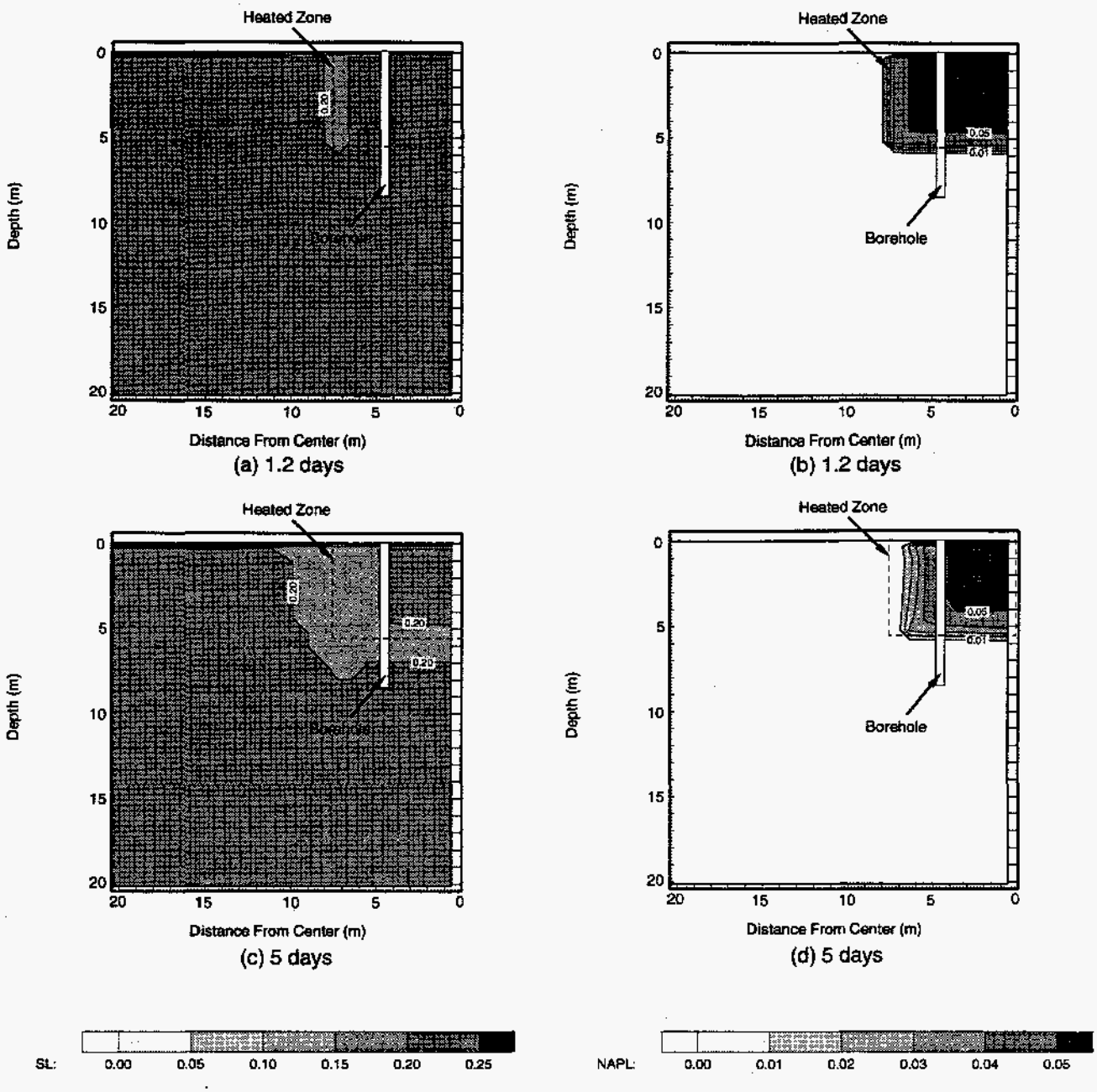

Figure 4-9. Early-time water (left diagram) and NAPL (right diagram) saturation contours, 2.5 kPa vacuum, long-side view, outside extraction, I=1 plane

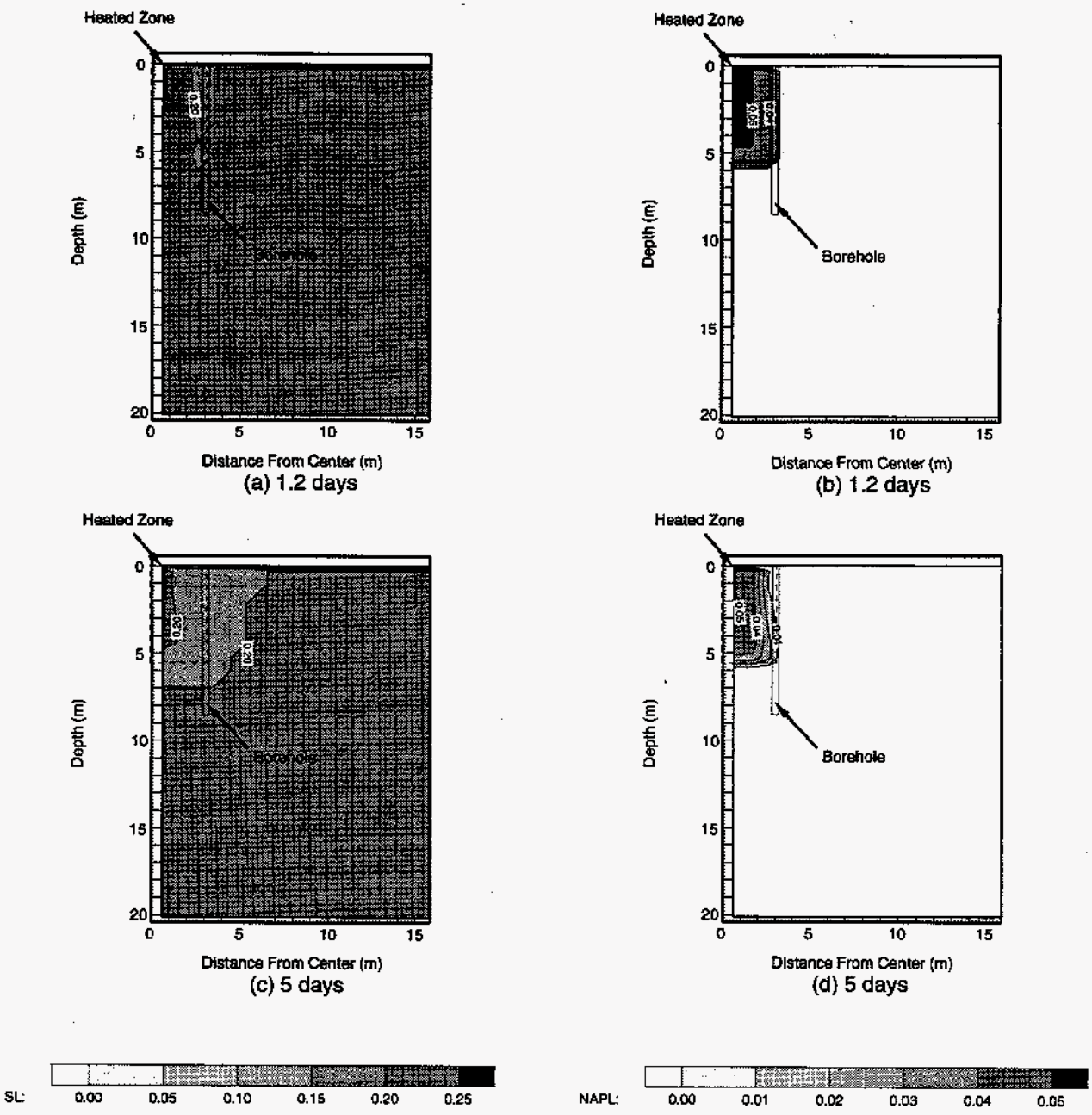

Figure 4-10. Early-time water (left diagram) and NAPL (right diagram) saturation contours, 2.5 kPa vacuum, short-side view, outside extraction, J=1 plane

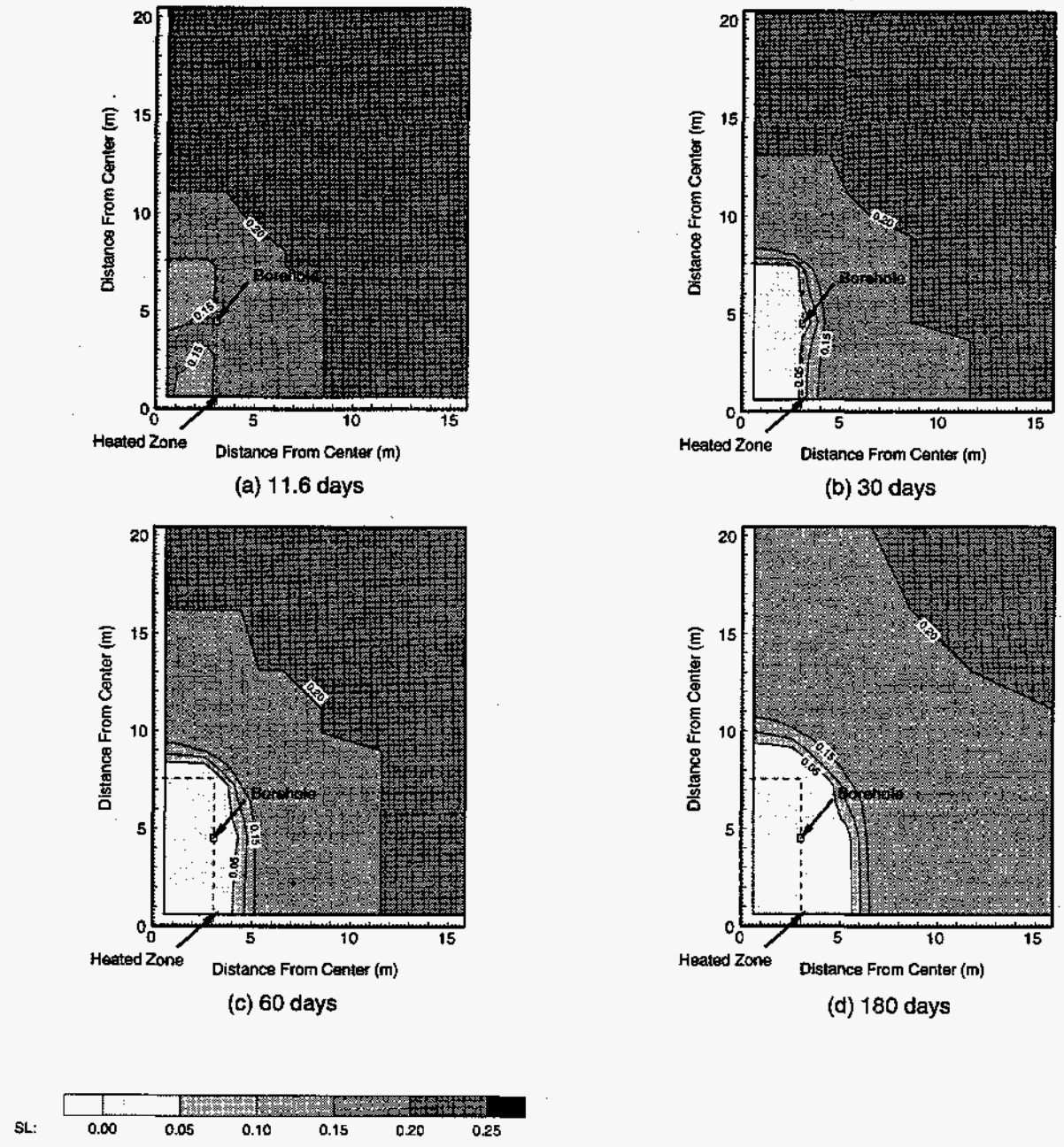

Figure 4-11. Late-time water saturation contours, 2.5 kPa vacuum, outside extraction, top view, K=4 plane

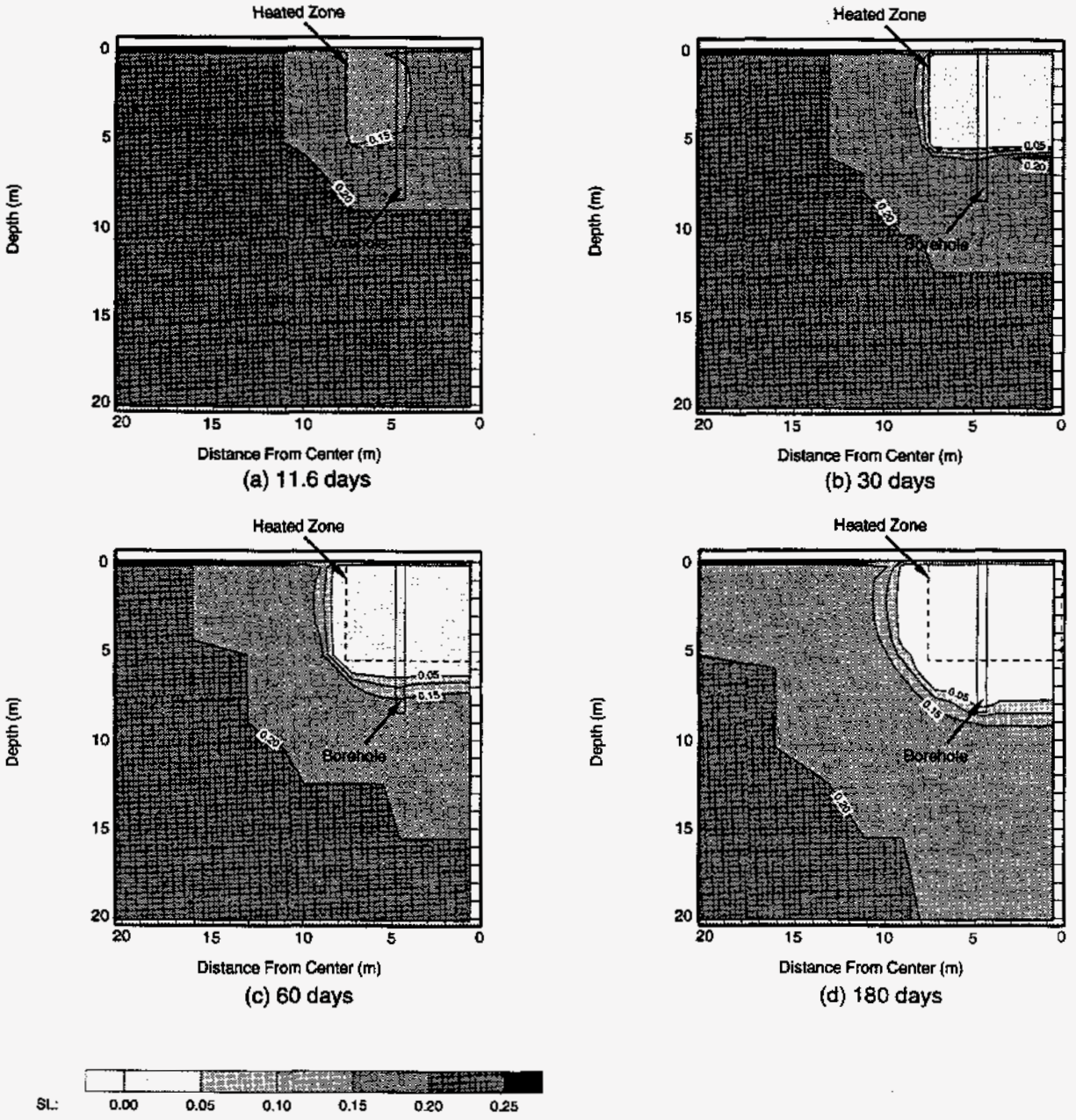

Figure 4-12. Late-time water saturation contours, 2.5 kPa vacuum, outside extraction, long-side view, I=1 plane

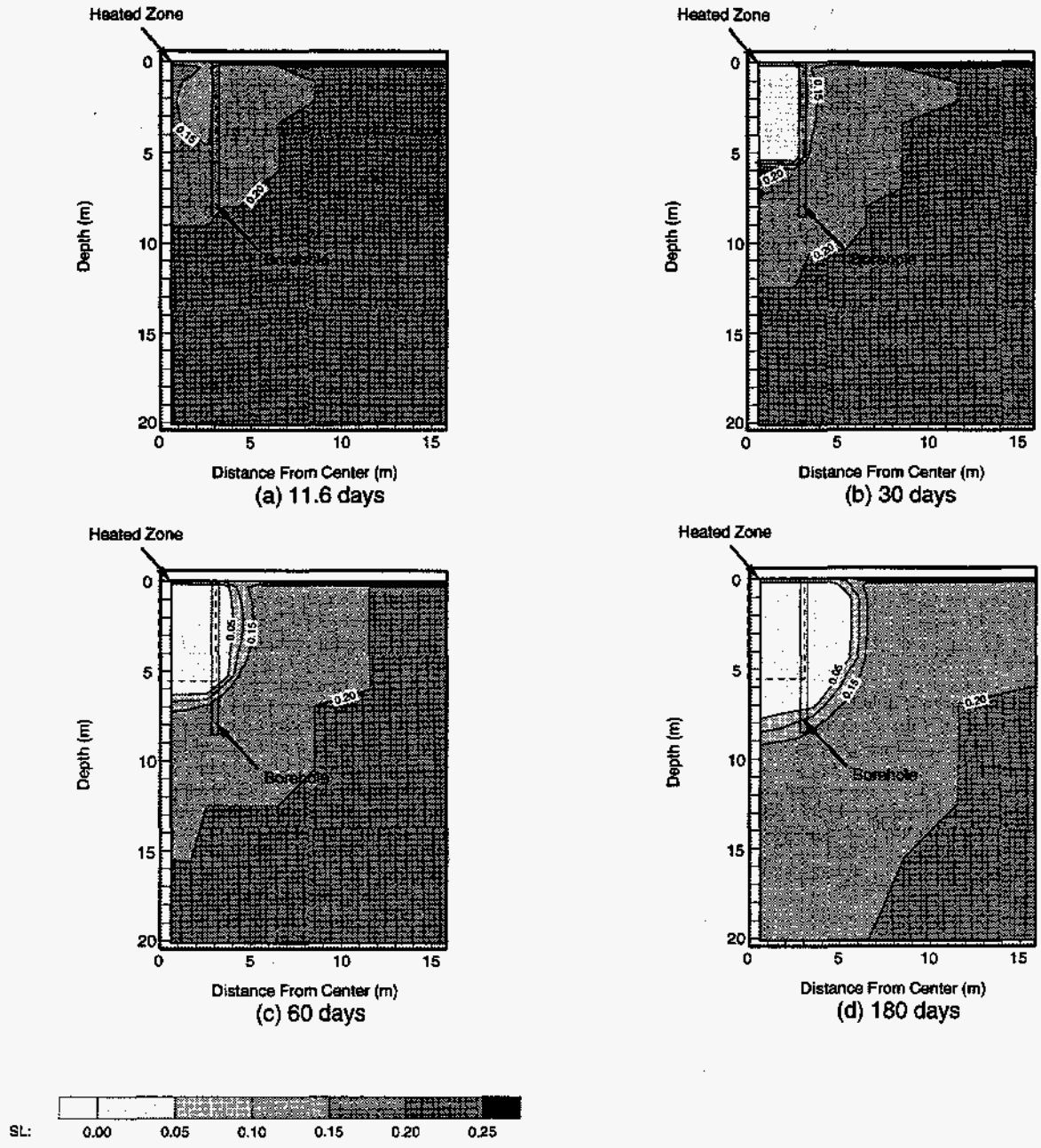

Figure 4-13. Late-time water saturation contours, 2.5 kPa vacuum, outside extraction, short-side view, J=1 plane

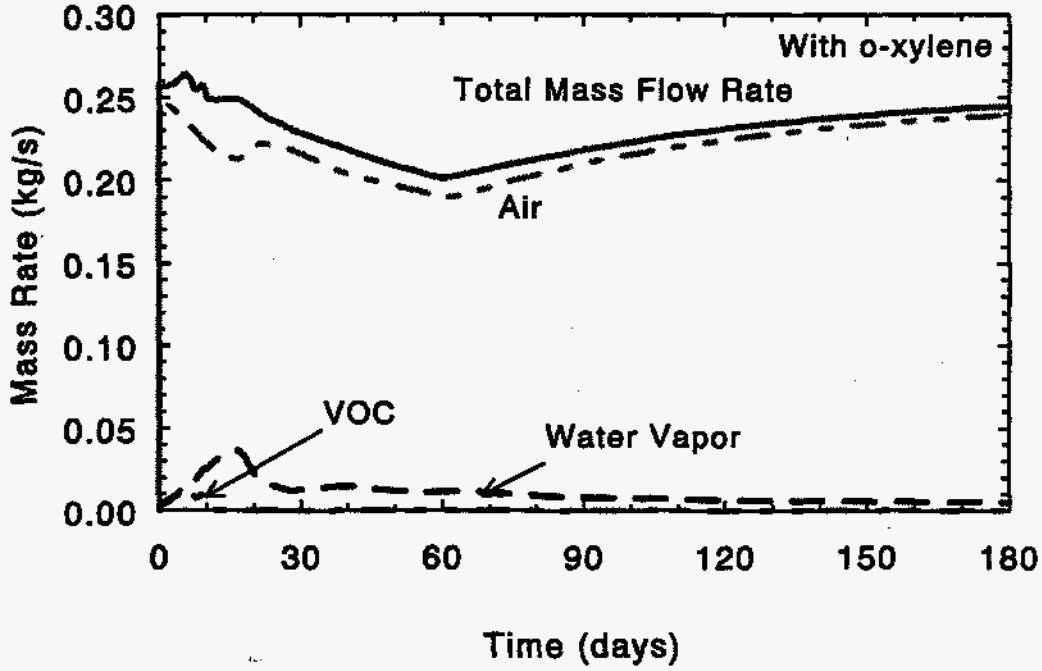

(a) Mass flow rates into boreholes

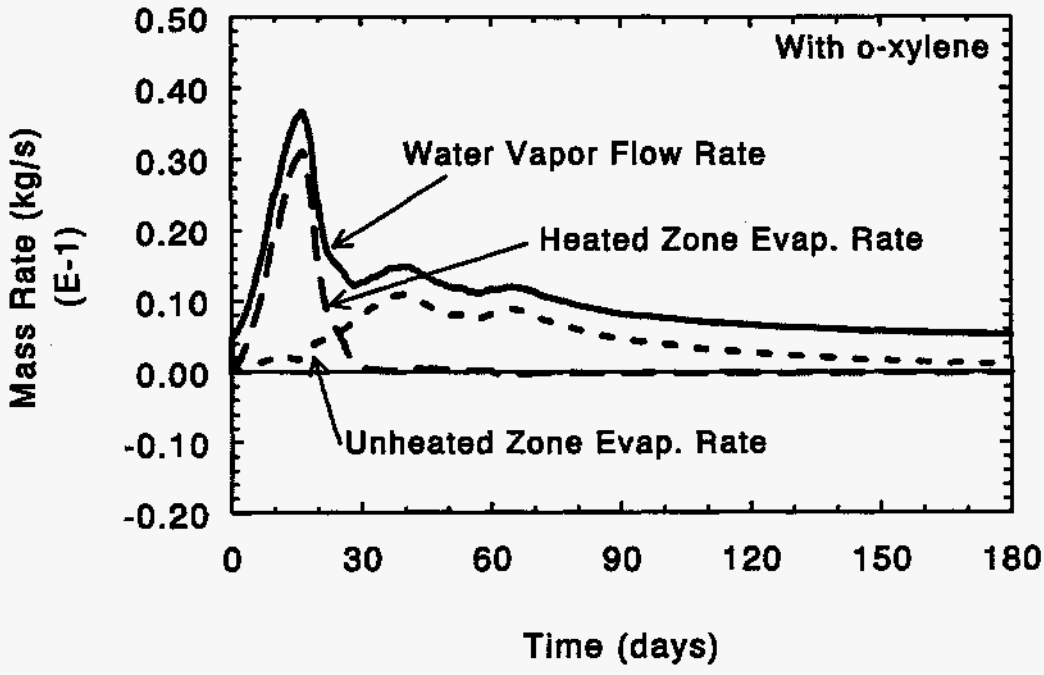

(b) Evaporation and water vapor mass rates

Figure 4-14. Mass rates, outside extraction, 100 kW, 2.5 kPa (10" water) BH vacuum

Similar to inside extraction, gas velocity vectors do not vary significantly with time. Gas flow velocity vectors at 60 days are shown in Figure 4-15 for all three views. As expected, the flow patterns are considerably different for outside extraction than for inside extraction. For inside extraction, all air flow passed through the heated zone before entering the borehole; in the outside extraction case, probably the majority of the flow comes from the unheated zone, so the air sweep is not as efficient as for inside extraction. A region of flow from the heated zone into the unheated soil is present in the lower corner of the long-side view since the borehole extraction depth is greater than the heated zone depth. Also, a low-flow region exists from the borehole towards the symmetry planes. This region is also obvious in the saturation plots shown earlier.

4.2 1.0 kPa Borehole Vacuum

Figures 4-16a and 4-16b show the heated and unheated zone temperatures, respectively. As for inside extraction, the temperature history is very similar to the 2.5 kPa borehole vacuum results presented earlier. The heated zone average, maximum, and minimum temperatures for the 1.0 kPa borehole vacuum are 258°C, 372°C, and 109°C, respectively, at 60 days, while the maximum unheated zone temperature is 155°C at 60 days. These temperatures are generally about 7°C higher than for 2.5 kPa. The temperature contours are very similar to the 2.5 kPa results; Figure 4-17 presents the temperature contours at 60 days.

Figure 4-18a summarizes the liquid water and NAPL mass variation in the heated zone with time. The evaporation rate is a little slower for the lower borehole vacuum, as the NAPL disappears within about 12 days compared to 10 days for the 2.5 kPa case. As shown in Figure 4-18b, migration of NAPL into the unheated zone occurs for this case starting at about 10 days. The maximum amount of NAPL in the unheated zone is about 370 kg, or just less than 5% of the initial NAPL mass in the heated zone. This maximum value occurs at about 13 days, or about the same time the NAPL disappears in the heated zone. Due to continued heating and venting, the NAPL eventually evaporates completely at 27 days.

Figures 4-19 through 4-21 show the various views of the liquid water and NAPL saturation contour plots at 1.2 days (10^5 seconds), 8 days, and 11.6 days. The early time liquid water and NAPL contours are very similar to the 2.5 kPa case, as a "dead" zone, or low flow rate zone, appears near the borehole toward the symmetry planes. However, in the lower borehole vacuum case, some NAPL pockets remain near the top and bottom of the heated zone toward the symmetry planes as seen in Figures 4-20f and 4-21f. The pocket at the bottom of the heated zone eventually migrates into the unheated soil.

Figures 4-22 through 4-24 present the liquid water saturation contours at 30 and 60 days for the various views. Liquid water saturations higher than 20% are seen at the same locations as the NAPL pockets described above, indicating water migration into the unheated zone. At 60 days, most of the migrated water has evaporated, although there still are some higher saturation zones.

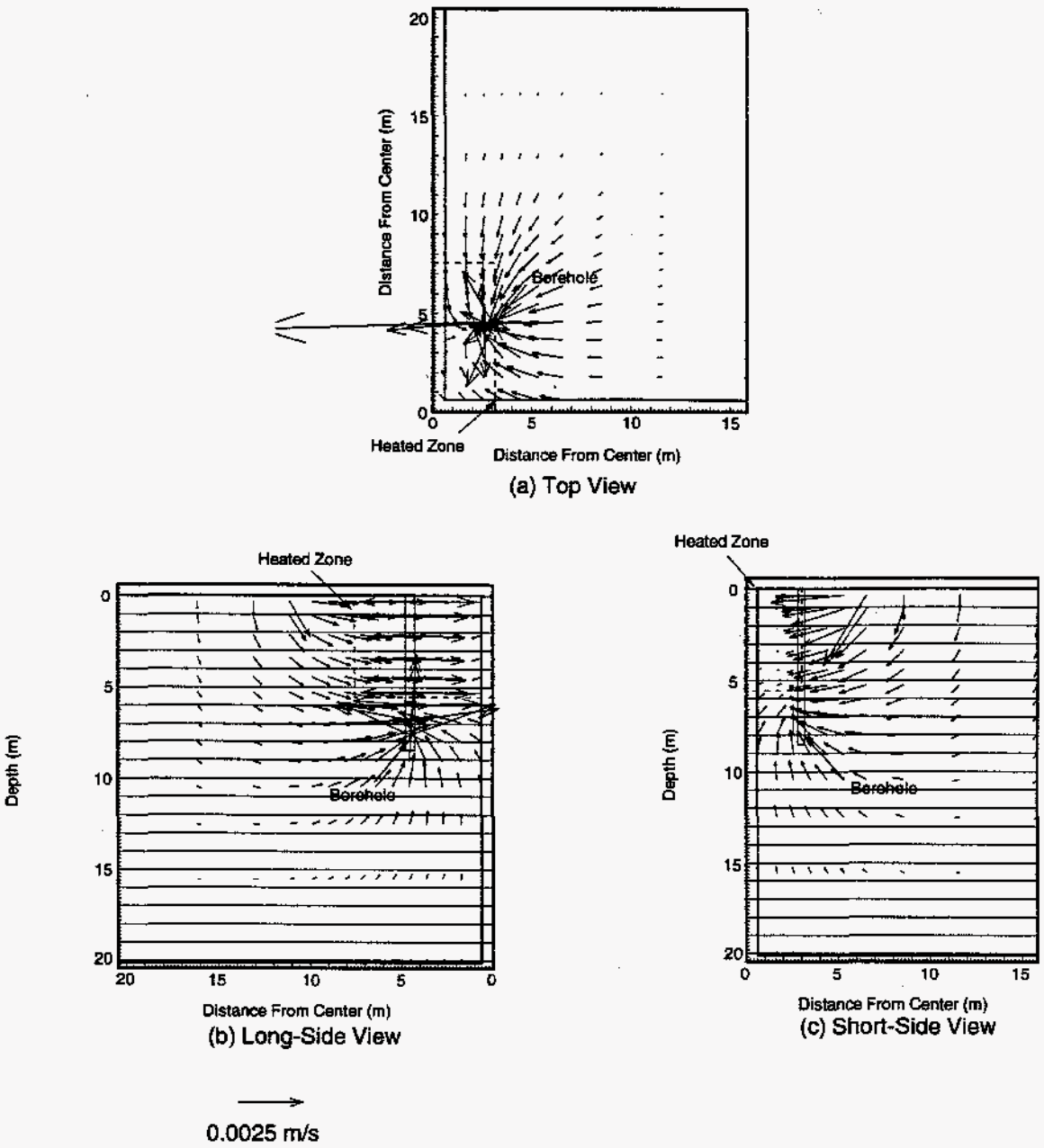

Figure 4-15. Gas velocity vectors at 60 days, 2.5 kPa vacuum, outside extraction
(a) Top view: K=4 plane
(b) Long-side view: I=3 plane
(c) Short-side view: J=3 plane

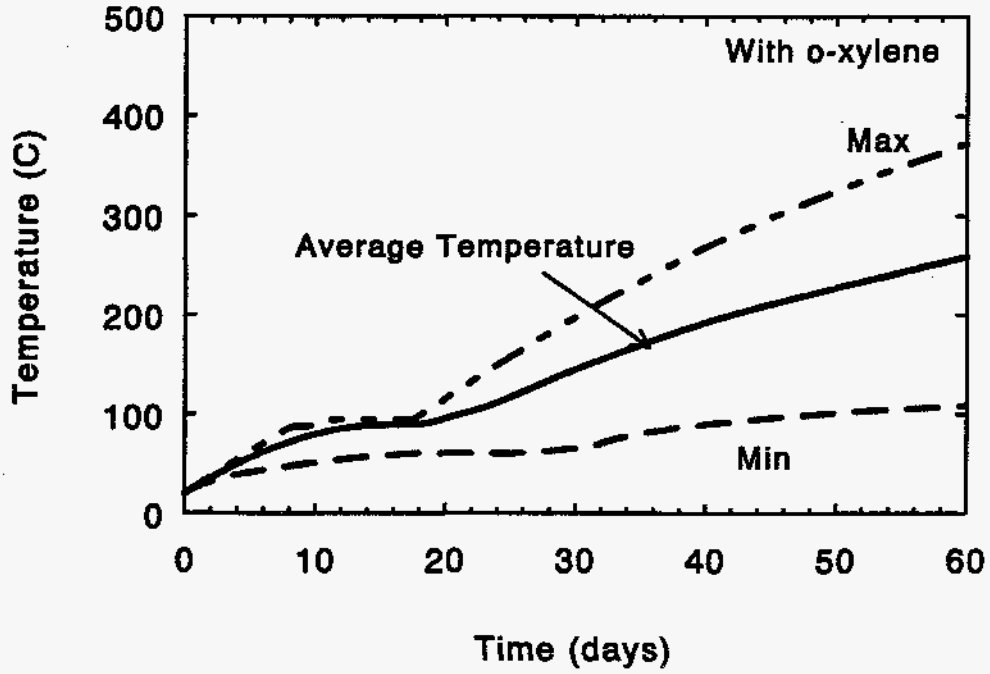

(a) Heated zone temperatures

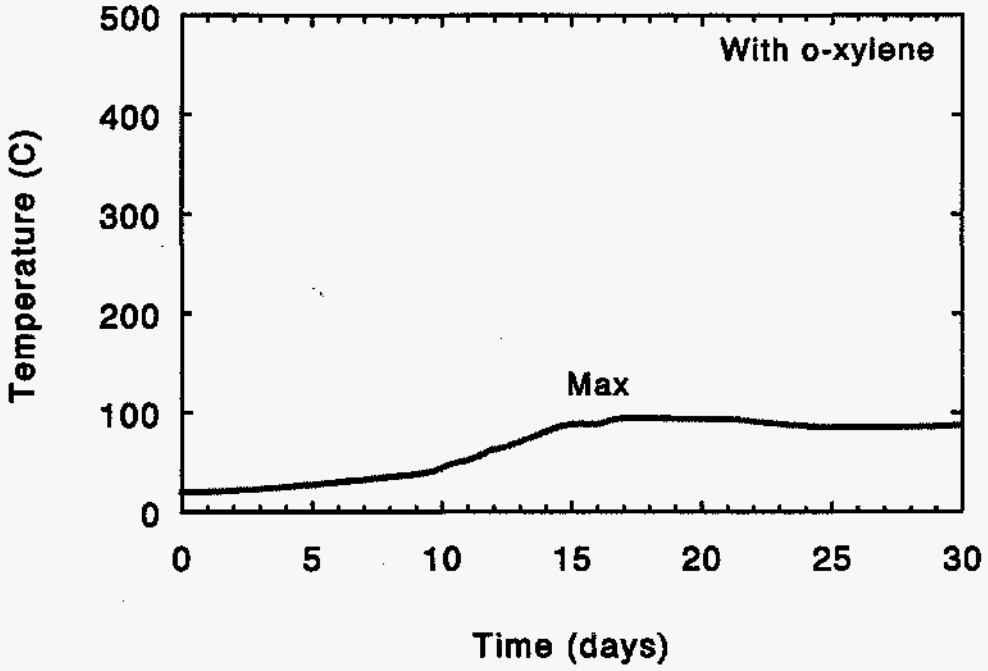

(b) Maximum unheated zone temperatures

Figure 4-16. Heated and unheated zone temperatures, outside extraction; 100 kW - 1.0 kPa (4" water) BH vacuum

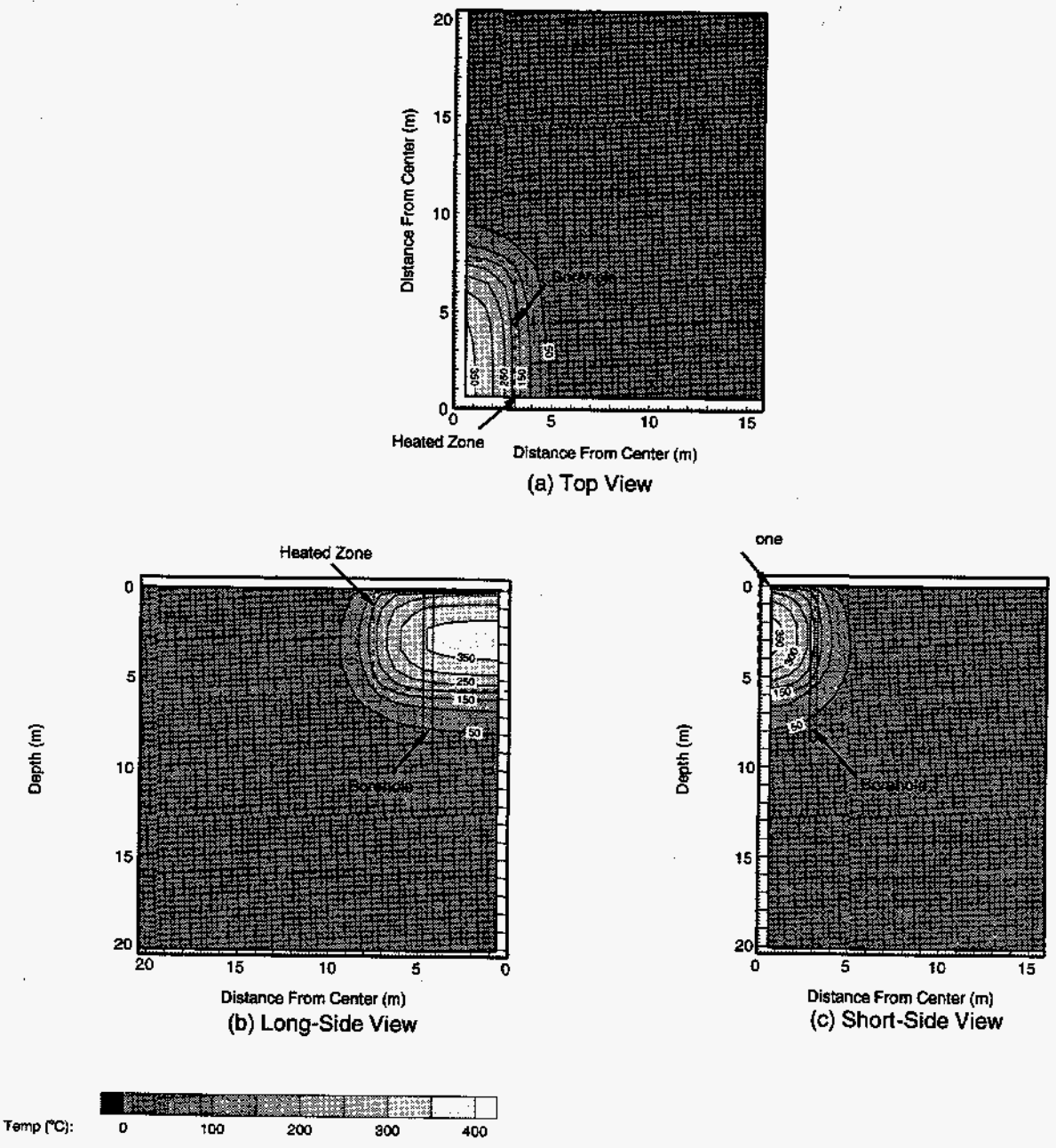

Figure 4-17. Temperature contours, at 60 days, outside extraction 1.0 kPa vacuum
(a) Top view: K=4 plane
(b) Long-side view: I=1 plane
(c) Short-side view: J=1 plane

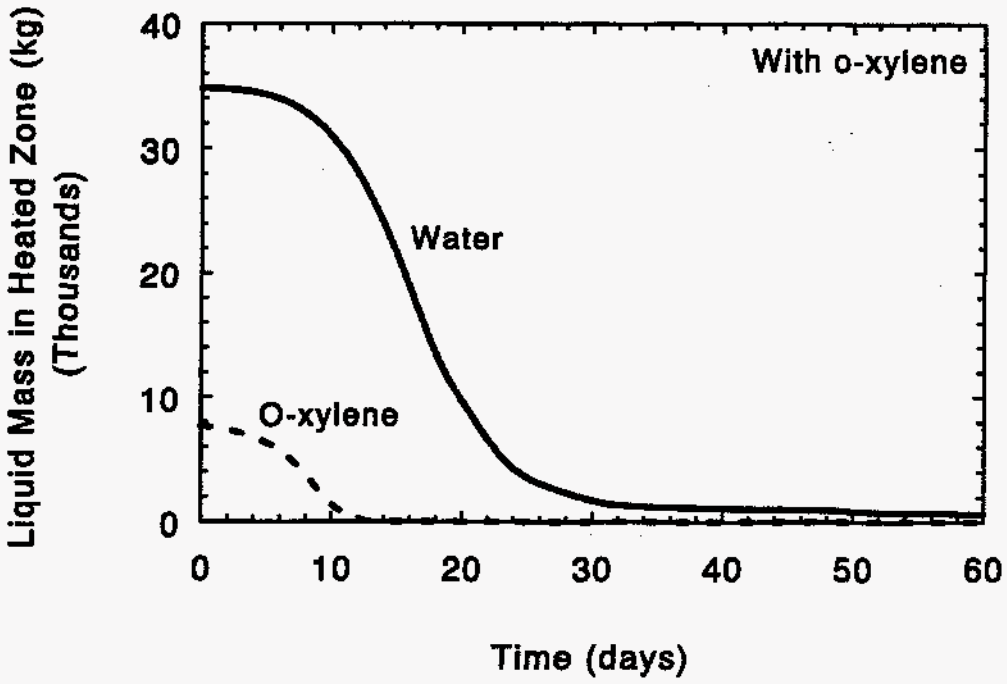

(a) Heated zone fluid mass

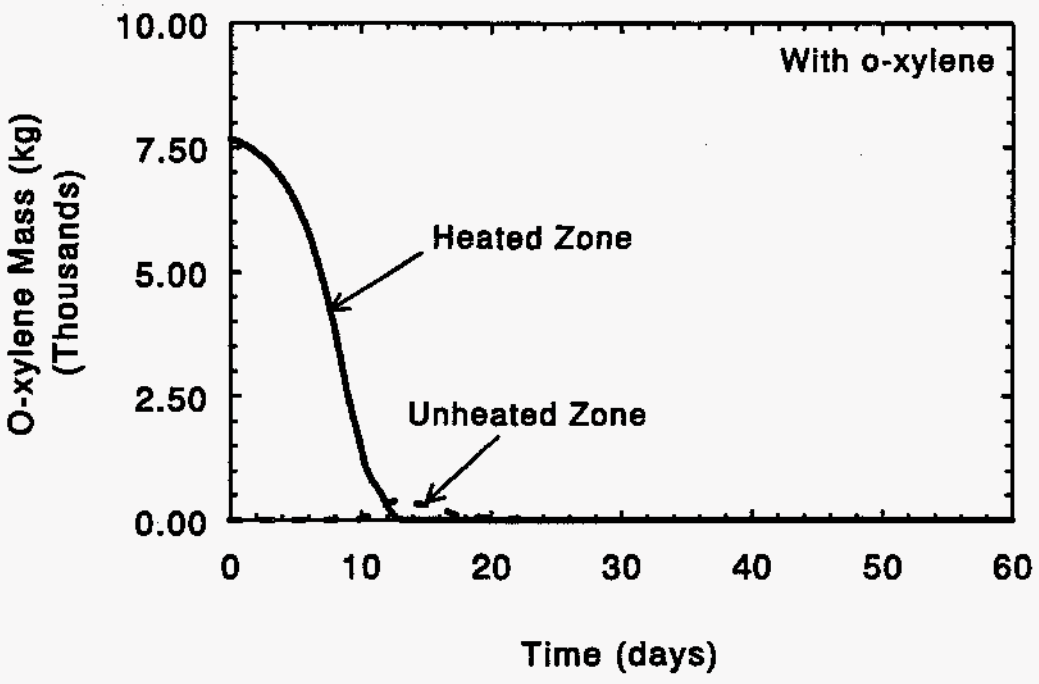

(b) O-xylene mas variation

Figure 4-18. Heated zone fluid masses and O-xylene mass variation, outside extraction, 100 kW, 1.0 kPa (4" water) BH vacuum

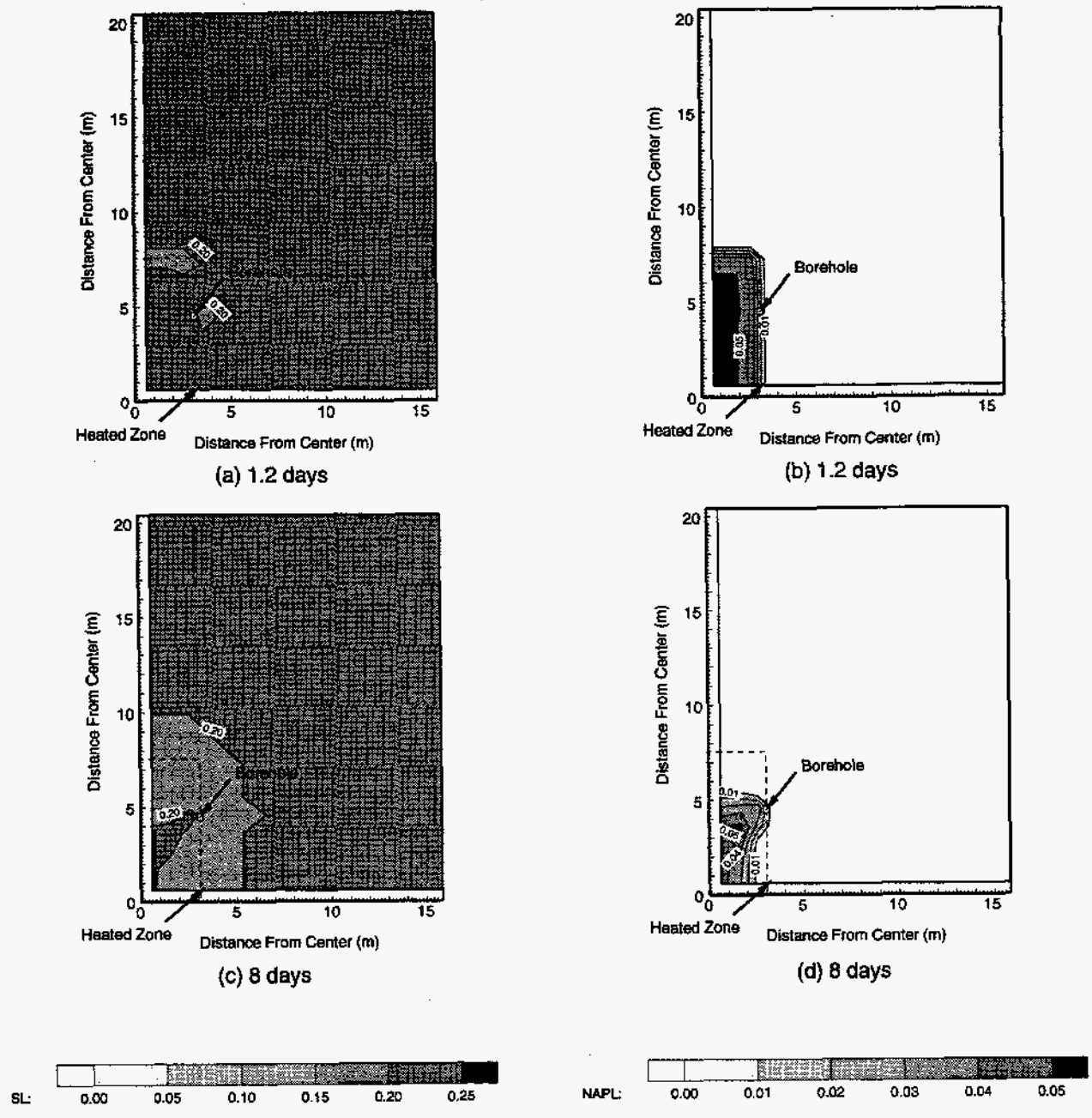

Figure 4-19. Early-time water (left diagram) and NAPL (right diagram) saturation contours, 1.0 kPa vacuum, top view, outside extraction, K=4 plane

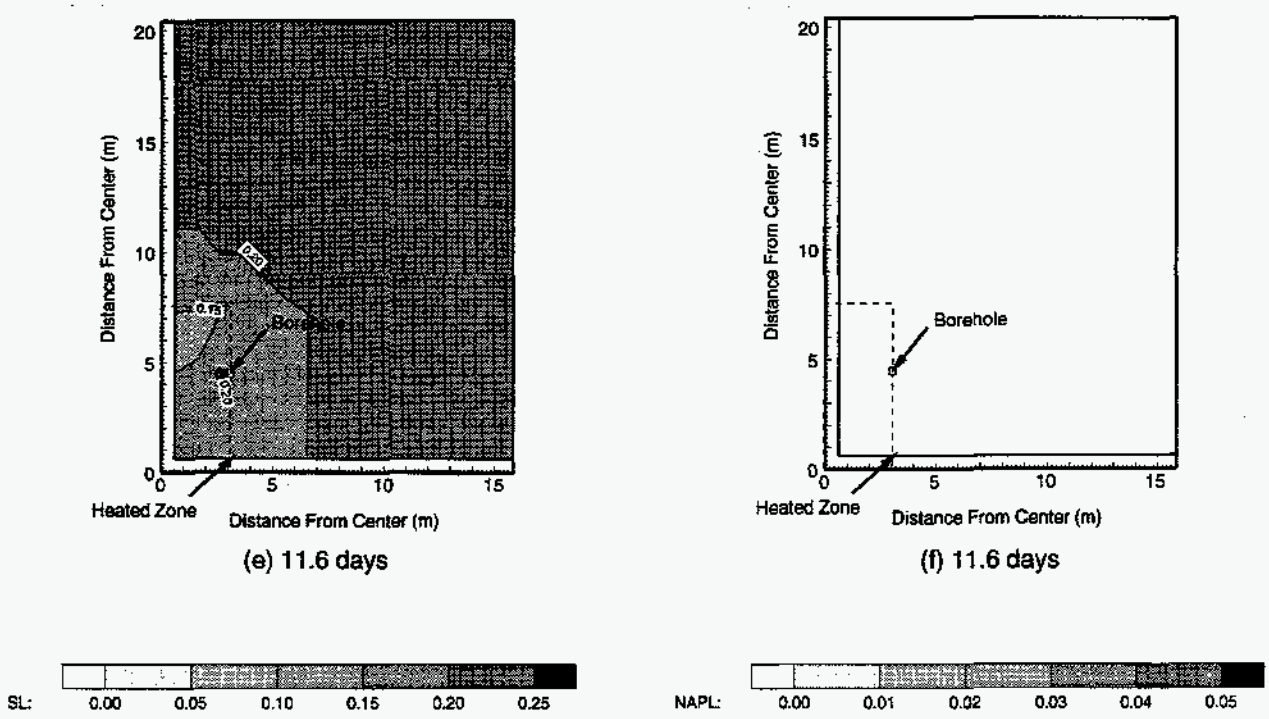

Figure 4-19. Early-time water (left diagram) and NAPL (right diagram) saturation contours, 1.0 kPa vacuum, top view, outside extraction, K=4 plane, continued

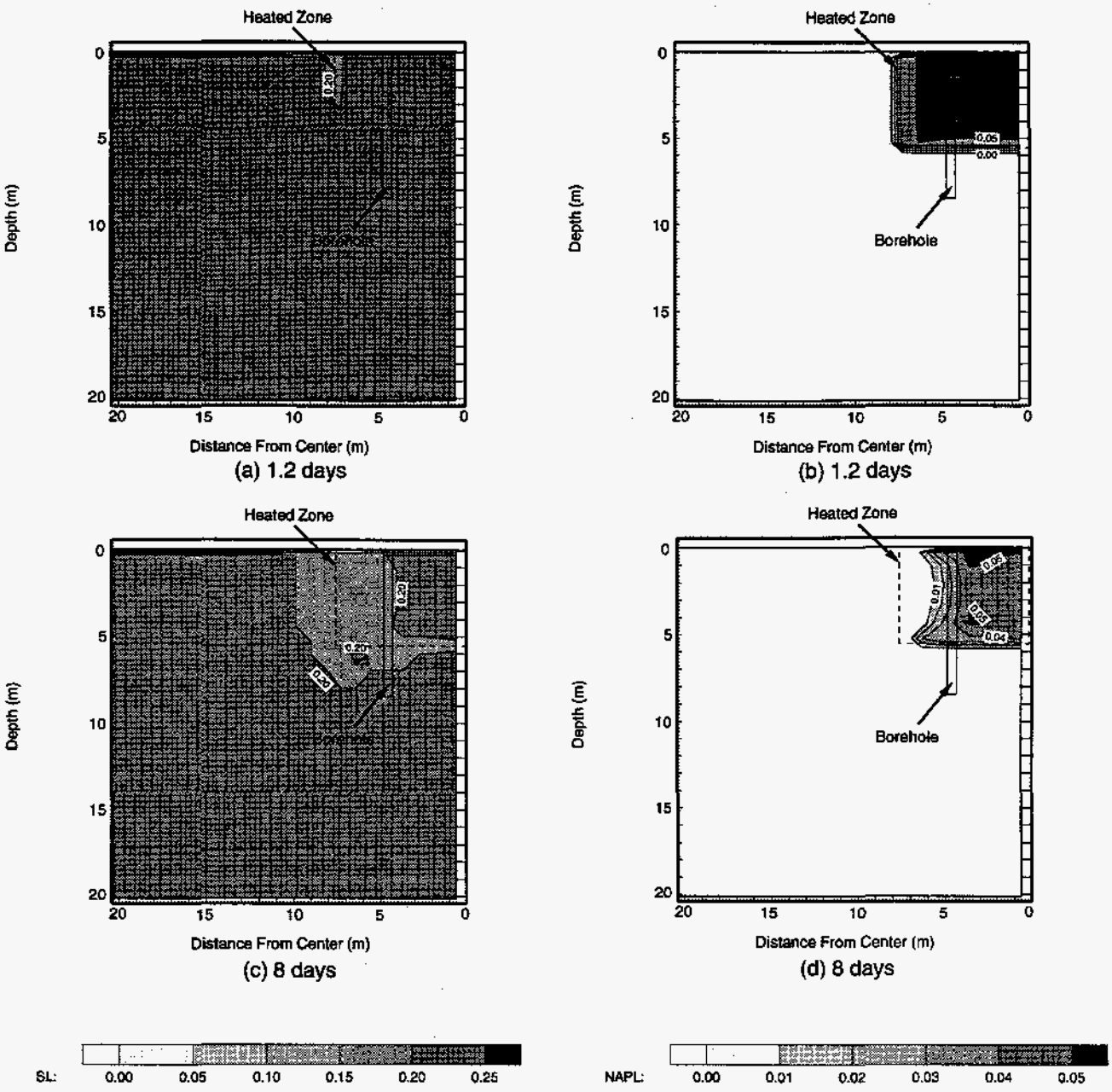

Figure 4-20. Early-time water (left diagram) and NAPL (right diagram) saturation contours, long-side view, 1.0 kPa vacuum, outside extraction, I=1 plane

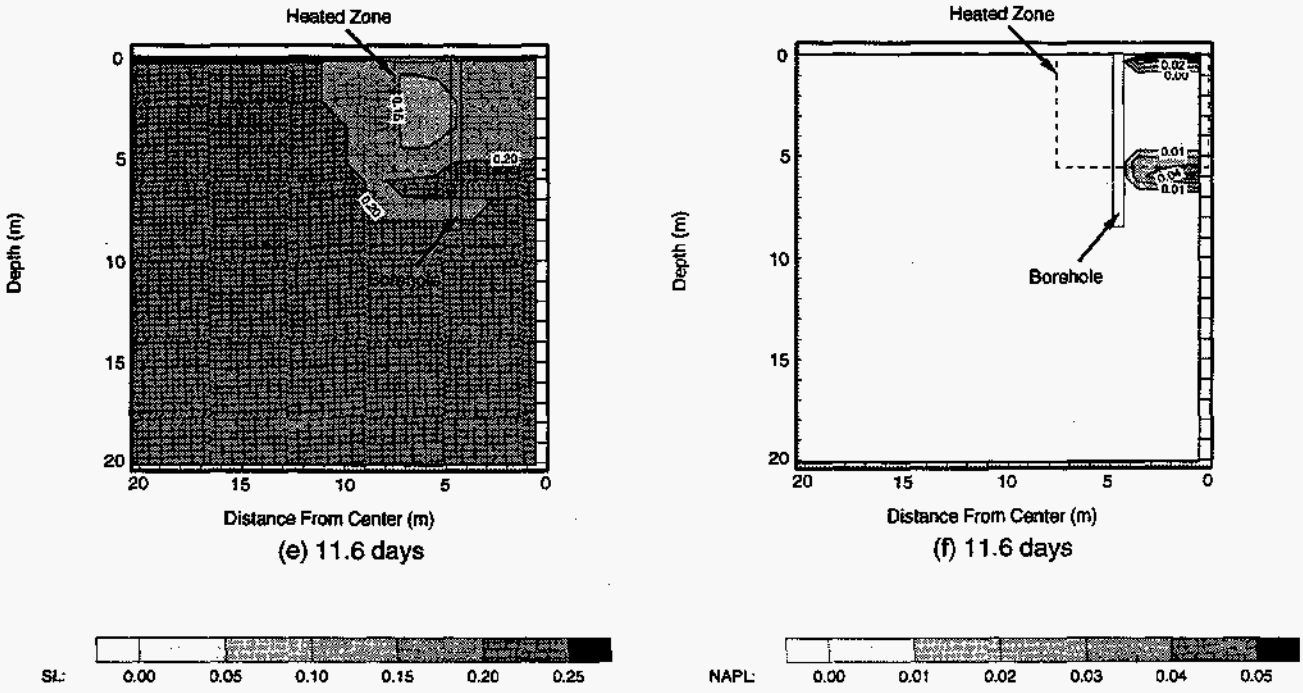

Figure 4-20. Early-time water (left diagram) and NAPL (right diagram) saturation contours, long-side view, 1.0 kPa vacuum, outside extraction, I=1 plane, continued

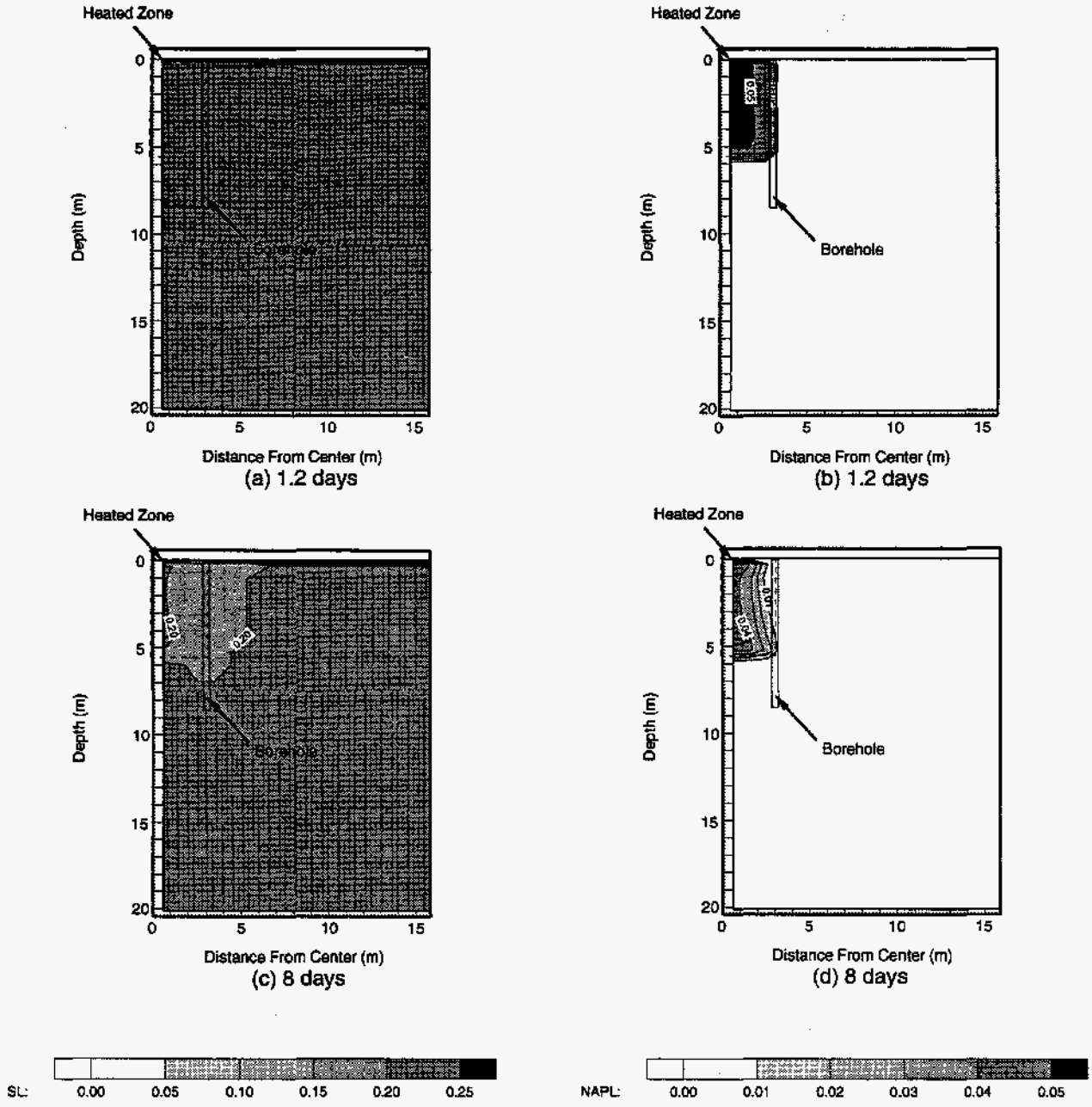

Figure 4-21. Early-time water (left diagram) and NAPL (right diagram) saturation contours, short-side view, 1.0 kPa vacuum, outside extraction, J=1 plane

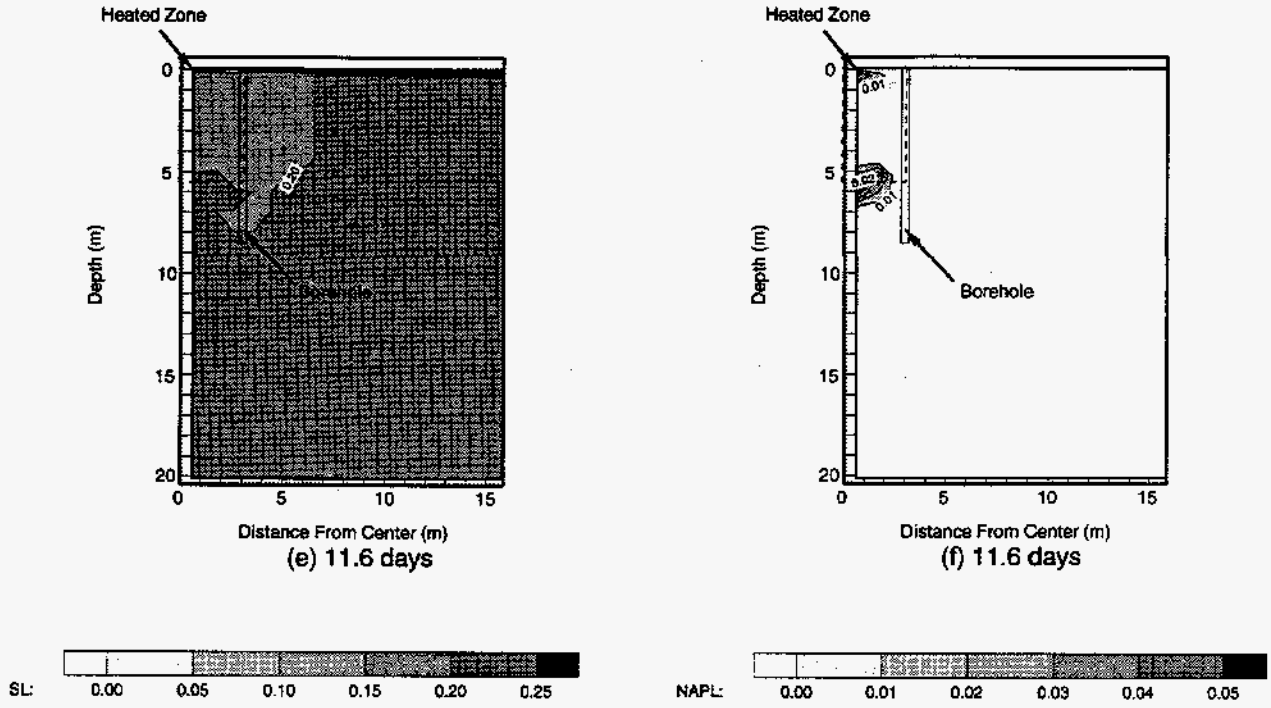

Figure 4-21. Early-time water (left diagram) and NAPL (right diagram) saturation contours, short-side view, 1.0 kPa vacuum, outside extraction, J=1 plane, continued

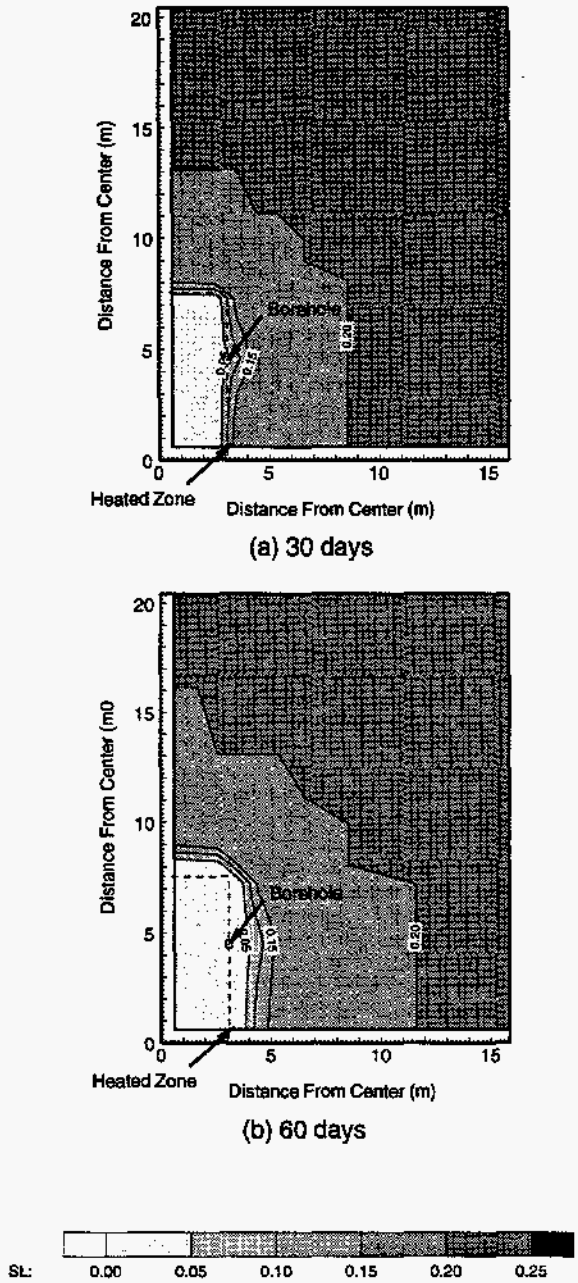

Figure 4-22. Late-time water saturation contours, 1.0 kPa vacuum, outside extraction, top view, K=4 plane

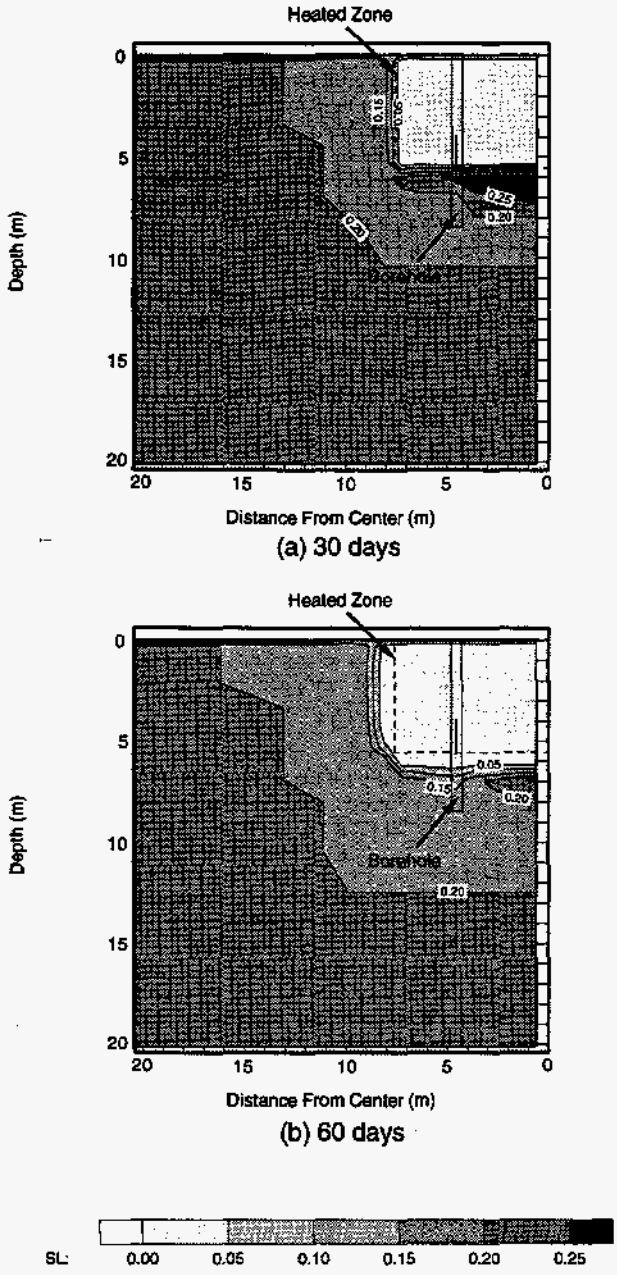

Figure 4-23. Late-time water saturation contours, 1.0 kPa vacuum, outside extraction, long-side view, I=1 plane

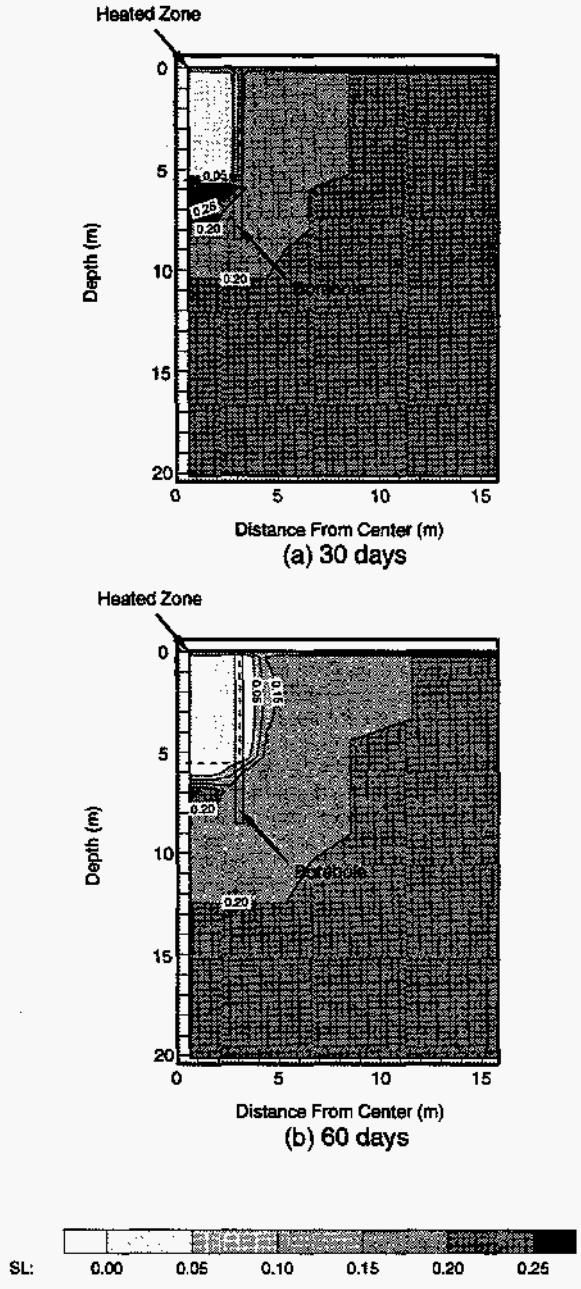

Figure 4-24. Late-time water saturation contours, 1.0 kPa vacuum, outside extraction, short-side view, J=1 plane

Figure 4-25a gives the various mass flow rates into the borehole. The flow is predominantly air, with smaller fractions of vapor and VOC. Figure 4-25b gives the vapor flow rate and the heated and unheated zone evaporation rates, indicating migration of water into the unheated zone from about 12 days to 18 days. Figure 4-26 presents the gas vector velocity plots; only the plots at 60 days are included. The general direction is towards the borehole as before.

Figure 4-27 shows details of the NAPL migration into the unheated soil; the results are given for 11.6 days, which corresponds to the maximum rate of NAPL flow into the unheated zone. Figure 4-27a shows the long-side view of the pressure difference referenced to a datum of 83200 Pa. This figure indicates higher pressures along the right side of the view at a symmetry plane. Figure 4-27b shows the resulting gas velocity vectors indicating significant convective gas flow from the heated zone into the unheated soil in this area. As shown in Figure 4-27c, this region corresponds to NAPL migration into the unheated soil.

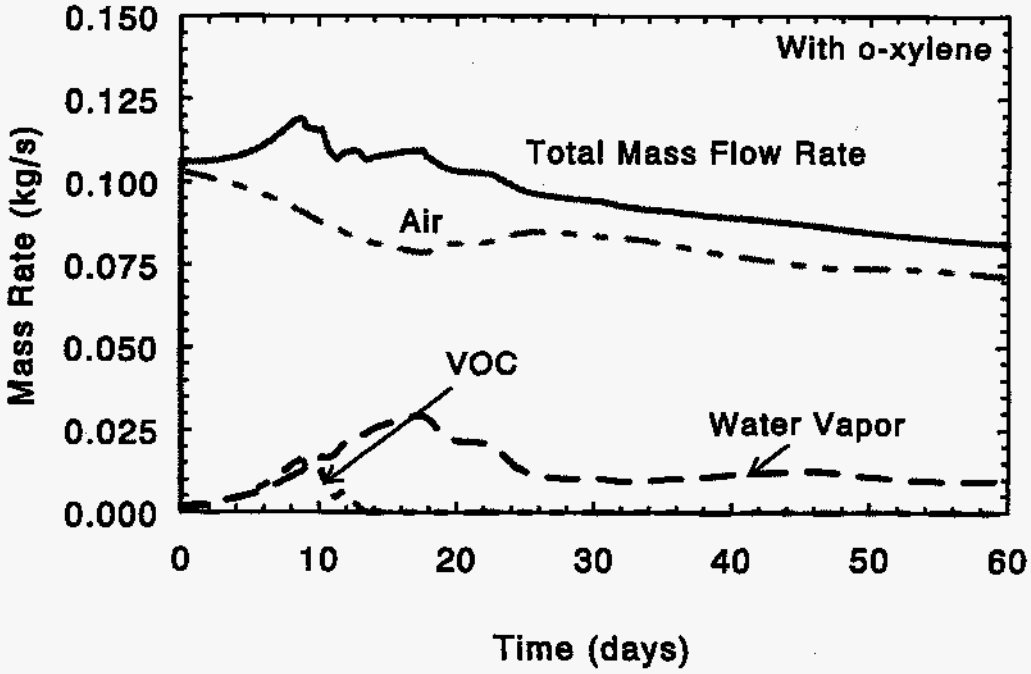

(a) Mass flow rates into boreholes

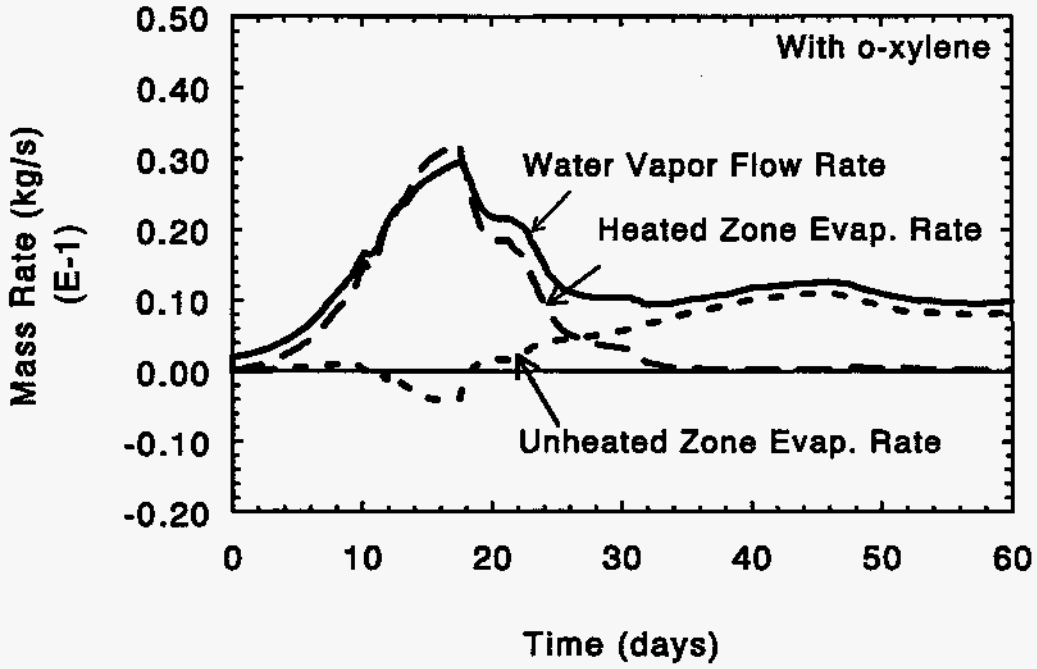

(b) Evaporation and water vapor mass rates

Figure 4-25. Mass rates, outside extraction, 100 kW - 1.0 kPa (4" water) BH vacuum

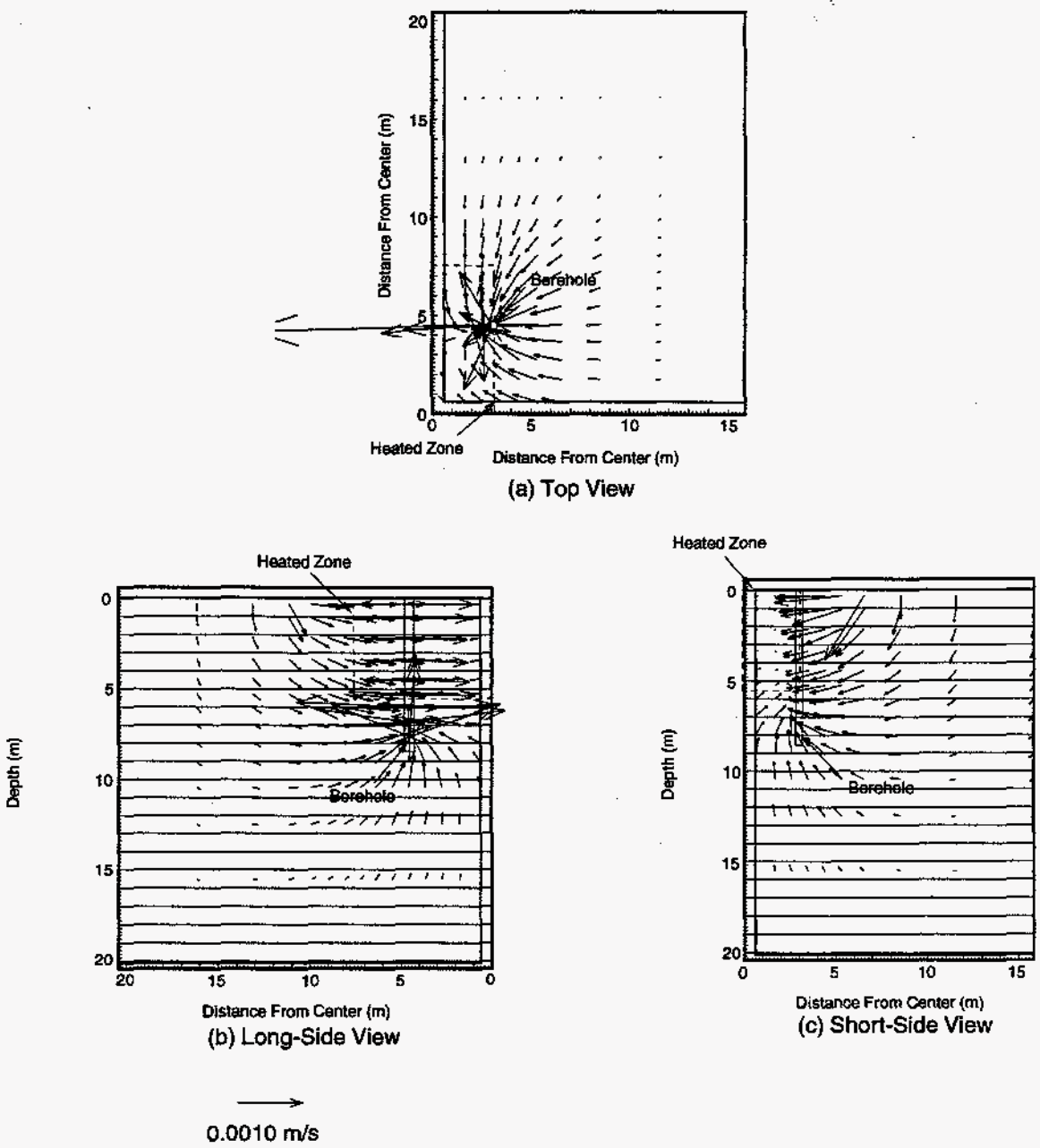

Figure 4-26. Gas velocity vectors at 60 days, 1.0 kPa vacuum, outside extraction
(a) Top view: K=4 plane
(b) Long-side view: I=3 plane
(c) Short-side view: J=3 plane

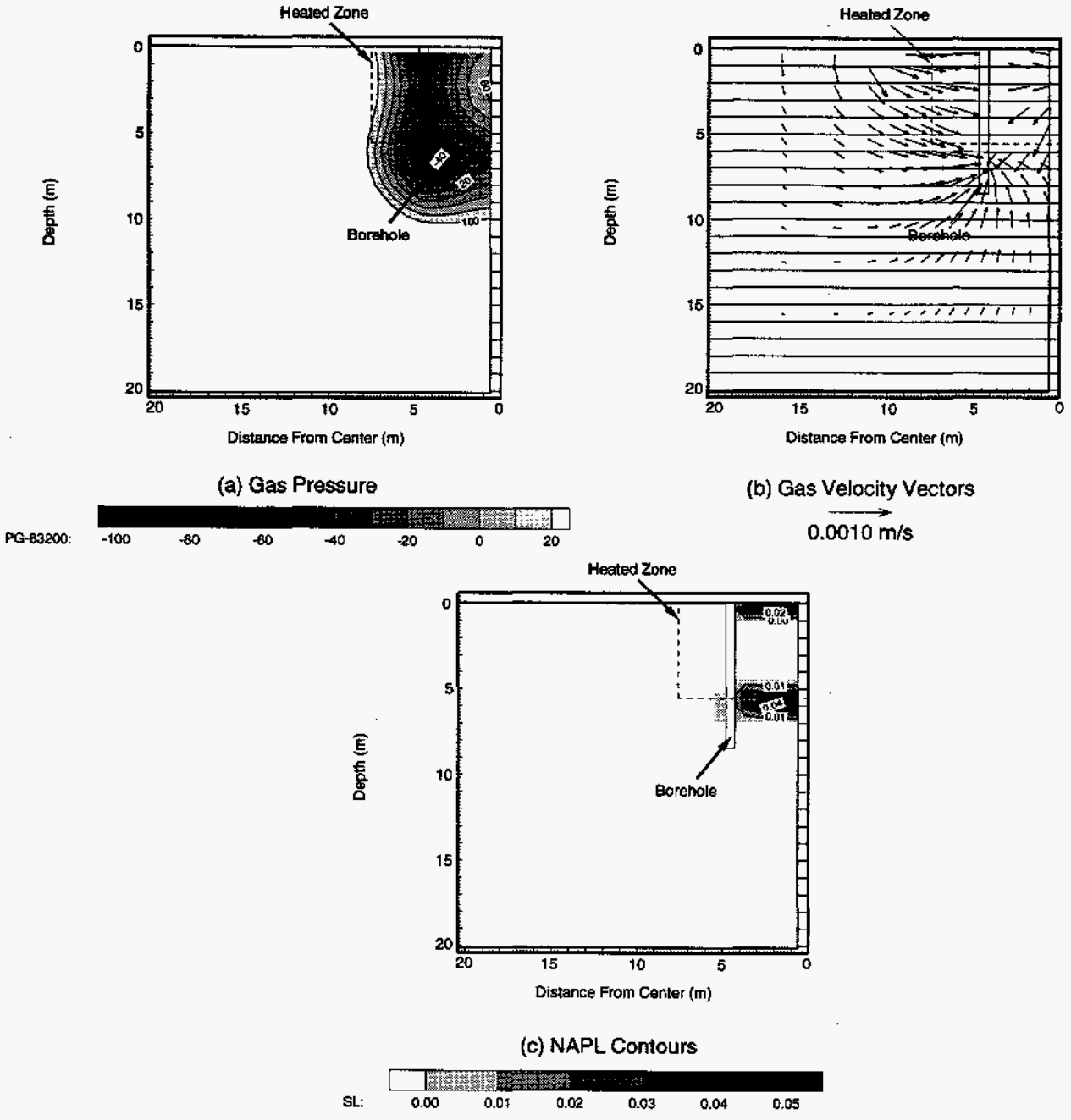

Figure 4-27. Details of NAPL migration into unheated zone at 11.6 days, 1.0 kPa vacuum, inside extraction, I=1 plane

5.0 Simulation Results - Soil Permeability Variation

In addition to the extraction location and borehole vacuum variations, the permeability of the soil was varied. The soil permeability should only effect the gas flow rate through the soil; all other parameters such as the heating rate are independent of the permeability in the present model. Based on Darcy's law, for a given path, the gas velocity is a function of the product of the intrinsic permeability and the imposed pressure difference. Therefore, the results from variation in the borehole vacuum or permeability should be equivalent. The present simulation was performed to confirm the similarity.

For inside extraction, a simulation with a soil permeability of 50 darcies and a borehole vacuum of 0.5 kPa was performed and discussed in Section 3.3. For this section, a simulation for a soil permeability of 10 darcies and 2.5 kPa borehole vacuum has been performed and the results compared with those in Section 3.3. Small differences can be expected since the pressure will be slightly different. However, the major results of the simulations should be very similar.

Figure 5-1 presents the temperature histories in the heated and unheated zones for the 10 darcy case. The average, minimum, and maximum heated zone temperatures at 60 days are 264°C, 376°C, and 136°C, respectively, while the maximum unheated zone temperature at 60 days is 150°C. All of these temperatures are within 1°C of the values for 50 darcies with a lower borehole vacuum. Figure 5-2 shows the temperature contours at 60 days; the contours are essentially the same as the 50 darcy results given earlier.

Figure 5-3a shows the heated zone fluid masses, while Figure 5-3b presents the NAPL masses in the heated and unheated zones. The results again are essentially the same as for 50 darcies. The maximum NAPL mass migrating to the unheated zone is 200 kg for 50 darcies, while the maximum value is about 210 kg for 10 darcies. Figures 5-4 through 5-6 show the liquid water and NAPL saturation contours for early times, while Figures 5-7 through 5-9 present the liquid water saturation contours at later times. While some minor differences exist between the present results and those for 50 darcies, the results are the same for all practical purposes.

Figure 5-10a gives the mass flow rates into the boreholes, while 5-10b has the water evaporation rates in the heated and unheated zones; again, the results are essentially the same as for 50 darcies. Figure 5-11 shows the gas velocity vectors which are the same as for 50 darcies.

As expected, the results for a different soil permeability scale with Darcy's law for all practical purposes. Some minor differences are noted, but the overall behavior is unchanged when the permeability is reduced by a factor of 5 while the borehole vacuum is increased by the same factor.

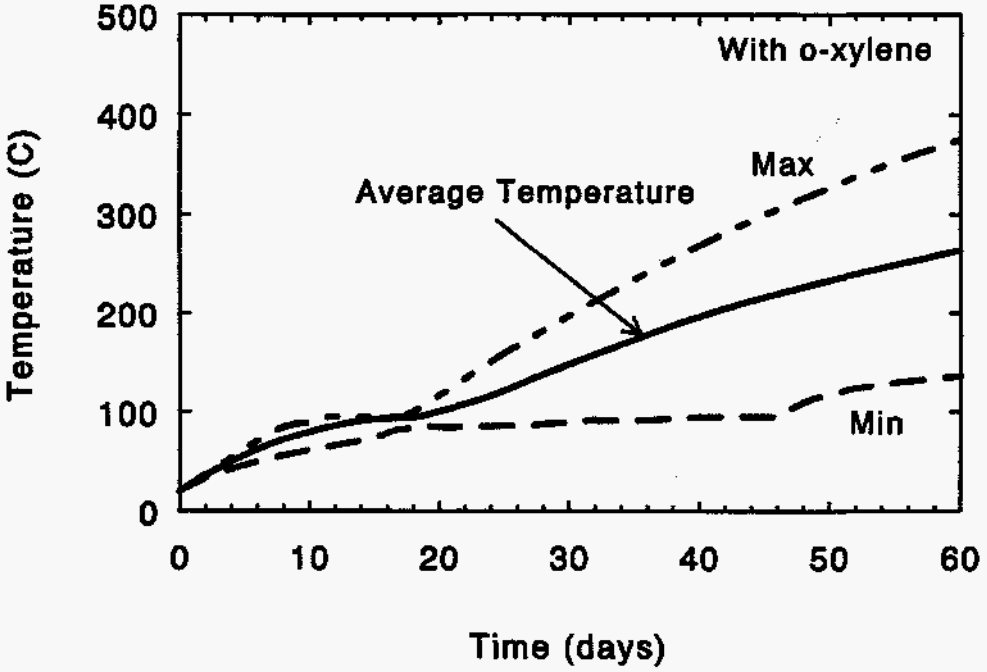

(a) Heated zone temperatures

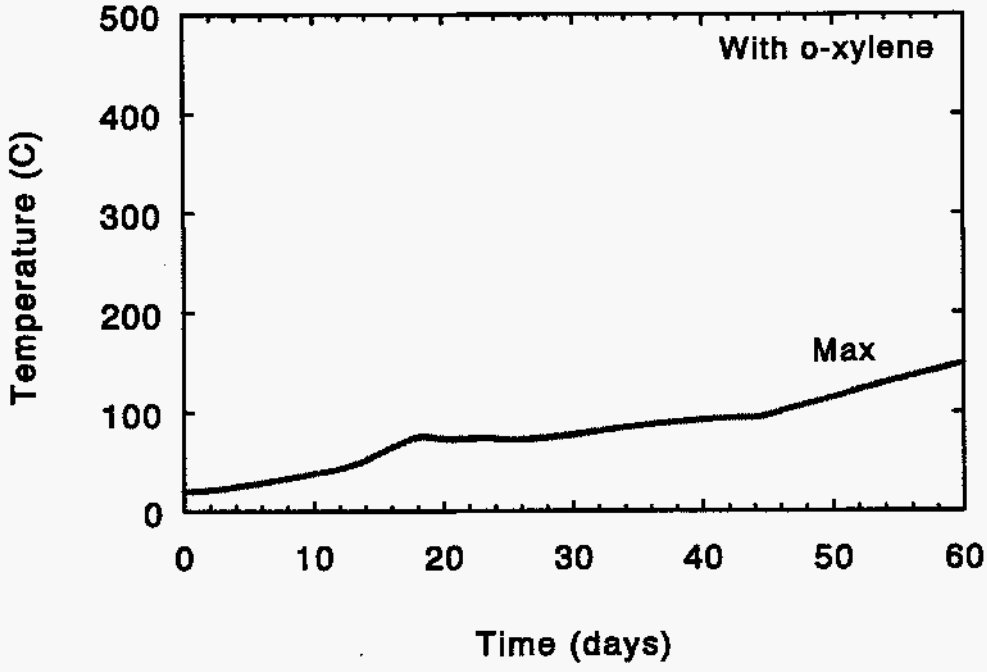

(b) Maximum unheated zone temperatures

Figure 5-1. Heated and unheated zone temperatures, inside extraction; 100 kW - 2.5 kPa BH vacuum - 10 darcies

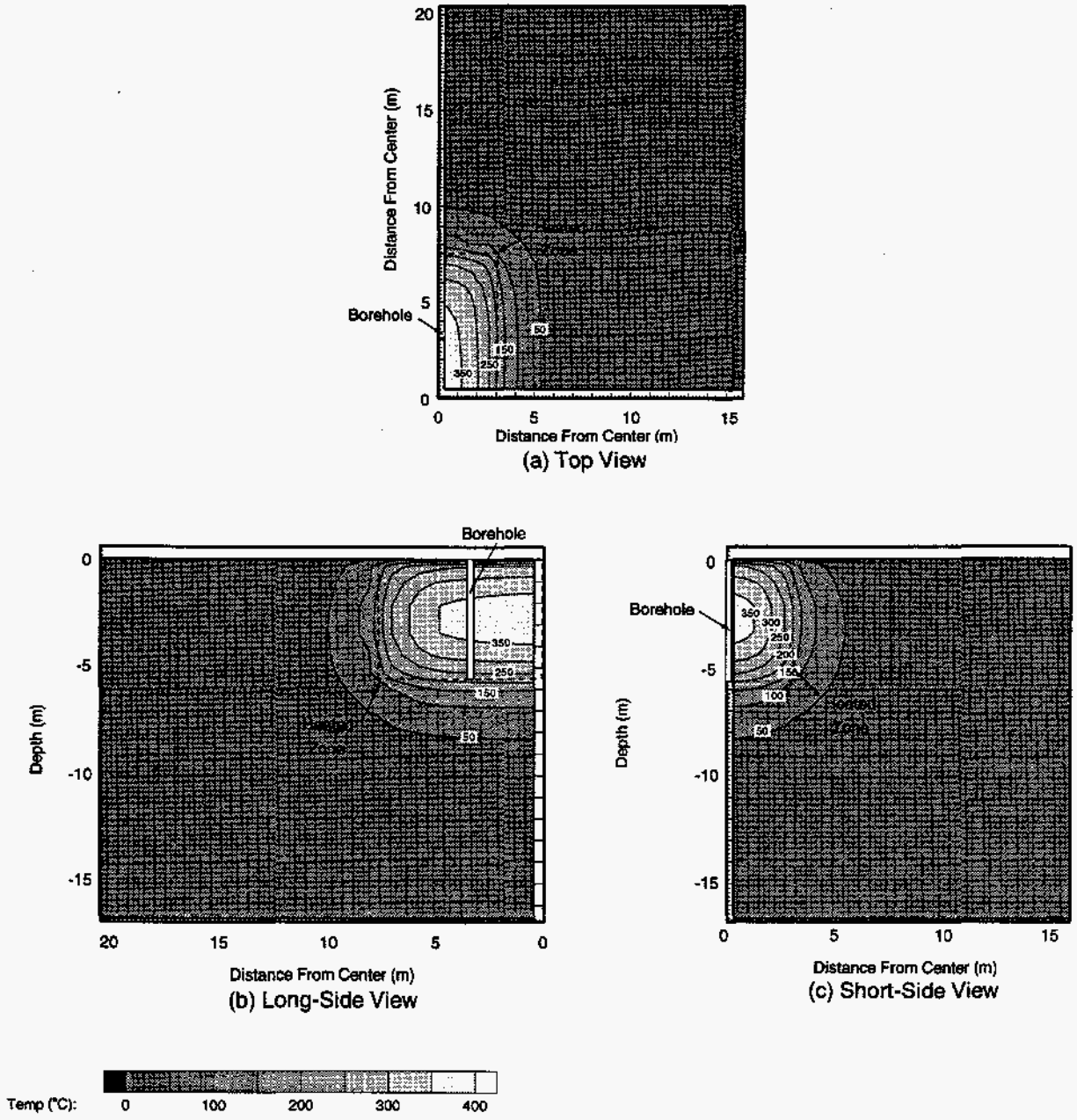

Figure 5-2. Temperature contours at 60 days, inside extraction, 10 darcies
(a) Top view: K=4 plane
(b) Long-side view: I=1 plane
(c) Short-side view: J=1 plane

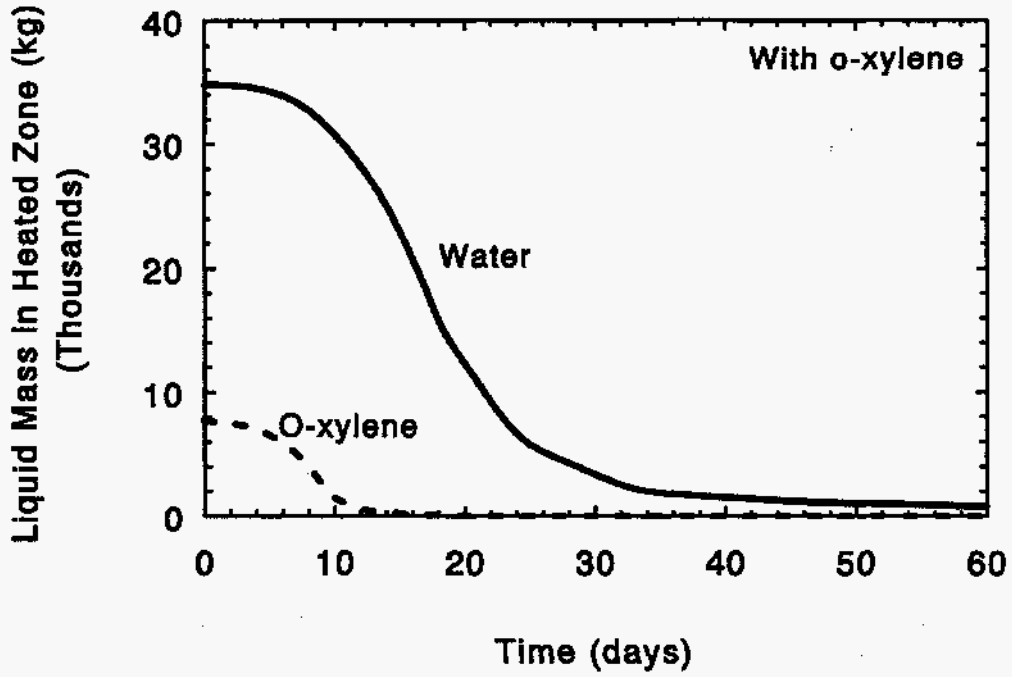

(a) Heated zone fluid masses

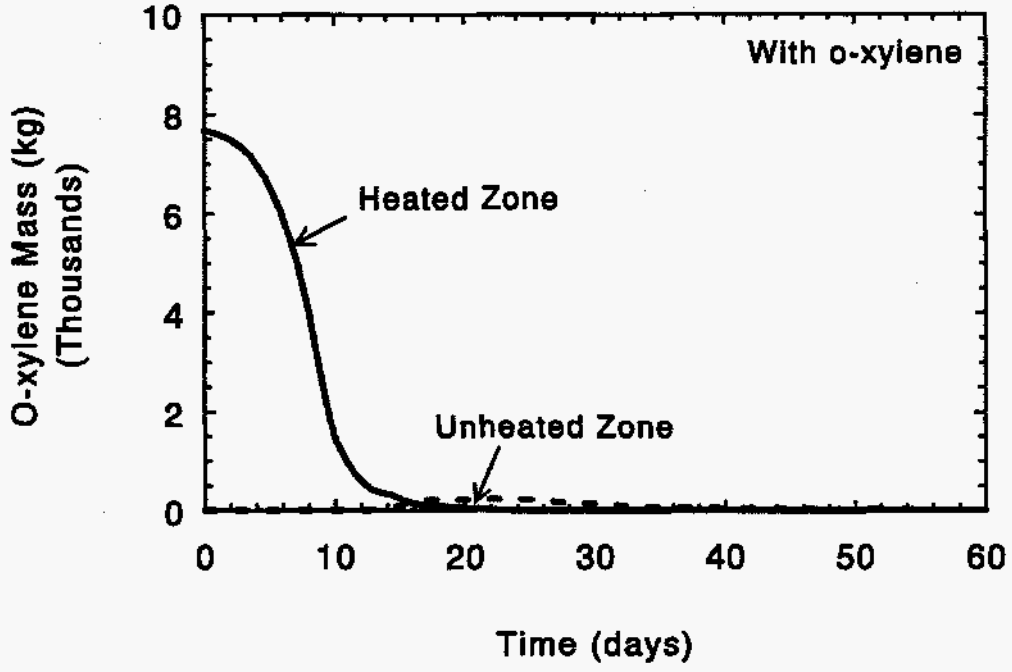

(b) O-xylene mass variation

Figure 5-3. Heated zone fluid masses and O-xylene mass variation, inside extraction, 100 kW, 2.5 kPa BH vacuum, 10 darcies

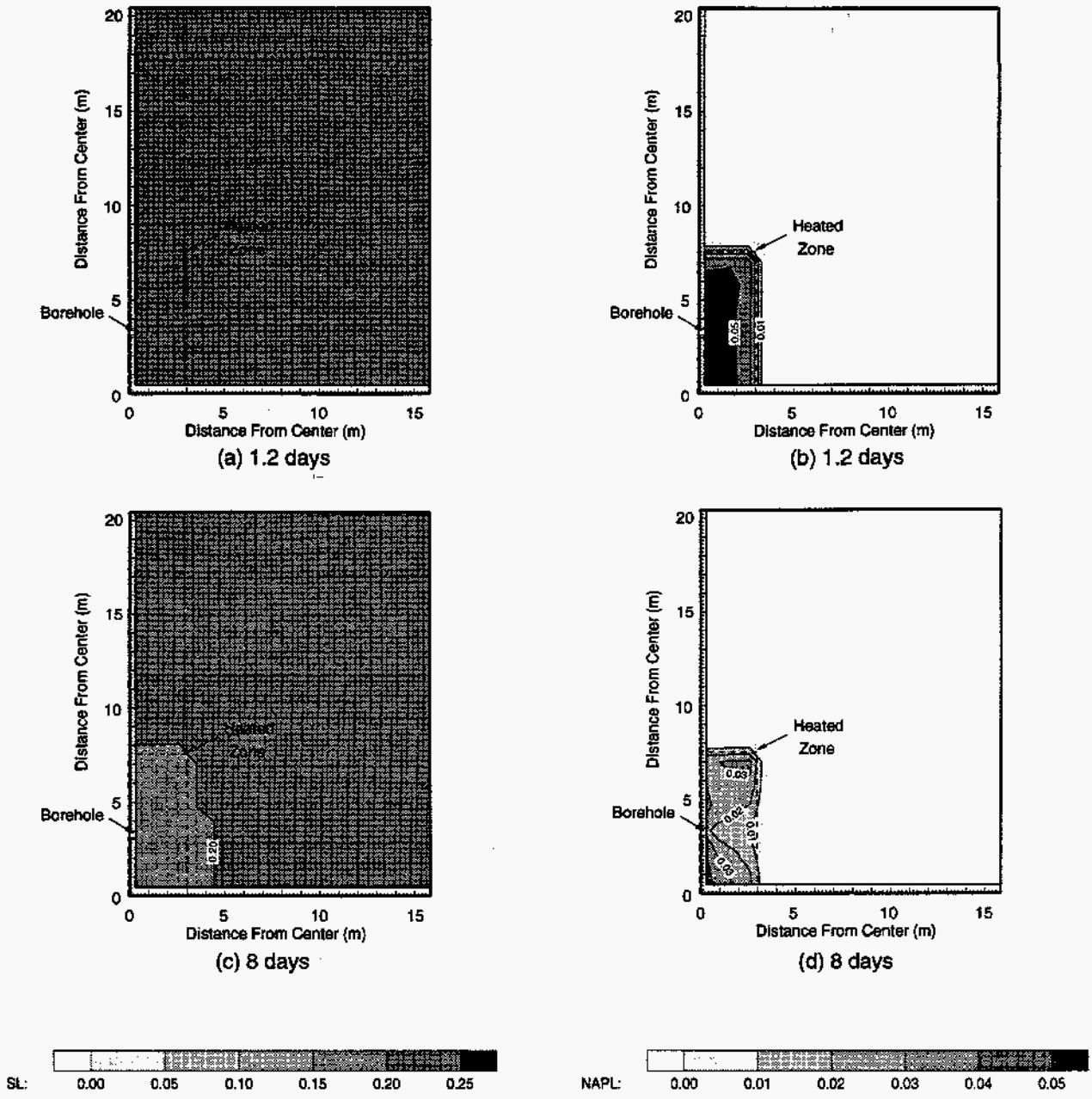

Figure 5-4. Early-time water (left diagram) and NAPL (right diagram) saturation contours, 10 darcies, top view, inside extraction, K=4 plane

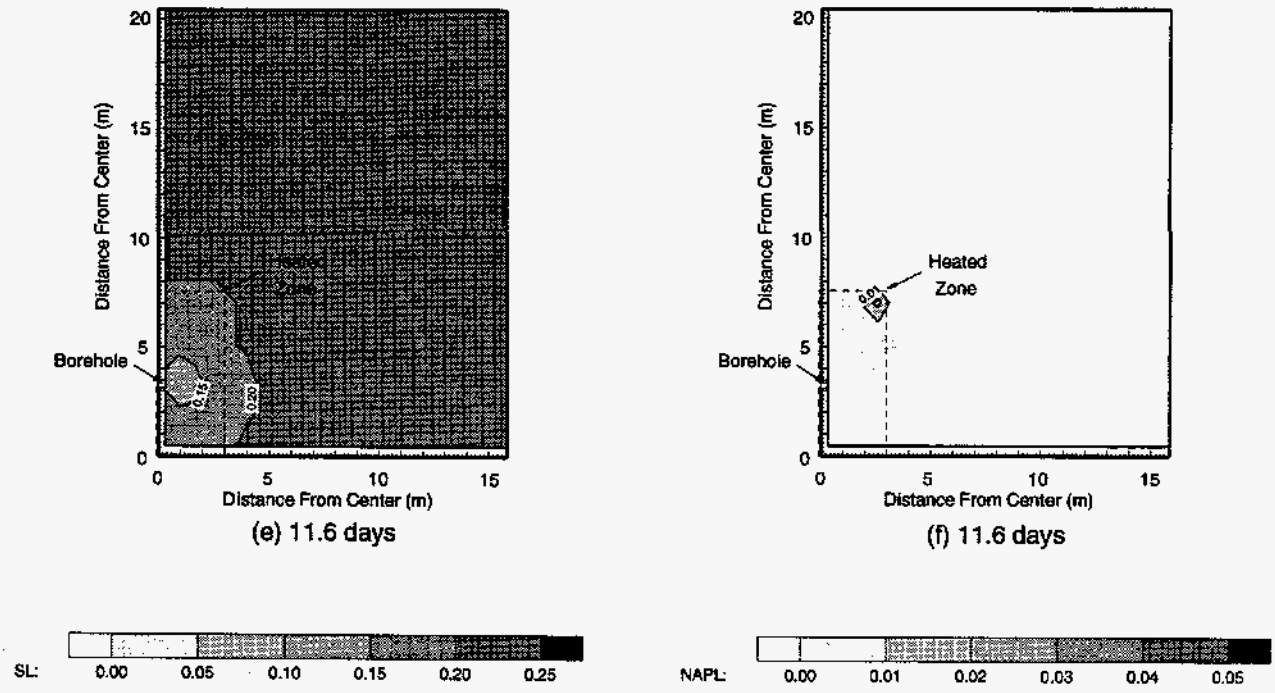

Figure 5-4. Early-time water (left diagram) and NAPL (right diagram) saturation contours, 10 darcies, top view, inside extraction, K=4 plane

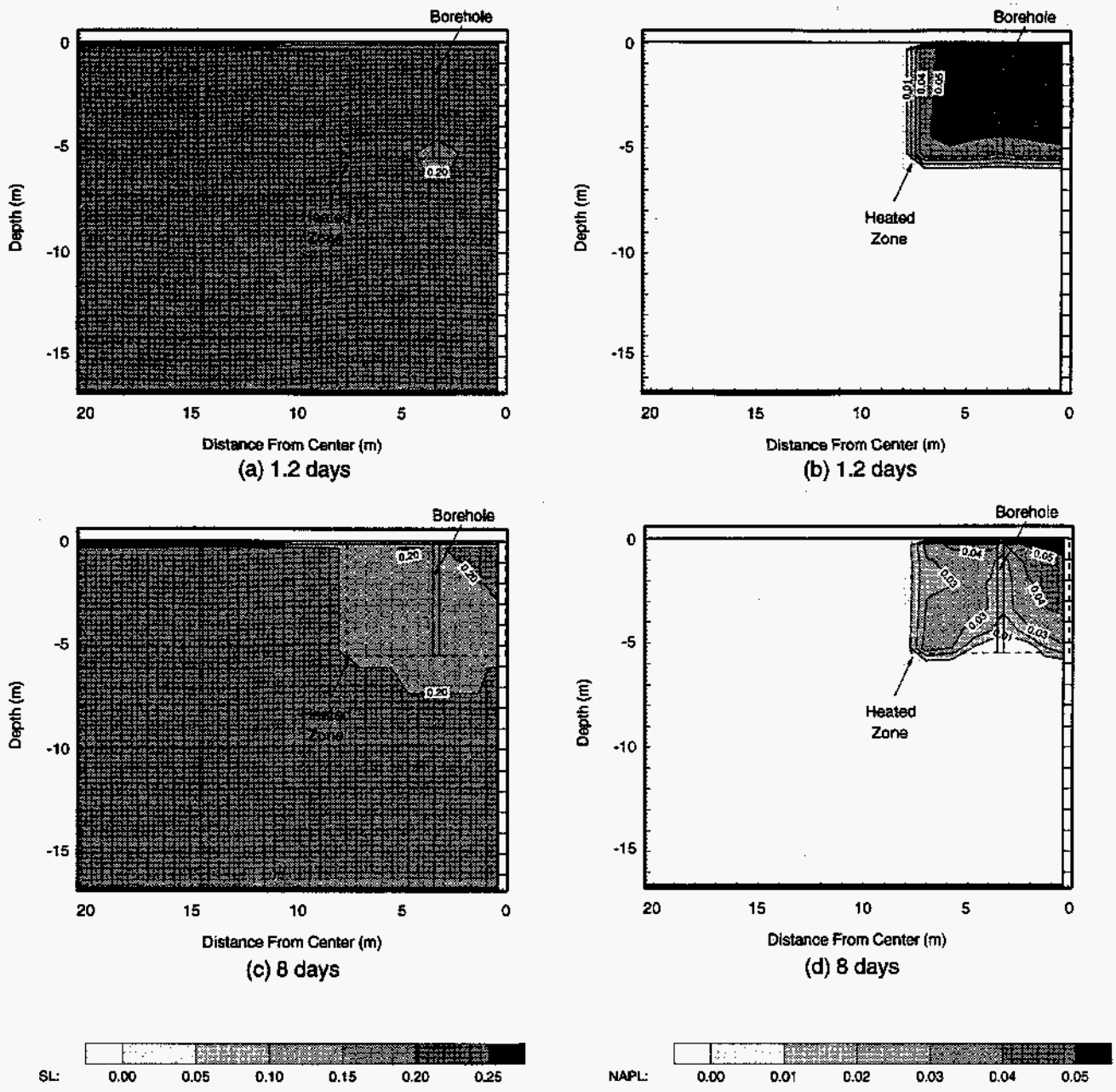

Figure 5-5. Early-time water (left diagram) and NAPL (right diagram) saturation contours, 10 darcies, long-side view, inside extraction, I=1 plane

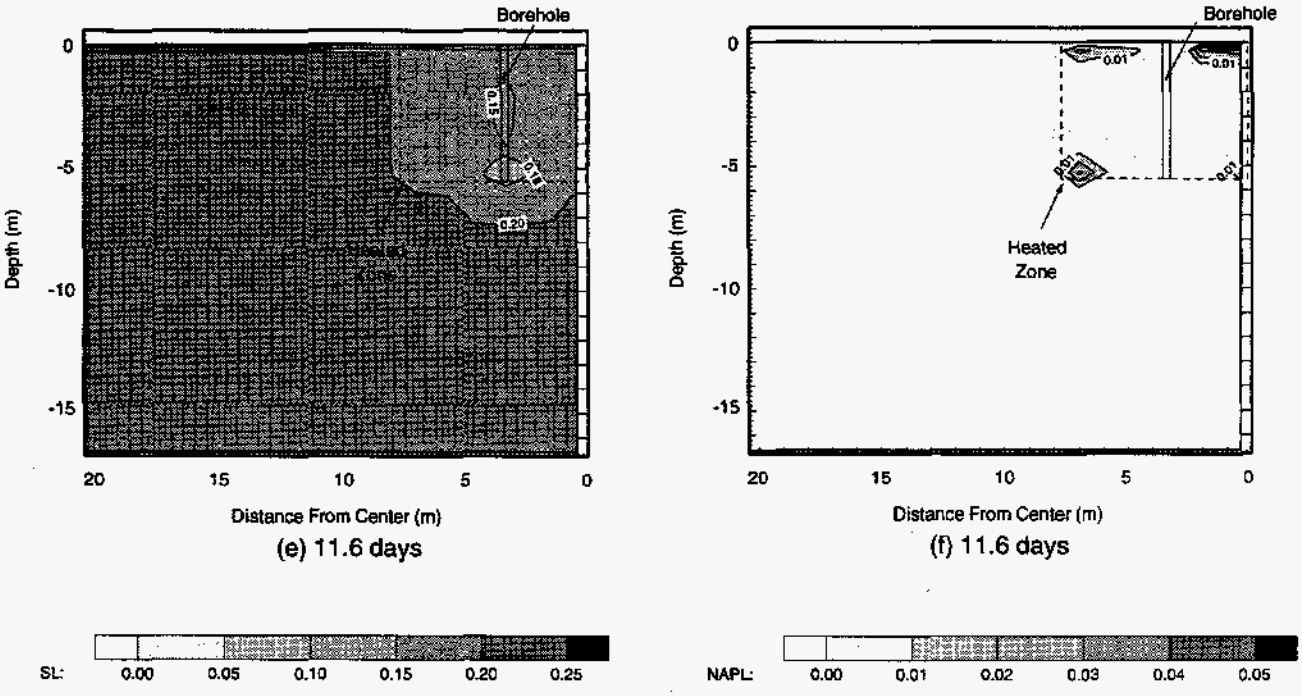

Figure 5-5. Early-time water (left diagram) and NAPL (right diagram) saturation contours, 10 darcies, long-side view, inside extraction, I=1 plane, continued

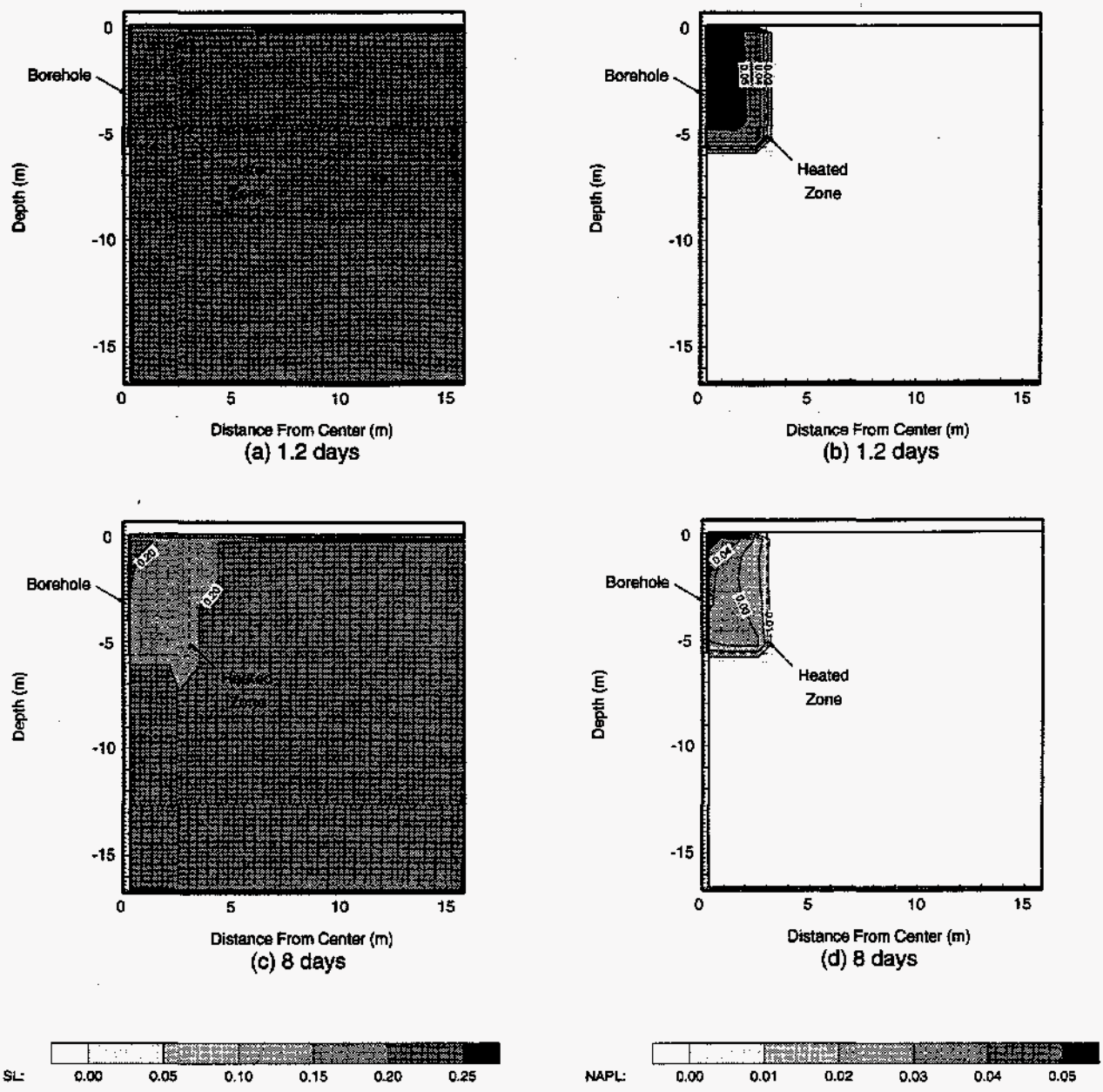

Figure 5-6. Early-time water (left diagram) and NAPL (right diagram) saturation contours, 10 darcies, short-side view, inside extraction, J=1 plane

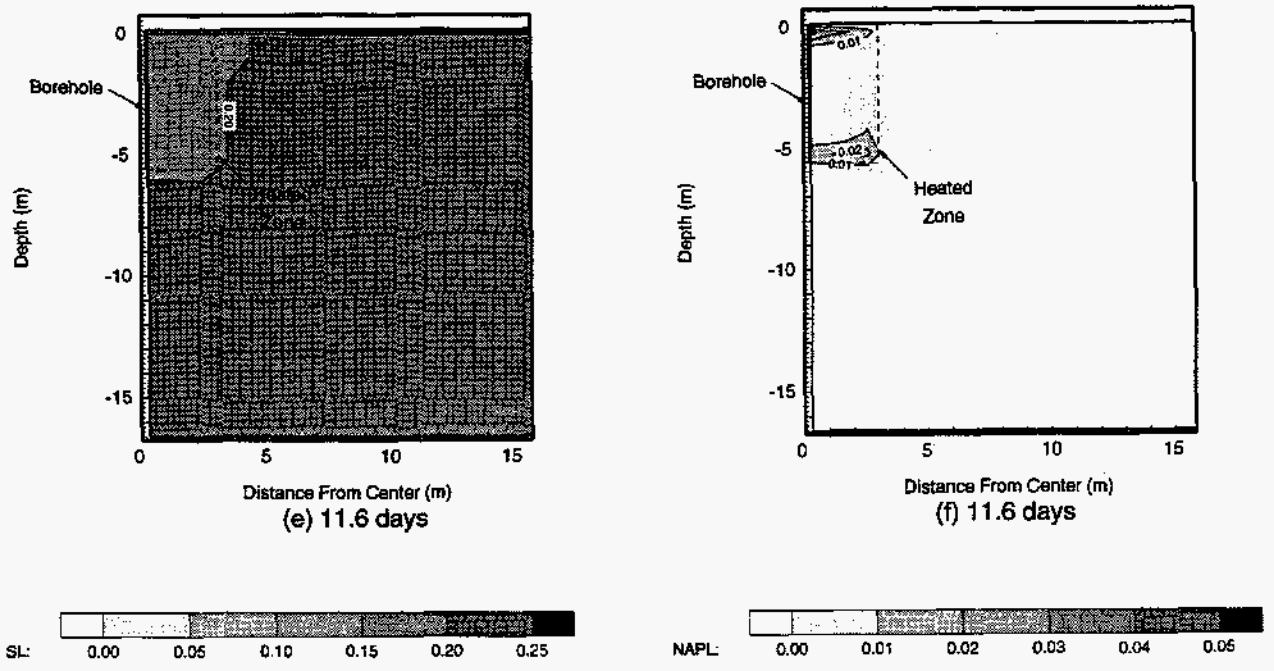

Figure 5-6. Early-time water (left diagram) and NAPL (right diagram) saturation contours, 10 darcies, short-side view, inside extraction, J=1 plane, continued

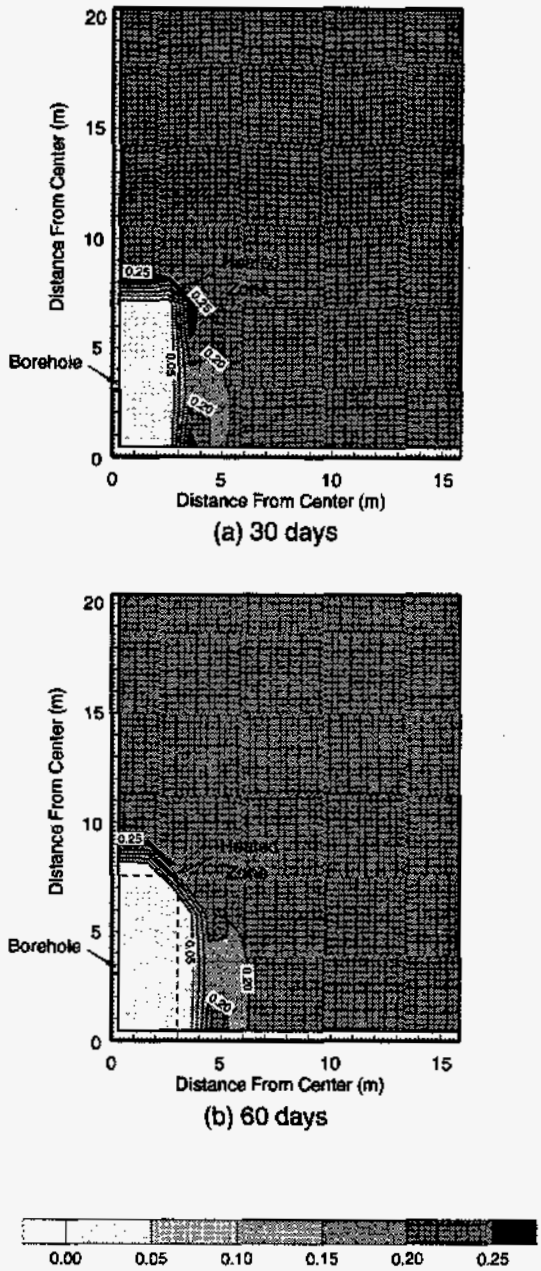

Figure 5-7. Late-time water saturation contours, 10 darcies, inside extraction, top view, K=4 plane

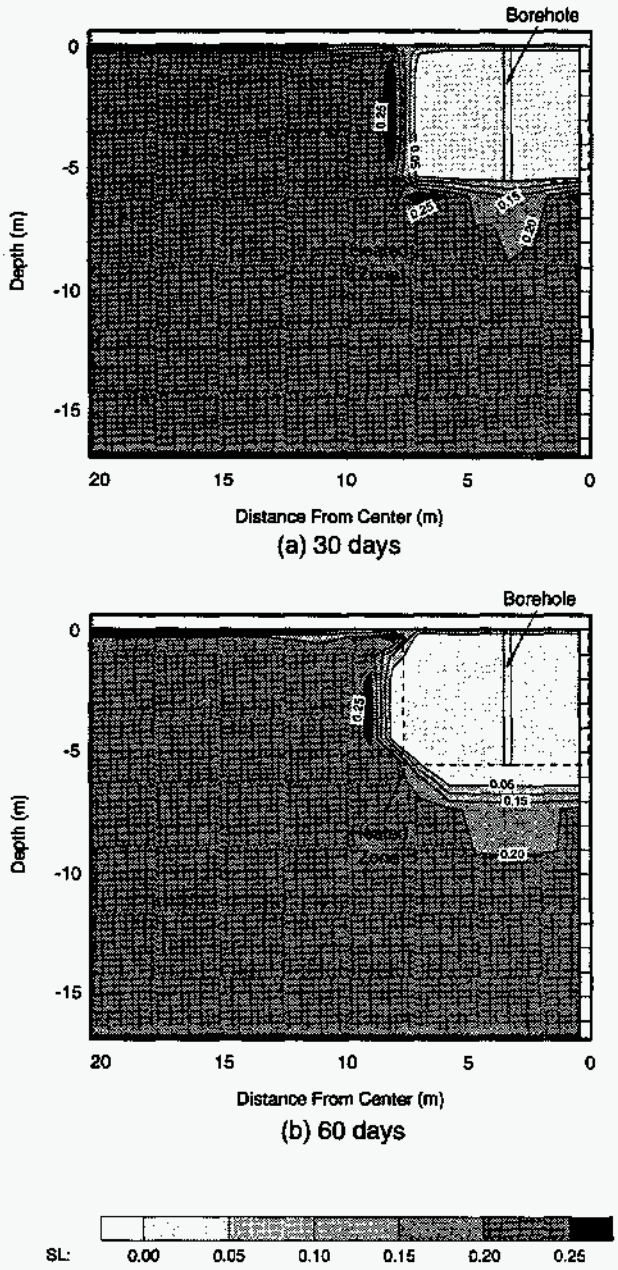

Figure 5-8. Late-time water saturation contours, 10 darcies, inside extraction, long-side view, I=1 plane

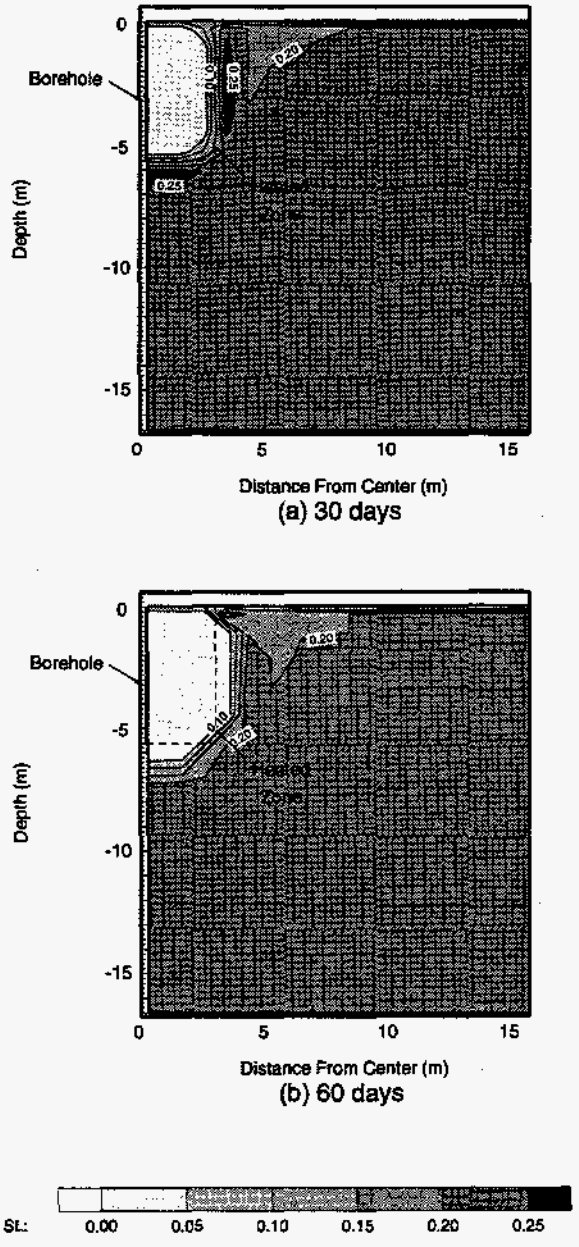

Figure 5-9. Late-time water saturation contours, 10 darcies, inside extraction, short-side view, J=1 plane

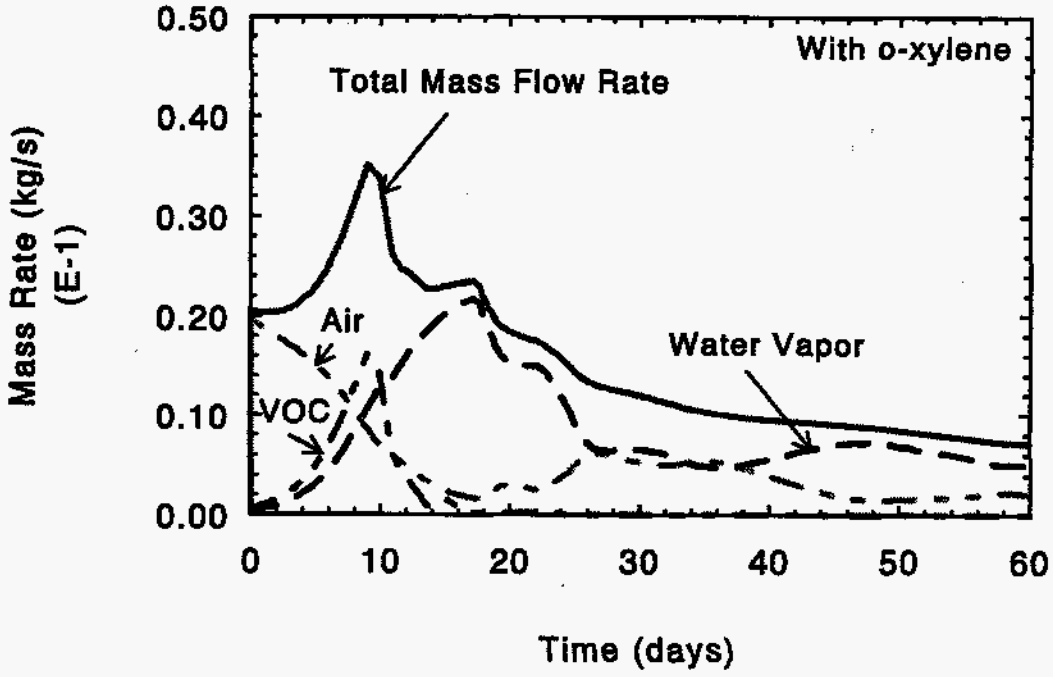

(a) Mass flow rates into boreholes

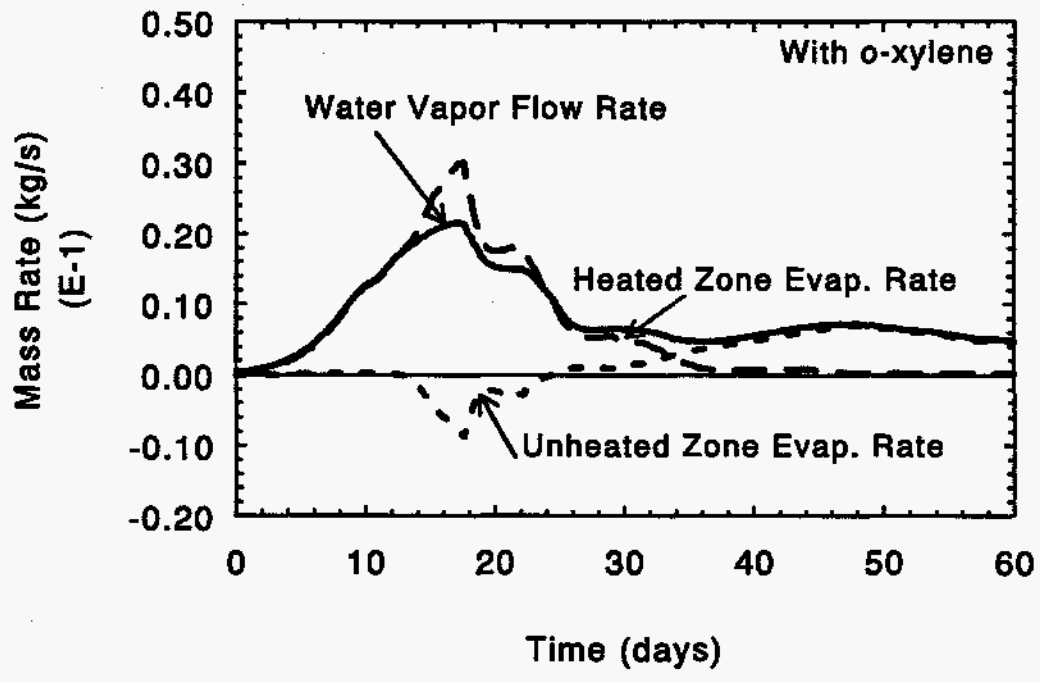

(b) Evaporation and water vapor mass rates

Figure 5-10. Mass rates, inside extraction, 100 kW, 2.5 kPa BH vacuum, 10 darcies

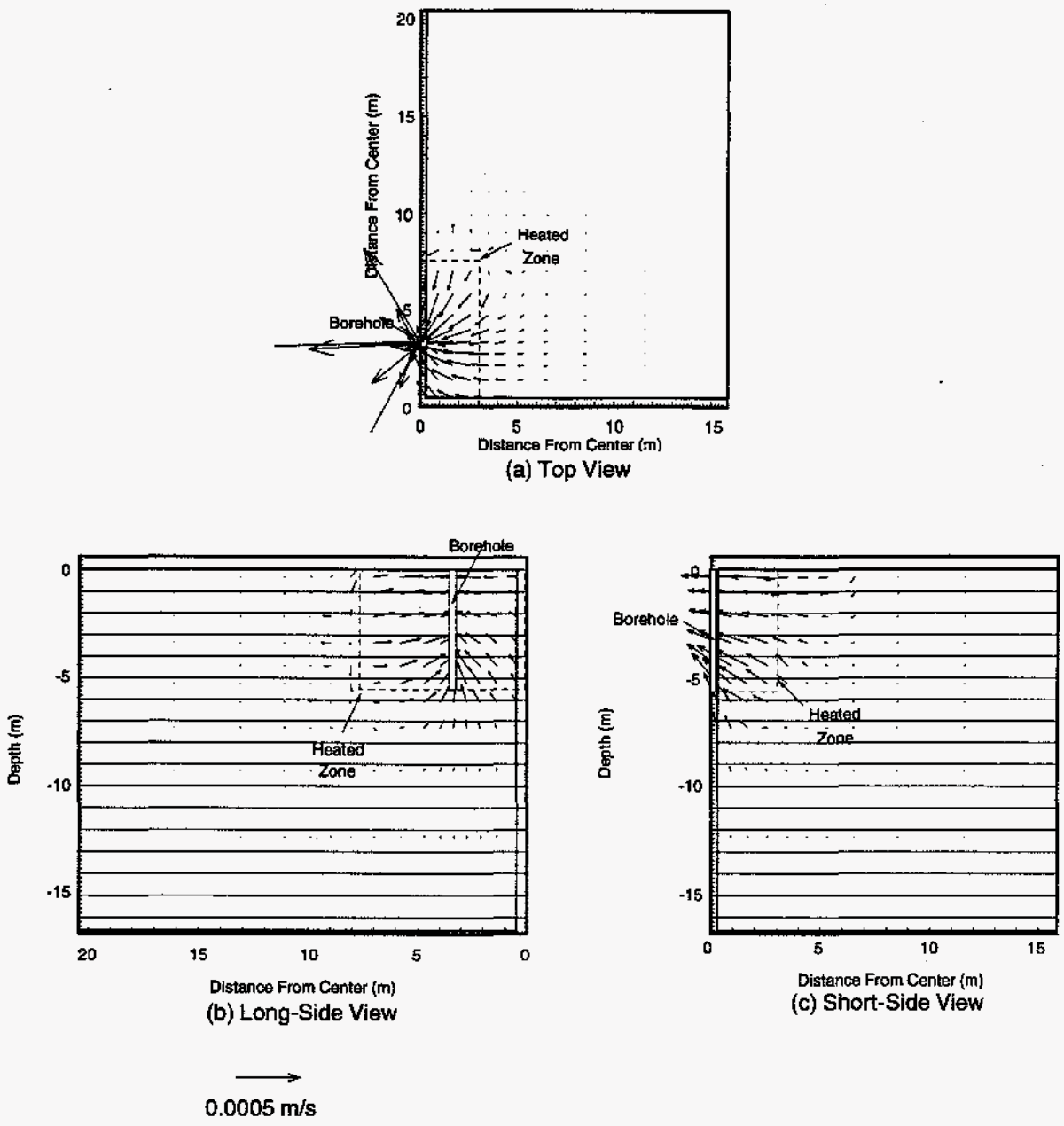

Figure 5-11. Gas velocity vectors at 60 days, 10 darcies, inside extraction
(a) Top view: K=4 plane
(b) Long-side view: I=3 plane
(c) Short-side view: J=3 plane

Intentionally left blank

6.0 Discussion

6.1 Inside Extraction

Three different borehole vacuums were investigated for the inside extraction case. As the borehole vacuum was reduced, the mass flow rate of air into the borehole decreased. The effect of the changing borehole vacuum was minimal on the temperature history and temperature distribution.

Saturation values and contours for liquid water and NAPL were significantly influenced by the borehole vacuum. As the vacuum, and therefore, borehole flow rate, was reduced, the potential for migration of liquid water and NAPL from the heated zone into the unheated soil increased. For the lowest borehole vacuum analyzed, liquid water and NAPL migrated from the heated zone into the unheated soil. Transport into the unheated zone is due to evaporation in the heated zone, convective transport into the unheated soil, and condensation in the cooler unheated region. Eventually, the migrated liquid evaporated due to heat losses to the unheated soil and continuing air flow through the soil. However, complete containment of the NAPL within the heated zone was lost for the lowest borehole vacuum case.

The mass flow rate composition entering the borehole changed dramatically as the vacuum was reduced, changing from air dominated to water vapor dominated. The gas velocity vectors indicated less uniform air sweep as the borehole vacuum was reduced, including directions directly away from the borehole.

6.2 Outside Extraction

Two borehole vacuums were investigated for outside extraction. The temperature values and contours are not significantly different for outside extraction than for inside extraction.

The liquid and NAPL saturation contours are significantly different for outside extraction. Due to the location of the borehole away from the symmetry planes, a "dead" zone, or low flow rate zone, exists near these planes where the air flow rate is low. In this region, pockets of liquid water and NAPL can exist due to the low air sweep, and migration of these liquids from the heated zone to the unheated soil can occur. Similar to inside extraction, transport into the unheated zone is due to evaporation in the heated zone, convective transport into the unheated soil, and condensation in the cooler unheated region.

The flow rate into the borehole is predominantly air in all cases since, with the location on the edge of the heated zone, most of the air will not pass through the heated zone. In addition, since the borehole length is longer than the heated zone, air can flow from the heated zone into the unheated soil, increasing the likelihood of liquid water and NAPL migration into the unheated soil.

6.3 Soil Permeability Variation

Scaling the present results with Darcy's law was investigated by decreasing the soil permeability by a factor of 5 while increasing the borehole vacuum by the same factor. Essentially all the results (temperature, liquid saturation, NAPL, and flow rates) were the same for the two cases indicating that Darcy's law may be used to estimate the effect of other conditions not explicitly analyzed.

7.0 Summary and Conclusions

Detailed simulations have been performed for the TEVES Project using the TOUGH2 code considering air, water, and a single-component NAPL. These studies investigated two different vapor extraction schemes. The first extraction scheme is through the two vapor extraction wells which are toward the middle of the heated zone, while the second approach uses the four outside guard electrodes located on the edge of the heated zone as extraction wells. Simulations have been performed with TOUGH2-VOC with an assumed initial NAPL inventory of 5% o-xylene in the heated zone to investigate possible contaminant migration into the unheated soil.

Contaminant migration from the heated zone into the unheated soil can occur if the borehole vacuum, or borehole flow rate, is not sufficient. If this occurs, evaporation of liquids (water and NAPL) due to the heating can cause flow from the heated zone into the unheated soil. The possibility of contaminant migration is much greater for outside extraction than inside extraction due to the location of the boreholes and the resulting less efficient air sweep in outside extraction. For conditions other than those analyzed (such as different soil permeability), Darcy's Law can be used to estimate the results.

The above analyses are simplified since they assume homogeneous soil properties and a single-component NAPL. Further investigation into heterogeneity effects including layering and the influence of multicomponent NAPLs on contaminant migration are recommended. In these cases, gas diffusion processes may dominate transport and must be included as investigated by Ho and Udell (1992).

From these results, sufficient air flow through the heated zone must be provided to contain the contaminants within the heated zone If the air flow rate is too low, water and NAPL may migrate into the unheated region outside the heated zone. For lower permeability soils, the borehole vacuum will have to be increased, or the heating rate decreased, to prevent contaminant migration.

Intentionally left blank

8.0 References

Adenekan, A.E., T.W. Patzek, and K. Pruess (1993), "Modeling of Multiphase Transport of Multicomponent Organic Compounds and Heat in the Subsurface: Numerical Model Formulation," Water Resour. Res., Vol. 29, No. 11, pp. 3727-3740, 1993.

Falta, R.W., and K. Pruess (1991), *STMVOC User's Guide*, Lawrence Berkeley Laboratory, LBL-30758.

Falta, R.W., K. Pruess, I. Javandel, and P.A. Witherspoon (1992a), "Numerical Modeling of Steam Injection for the Removal of Nonaqueous Liquids From the Subsurface, 1. Numerical Formulation," Water Resour. Res., Vol. 28, No. 2, pp. 433-449.

Falta, R.W., K. Pruess, I. Javandel, and P.A. Witherspoon (1992b), "Numerical Modeling of Steam Injection for the Removal of Nonaqueous Liquids From the Subsurface, 2. Code Validation and Approximation," Water Resour. Res., Vol. 28, No. 2, pp. 451-465.

Finsterle, S., and K. Pruess (1993), *T2VOC, a 3-phase Water/Air/NAPL Module for TOUGH2*, Version 0.5, Lawrence Berkeley Laboratory.

Ho, C.K., and K.S. Udell (1992), "An experimental investigation of air venting of volatile liquid hydrocarbon mixtures from homogeneous and heterogeneous porous media," J. Contaminant Hydrology, Vol. 11, pp. 291-316.

Moridis, G.J., and K. Pruess (1992), *TOUGH Simulations of Updegraff's Set of Fluid and Heat Flow Problems*, LBL-32611, Lawrence Berkeley Laboratory.

Moridis, G.J., and K. Pruess (1993), *TOUGH2 Conjugate Gradient Package*, Lawrence Berkeley Laboratory.

Parker, J.C., R.J. Lenhard, and T. Kuppusamy (1987), "A Parametric Model for Constitutive Properties Regarding Multiphase Flow in Porous Media," Water Resour. Res., Vol. 23, No. 4, pp. 618-624.

Phelan, J.M. (1993), *Field Measurements of Soil Air Permeability at the Chemical Waste Landfill*, Sandia National Laboratories, September 1993.

Phelan, J.M., and S.W. Webb (1994), "Thermal Enhanced Vapor Extraction Systems - Design, Application, and Performance Prediction Including Contaminant Behavior," 33rd Hanford Symposium on Health and the Environment.

Pruess, K. (1987), *TOUGH User's Guide*, LBL-20700, Lawrence Berkeley Laboratory.

Pruess, K., ed. (1990), *Proceedings of the TOUGH Workshop*, LBL-29710, Lawrence Berkeley Laboratory, Berkeley, CA.

Pruess, K. (1991), *TOUGH2 - A General-Purpose Numerical Simulator for Multiphase Fluid and Heat Flow*, LBL-29400, Lawrence Berkeley Laboratory.

Snow, R., and T. Bajzek (1993), *Thermal Enhanced Vapor Treatment System Demonstration Phase III - Design Report*," IITRI Project No. C06763.

Stephens, D.B. (1989), *Laboratory Analysis of Soil Hydraulic Properties From Chemical Waste Landfill CAP Verifications Project*, Daniel B. Stephens & Associates.

Appendix A
Early Simulation Results

Early simulation results for the TEVES Project are summarized in Phelan and Webb (1994). These simulations were performed with essentially the same model as discussed in the main report except for the borehole boundary condition. In the early results, heat transfer from the soil to the borehole was included. Due to the constant pressure and temperature boundary condition of the borehole, the temperature in the vicinity of the borehole was depressed, and local water and NAPL condensation around the borehole was observed. This behavior is not considered realistic since the actual borehole temperatures will approach those of the heated soil. Subsequently, heat transfer to the borehole was eliminated, and the simulations were redone. Other than the local conditions around the borehole, the general behavior is essentially the same for these early simulations and for the results presented in the main report. Some results from the early simulations as given by Phelan and Webb (1994) are presented in this Appendix for comparison purposes.

Results are shown for the inside extraction case of 0.5 kPa borehole vacuum; this case was chosen since contaminant migration into the unheated soil occurs. The temperature plots for the early simulation is shown in Figure A-1; the average, maximum, and minimum temperatures for the heated zone at 60 days are 249°C, 365°C, and 135°C, respectively; the unheated zone maximum temperature is 142°C. The values are about 10-15°C lower than the results given in Section 3.3 due to heat transfer to the borehole. The temperature contours at 60 days are shown in Figure A-2. The only difference compared to Section 3.3 is the local temperature depression around the borehole.

Figure A-3a shows the liquid masses in the heated zone, while Figure A-3b shows the NAPL masses in the heated and unheated zones; the results are similar to those in the main report. The maximum amount of NAPL migrating to the unheated zone is about 225 kg for this early model; about 200 kg migrated in the final model. Figure A-4 shows NAPL saturation contours at 8 days; the results are the same as in Section 3.1 except for the area right around the borehole.

Finally, Figure A-5 shows the mass flow rates into the borehole and the evaporation rates; again, the results are essentially the same as in Section 3.3.

While the borehole model used in the simulation presented in Phelan and Webb (1994) and in the present report is different, the overall results are essentially the same except for local conditions right around the borehole. The general conclusions from the study are unchanged.

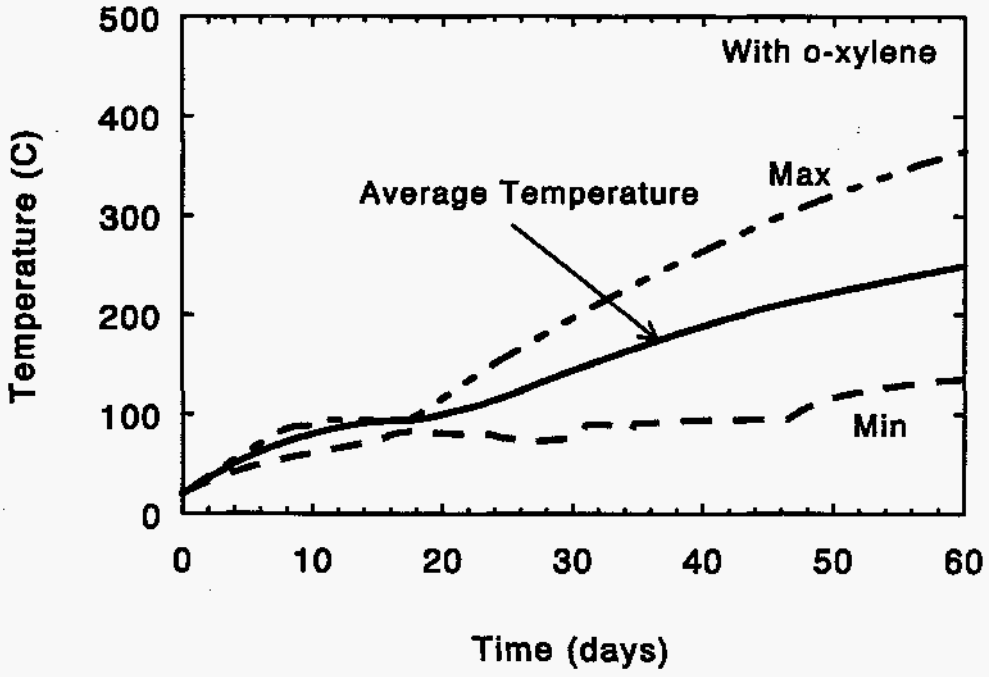

(a) Heated zone temperatures

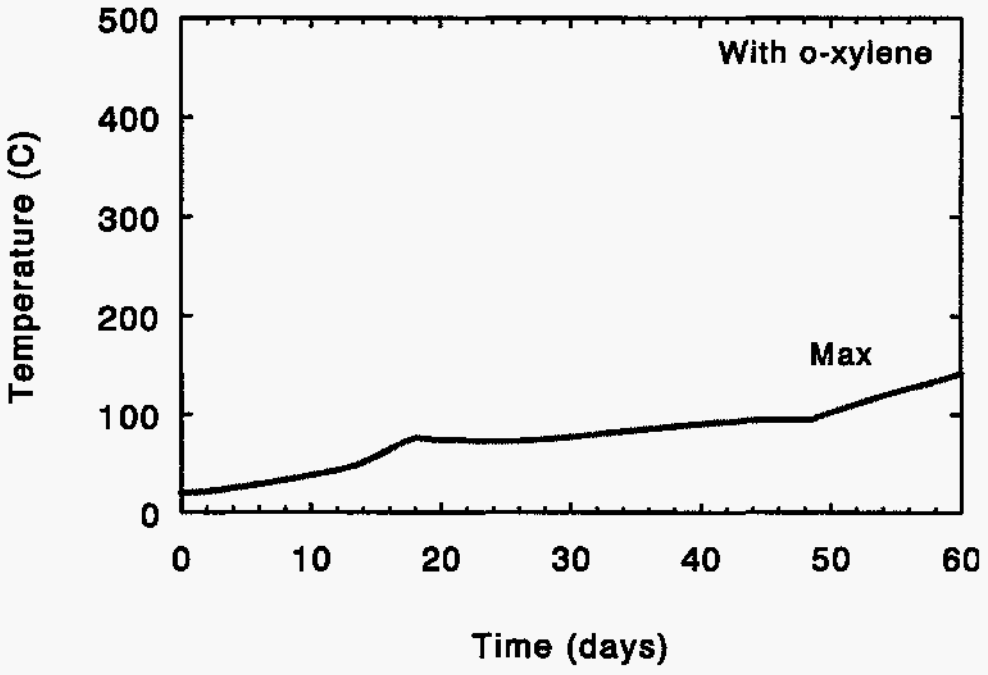

(b) Maximum unheated zone temperatures

Figure A-1. Heated and unheated zone temperatures, inside extraction, 100 kW, 0.5 kPa (2" water) BH vacuum

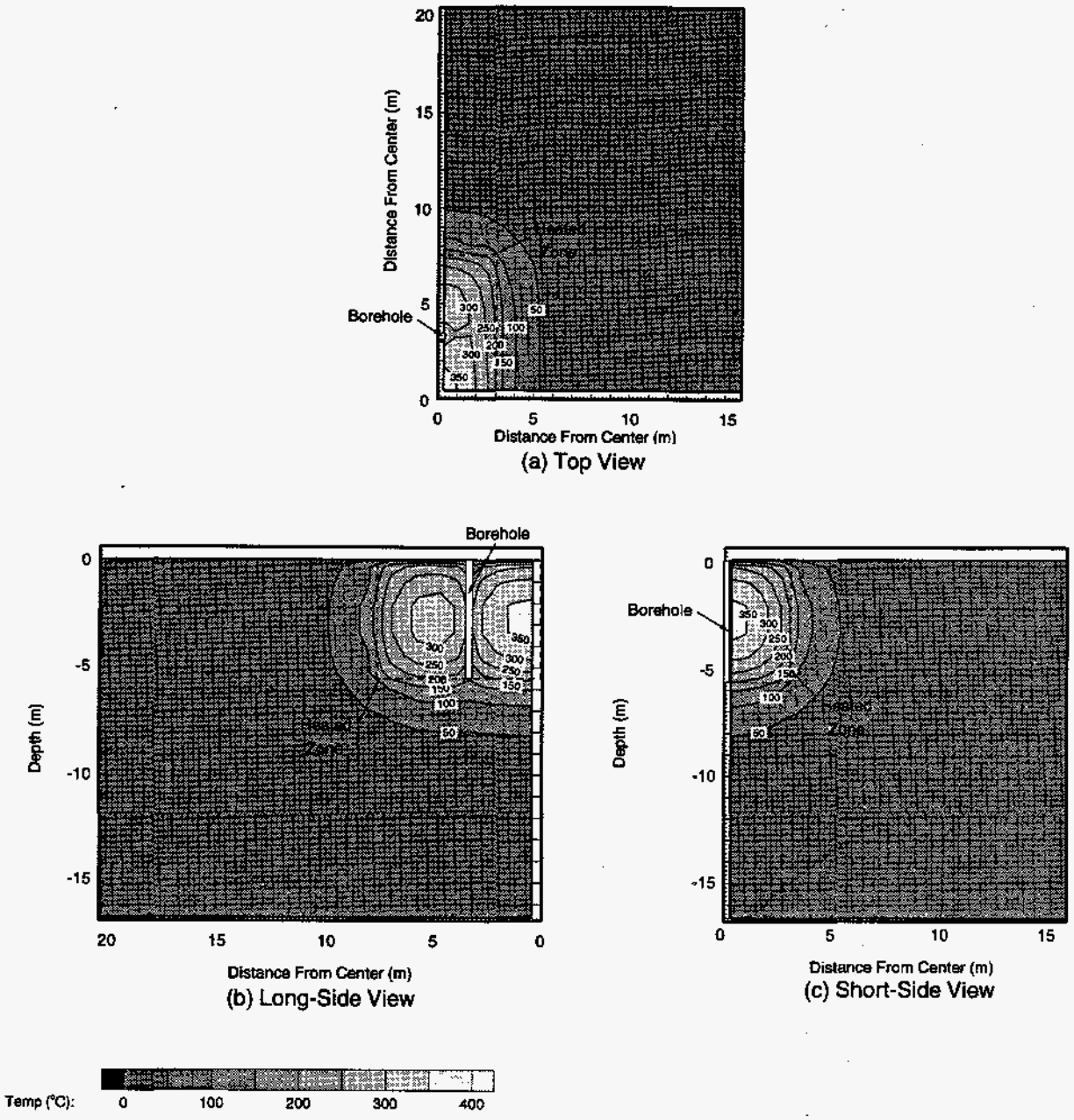

Figure A-2. Temperature contours at 60 days, inside extraction, 0.5 kPa vacuum
(a) Top view: K=4 plane
(b) Long-side view: I=1 plane
(c) Short-side view: J=1 plane

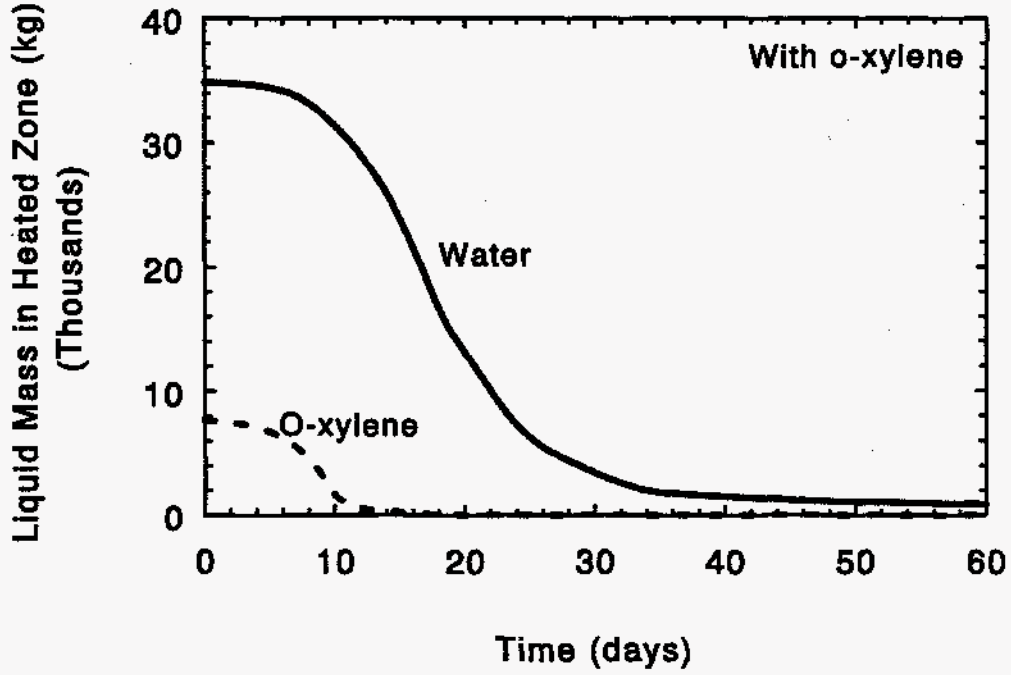

(a) Heated zone fluid masses

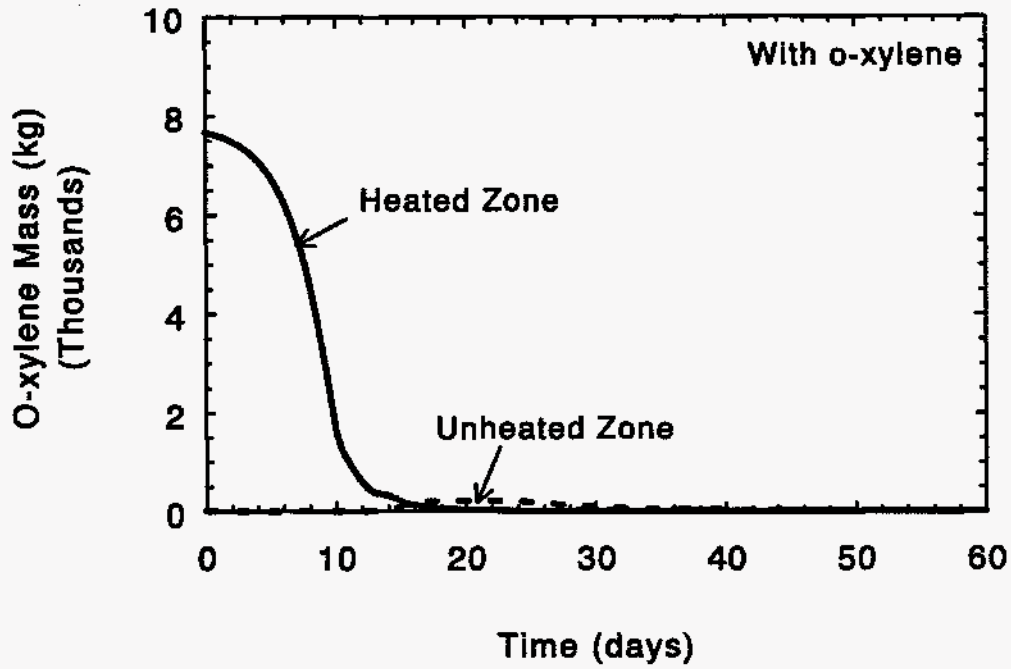

(b) O-xylene mass variation

Figure A-3. Heated zone fluid masses and O-xylene mass variation, inside extraction, 100 kW, 0.5 kPa (2" water) BH vacuum

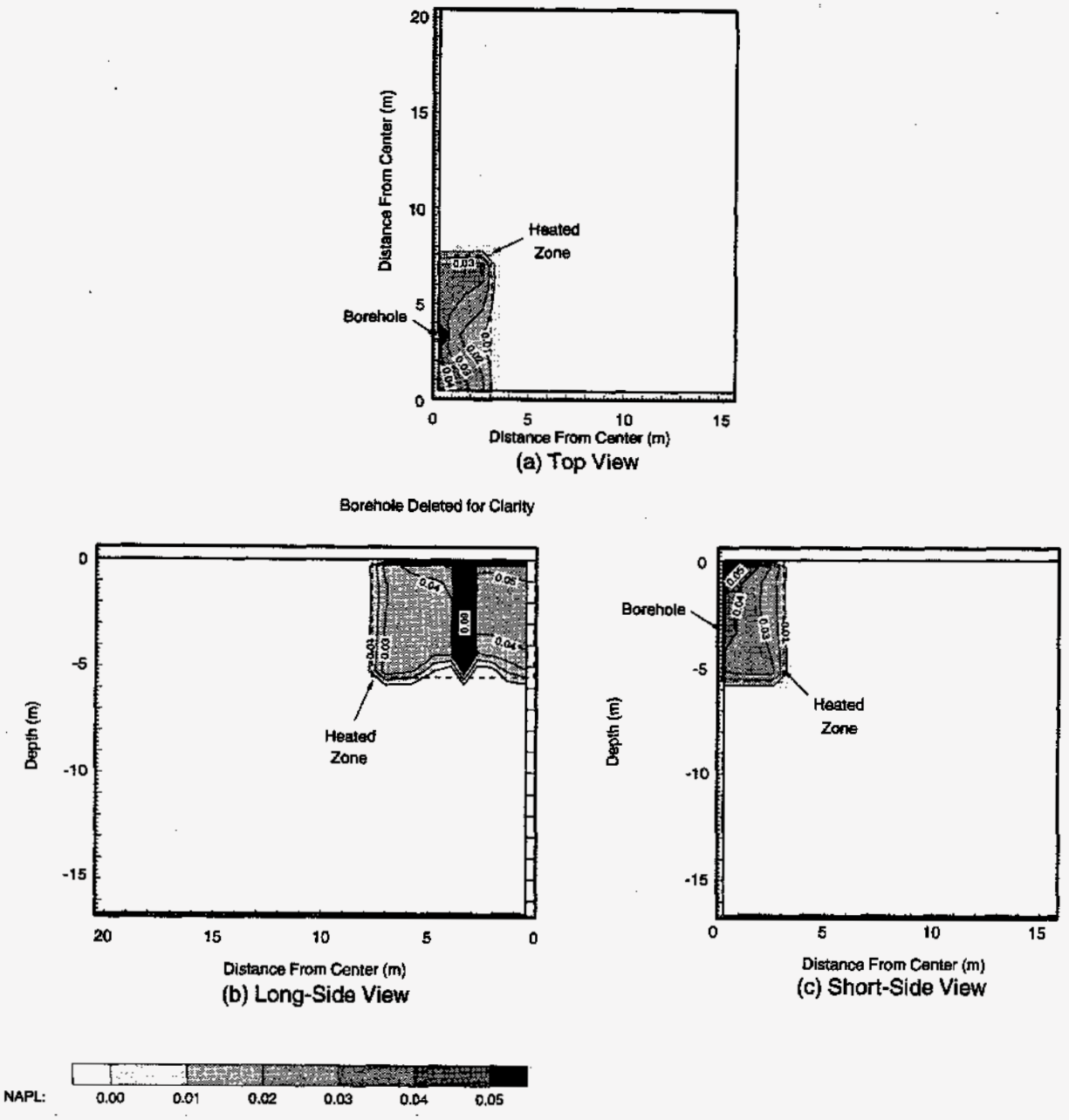

Figure A-4. NAPL saturation contours at 8 days, 0.5 kPa vacuum
(a) Top view: K=4 plane
(b) Long-side view: I=1 plane
(c) Short-side view: J=1 plane

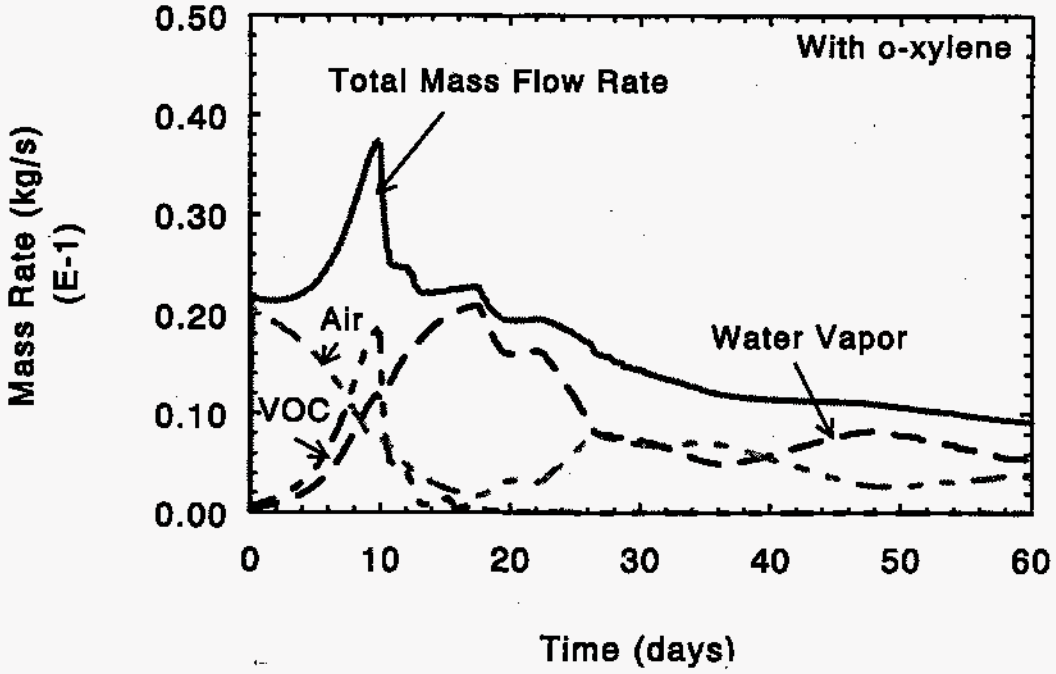

(a) Mass flow rates into boreholes

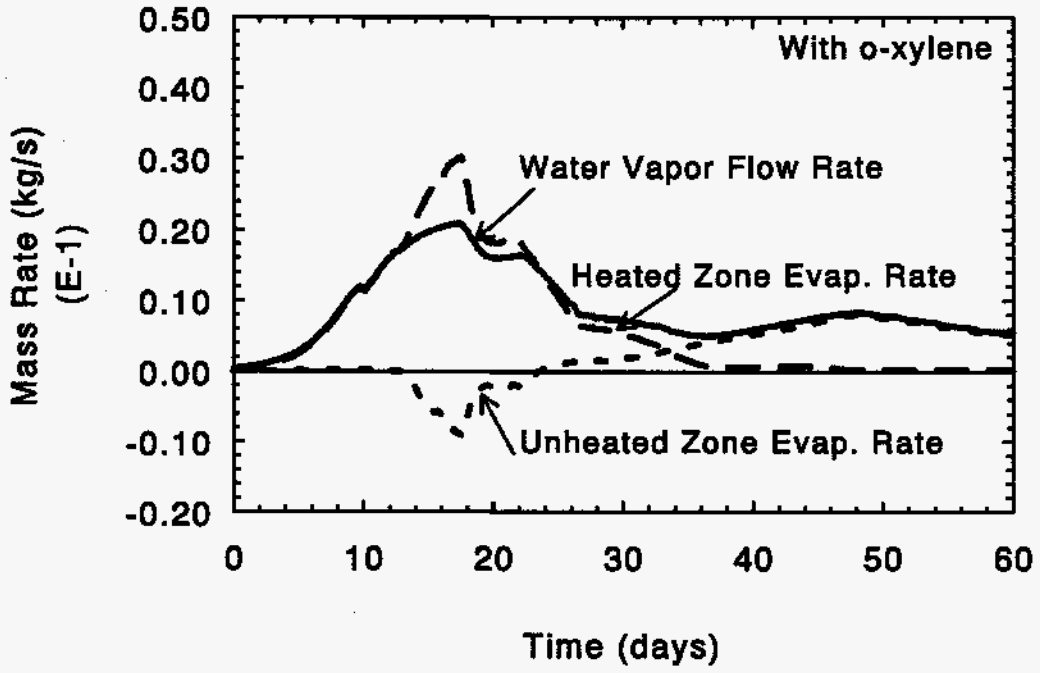

(b) Evaporation and water vapor mass rates

Figure A-5. Mass rates, inside extraction, 100 kW, 0.5 kPa (2" water) BH vacuum

DISTRIBUTION:

1 Cindy Ardito
Intera, Inc.
1650 University Blvd., N.E.
Albuquerque, NM 87102

1 T. Bergsman
Pacific Northwest Laboratories
Battelle Boulevard
Richland, WA 99352

1 Skip Chamberlain
U.S. Department of Energy
EM-541, H17 Cloverleaf Gtn.
19901 Germantown Rd.
Germantown, MD 20874-1290

1 David Daniel
University of Texas at Austin
Cockrell Hall, Room 9. 102
Austin, TX 78712

1 Harsh Dev
IIT Research Institute
10 West 35th St.
Chicago, IL 60616-3799

1 Tom Early
Oak Ridge National Laboratory
P.O. Box 2008
Oak Ridge, TN 37831-6317

1 Elizabeth Fiedler
Oak Ridge National Laboratory
Blair Road
Portal #5
MS-7328
Bldg. 303-7, Rm. 42
Oak Ridge, TN 37831-7328

1 Phillip Gauglitz, Ph.D.
Pacific Northwest Laboratories
Battelle Boulevard
Richland, WA 99352

1 Thomas Hicks
U.S. Department of Energy
Savannah River Operations Office
P.O. Box A, Building 703-46A
Aiken, SC 29802

1 Tim Jarosch
Westinghouse Savannah River Company
Road SR-1
Bldg. 773-42A
Aiken, SC 29808

1 Daniel Krivitzky
U.S. Department of Energy
Albuquerque Operations Office
P.O. Box 5400
Albuquerque, NM 87185

1 B. Looney
Westinghouse Savannah River Company
Road SR-1
Bldg. 773-42A
Aiken, SC 29808

1 Andrew Murray, P.E.
SubTerra Remedial Engineers, Inc.
1830 Bering Drive
Suite 23
San Jose, CA 95112-4212

1 Mary Peterson
Pacific Northwest Laboratories
P.O. Box 999
MS P7-41
Battelle Blvd.
Richland, WA 99352

1 Gug Sresty
IIT Research Institute
10 West 35th St.
Chicago, IL 60616-3799

1 Jim Studer
Intera, Inc.
1650 University Blvd., N.E.
Albuquerque, NM 87102

1 Terry Walton
Pacific Northwest Laboratories
Battelle
P.O. Box 999, K9-08
Richland, WA 99352

1 Jim Wright
U.S. Department of Energy
Savannah River Operations Office
P.O. Box A, Bldg. 703-46A
Aiken, SC 29802

1	MS	0701	Dick Lynch, 6100
1		0719	Jennifer Nelson, 6621
5		0719	James Phelan, 6621
1		0726	James Rice, 6600
1		0834	Roger Eaton, 9112
1		0834	Mario Martinez, 9112
1		1324	Peter Davies, 6115
1		1324	Cliff Ho, 6115
5		1324	Steve Webb, 6115
2	MS	0100	Document Processing for DOE/OSTI, 7613-2
1		0619	Print Media, 12615
5		0899	Technical Library, 4414
1		9018	Central Technical Files, 8523-2